State space model extraction of thermohydraulic systems

Thesis submitted for the degree Doctor of Philosophy

at the Potchefstroom campus of the North-West University

Kenneth R. Uren

Promoter: Prof. G. van Schoor
Co-promoter: Prof. C.P. Bodenstein
May 2009

PREFACE

During my studies from graduate to post graduate, my interest in systems modelling and control was initiated by my promotor Prof. George van Schoor. My favourite readings included "System dynamics and response" [1], "Predictive control with constraints" [2] and "Process modelling and model analysis" [3]. My Masters' study investigated optimal control schemes for a PBMR PCU which initiated an interest in the modelling of thermohydraulic systems for control purposes. This lead to the study presented in this thesis.

I want to thank my Lord Jesus Christ for his grace, blessings and strength during this study. All the glory and honour to Him. I am so grateful for such a competent and understanding promotor, Prof. George van Schoor. To me, he is a father, a spiritual leader, a friend and a colleague. I have learned so much from him about research and life. My thanks to Prof. Charles Bodenstein, for sharing with me his vast amount of experience in the areas of modelling and control. Thanks for your support and encouragement.

I want to thank my wonderful wife Grethe, for her love, support, prayers and encouragement. Thanks for believing in me and thank you for the coffee in the late nights. This thesis is dedicated to you. I want to express also my deepest thanks to my family and parents Bertha and Basie Uren; and Louise and Speedy Cilliers for standing behind me during this study. You are pillars of strength.

I would like to thank M-Tech Industrial (Pty) Ltd for their contribution in identifying the need for this study. Thank you for the supportive documentation and access to the *Flownex®* simulation software. Thank you for the financial support without which this study would not have been possible.

For God had not given us a spirit of fear; but of power, and of love, and of a sound mind.

II Timothy 1:7

ABSTRACT

Many hours are spent by system and control engineers deriving reduced order dynamic models portraying the dominant system dynamics of thermohydraulic systems. A need therefore exists to develop a method that will automate the model derivation process. The model format preferred for control system design and analysis during preliminary system design is the state space format. The aim of this study is therefore to develop an automated and generic state space model extraction method that can be applied to thermohydraulic systems.

Well developed system identification methods exist for obtaining state space models from input-output data, but these models are not transparent, meaning the parameters do not have any physical meaning. For example one cannot identify system parameters such as heat or mass transfer coefficients. Another approach is needed to derive state space models automatically. Many commercial thermohydraulic simulation codes follow a network approach towards the representation of thermohydraulic systems. This approach is probably one of the most advanced approaches in terms of technical development. It would therefore be useful to develop a state space extraction algorithm that would be able to derive reduced order state space models from network representations of thermohydraulic systems. In this regard a network approach is followed in the development of the state space extraction algorithm. The advantage of using a network-based extraction method is that the extracted state space model is transparent and the algorithm can be embedded in existing simulation software that follow a network approach.

In this study an existing state space extraction algorithm, used for electrical network analysis, is modified and applied in a new way to extract state space models of thermohydraulic systems. A thermohydraulic system is partitioned into its respective physical domains which, unlike electrical systems, have multiple variables. Network representations are derived for each domain. The state space algorithm is applied to these network representations to extract symbolic state space models. The symbolic parameters may then be substituted with numerical values. The state space extraction algorithm is applied to small scale thermohydraulic systems such as a U-tube and a heat exchanger, but also to a larger, more complex system such as the Pebble Bed Modular Reactor Power Conversion Unit (PBMR PCU). It is also shown

that the algorithm can extract linear, nonlinear, time-varying and time-invariant state space models. The extracted state space models are validated by solving the state space models and comparing the solutions with *Flownex*® results. *Flownex*® is an advanced and extensively validated thermo-fluid simulation code. The state space models compared well with *Flownex*® results.

The usefulness of the state space model extraction algorithm in model-based control system design is illustrated by extracting a linear time-invariant state space model of the PBMR PCU. This model is embedded in an optimal model-based control scheme called Model-Predictive Control (MPC). The controller is compared with standard optimised control schemes such as PID and Fuzzy PID control. The MPC controller shows superior performance compared to these control schemes.

This study succeeded in developing an automated state space model extraction method that can be applied to thermohydraulic networks. Hours spent on writing down equations from first principles to derive reduced order models for control purposes can now be replaced with a click of a button. The need for an automated state space model extraction method for thermohydraulic systems has therefore been resolved.

Keywords: State space models, model extraction, thermohydraulic systems

OPSOMMING

Stelsel- en beheeringenieurs spandeer baie ure om lae orde dinamiese modelle af te lei wat die dominante dinamika van termo-hidroliese stelsels reflekteer. Daar is dus 'n behoefte om 'n metode te ontwikkel wat die modelafleidingsproses outomatiseer. Die model formaat wat verkies word vir die ontwikkeling van beheerskemas en voorlopige stelselontwerp is toestandsruimtemodelle. Die doel van die studie is dus om 'n outomatiese en generiese toestandsruimtemodel onttrekkingsmetode te ontwikkel wat op termo-hidroliese stelsels toegepas kan word.

Goeie stelselidentifikasiemetodes bestaan wel, en kan gebruik word om toestandsruimte-modelle uit data af te lei. Die nadeel van hierdie metodes is egter dat die modelle nie deursigtig is nie. Dit beteken dat die parameters nie enige fisiese betekenis het nie. 'n Mens sou byvoorbeeld nie parameters soos hitte en massa oordrag koëffisiënte kon identifiseer nie. 'n Ander benadering word benodig om toestandsruimtemodelle outomaties af te lei. Baie kommersiële termo-hidroliese simulasiekodes maak gebruik van 'n netwerkbenadering om termo-hidroliese stelsels voor te stel. Hierdie benadering is waarskynlik tegnies, een van die mees gevorderde benaderings. Dit is dus baie sinvol om 'n toestandsruimtemodel onttrekkingsmetode te ontwikkel wat gereduseerde toestandsruimtemodelle van netwerkvoorstellings onttrek. In hierdie opsig is 'n netwerkgebaseerde benadering gevolg in die ontwikkeling van die toestandsruimtemodel onttrekkingsalgoritme. Die voordele van 'n netwerkgebaseerde benadering is dat die modelle deursigtig is en dat die onttrekkingsalgoritme in 'n bestaande simulasiepakket, wat 'n netwerkbenadering volg, ingebou kan word.

In hierdie studie word 'n toestandsruimtemodel onttrekkingsalgoritme, wat gebruik word in elektriese netwerkanalise, aangepas en op 'n nuwe manier toegepas om toestandsruimte modelle van termo-hidroliese stelsels te onttrek. Die termo-hidroliese stelsel word opgedeel in die verskillende fisiese domeine. Anders as elektriese stelsels, het termo-hidroliese stelsels 'n groter aantal veranderlikes. Netwerkvoorstellings word dan vir elke domein afgelei. Die toestandsruimtemodel onttrekkingsalgoritme word dan toegepas op die netwerkvoorstellings om simboliese toestandruimtemodelle te onttrek. Die simboliese parameters kan dan met

numeriese waardes vervang word. Die toestandsruimtemodel onttrekkingsalgoritme is toegepas op kleinskaalse termo-hidroliese stelsels soos 'n U-buis en 'n hitteruiler, maar ook op 'n groter en meer komplekse stelsel soos die Korrelbed Modulêre Reaktor Drywings Omskakelings Eenheid (KMR DOE). Dit word ook gewys dat die algoritme liniêre, nie-liniêre, tyd-afhanklike en tyd-onafhanklike toestandsmodelle kan onttrek. Die onttrekte toestandsmodelle is gevalideer deur die toestandsmodelle op te los en die oplossings met *Flownex*® resultate te vergelyk. *Flownex*® is 'n gevorderde en intensief gevalideerde termo-vloei simulasie pakket. Die toestandsruimte modelle het goed vergelyk met die *Flownex*® resultate.

Die nut van die toestandsruimtemodel onttrekkingsalgoritme vir modelgebaseerde beheerstelselontwerp word geïllustreer deur 'n liniêre tyd-onafhanklike toestandsruimte model van die KMR DOE te onttrek. Hierdie model is gebruik in 'n optimale modelgebaseerde beheerskema naamlik Model-Voorspellings Beheer (MVB). Hierdie beheerder is vergelyk met standaard ge-optimaliseerde beheerskemas soos PID en Wasige PID beheer. MVB beheer het baie beter as die ander standaard skemas presteer.

Hierdie studie het daarin geslaag om 'n ge-outomatiseerde toestandsruimtemodel onttrekkingsmetode te ontwikkel wat op termo-hidroliese stelsels toegepas kan word. Ure se werk om vergelykings van eerste beginsels af te lei om gereduseerde modelle vir beheerdoeleindes af te lei kan nou met die druk van 'n knoppie gedoen word. Die behoefte vir 'n outomatiese toestandsruimtemodel onttrekkingsmetode vir termo-hidroliese stelsels is dus aangespreek.

CONTENTS

List of figures **xi**

List of tables **xvi**

Nomenclature **xvii**

1 Introduction **1**

1.1 Introduction 1

1.2 Models of thermohydraulic systems for control purposes 3

1.2.1 Mechanistic models 3

1.2.2 Empirical models 4

1.2.3 Qualitative models 4

1.3 Model-based control 5

1.4 Conclusion on modelling methods for control 7

1.5 Problem statement 7

1.6 Objective of this study 8

1.7 Outline of the thesis 9

2 Literature survey **11**

2.1 Introduction . . . 11
2.2 State space models of thermohydraulic systems . . . 11
2.2.1 The scope of modelling methods and structures for control . . . 11
2.2.2 Previous state space model applications . . . 13
2.2.3 The necessity of state space models . . . 15
2.3 Dedicated codes for control system development . . . 17
2.3.1 Object-oriented approach . . . 17
2.3.2 Bond graph approach . . . 18
2.3.3 Block diagram approach . . . 18
2.3.4 Analytical approach . . . 19
2.4 State space model extraction methods . . . 19
2.5 Limitations of current approaches . . . 20
2.6 Conclusion . . . 20

3 State space models **21**
3.1 Introduction . . . 21
3.2 The notion of a system . . . 21
3.3 State space representation . . . 23
3.4 State space modelling of networks . . . 25
3.5 Conclusions . . . 29

4 Extraction of State Space models **30**
4.1 Introduction . . . 30
4.2 Generalised system variables and elements . . . 30
4.3 State space modelling using a network approach . . . 32
4.3.1 Algebraic description of a network . . . 32
4.3.2 Comparison with algebraic representation used in *Flownex*® . . . 35
4.3.3 System structural and elemental equations . . . 37

4.3.4 State space extraction algorithm . . . 43
4.4 Conclusion . . . 44

5 Applications of state space model extraction **45**
5.1 Introduction . . . 45
5.2 Thermohydraulic element characterisation . . . 45
5.2.1 Generalised hydraulic and thermal elements . . . 46
5.2.2 Turbomachines and shafts in terms of generalised elements . . . 52
5.3 Thermohydraulic applications . . . 58
5.3.1 State space model extraction of a U-tube . . . 58
5.3.2 State space model extraction of a heat exchanger . . . 65
5.3.3 State space model extraction of a PBMR PCU . . . 72
5.3.4 Helium injection . . . 80
5.3.5 Helium extraction . . . 82
5.3.6 Helium bypass . . . 84
5.4 Conclusion . . . 86

6 Model-based control **87**
6.1 Introduction . . . 87
6.2 Brief plant description . . . 87
6.3 Power output control . . . 88
6.4 Linear state space model of the PCU . . . 89
6.4.1 Hydraulic flow sources . . . 95
6.4.2 Mechanical flow sources . . . 97
6.4.3 Symbolic matrix elements . . . 98
6.5 Extracted linear state space model validation . . . 99
6.6 Model based control . . . 103
6.7 Conclusion . . . 109

7 Conclusions **110**

7.1 Introduction 110

7.2 Overview 110

7.3 Unique contribution 111

7.4 Recommendations 113

7.5 Closure 113

Bibliography **115**

A Review of graph theory **120**

A.1 Notation and basic definitions 120

A.2 Trees and co-trees 123

A.3 Matrix representation of graphs 124

B Symbolic state space model extraction **128**

B.1 Symbolic **A** and **B** matrix elements 128

C Code implementation **130**

C.1 State space model extraction: U-tube 130

LIST OF FIGURES

1.1 Schematic description of advanced control 2

1.2 Model types for control [4] 3

1.3 Model-based advanced control strategy [5] 6

1.4 State space representation of a system 6

1.5 Automatic model generation using *Symbols 2000*® [6] 8

1.6 Thermohydraulic network [7] 8

1.7 Simulation and control analysis code based on the network approach 9

2.1 Controlled Reference Value (CRV) approach [8] 16

2.2 Control Action Control (CAC) approach [8] 16

3.1 System mapping input functions to output functions [3] 22

3.2 System descriptions 22

3.3 Conceptual diagram of the state space representation 23

3.4 Illustration of time invariance [9] 24

3.5 Electrical network: Example 1 26

3.6 Electrical network: Example 2 28

4.1 Generalised system variables 31

4.2 Generalised system elements [10] . . . 33
4.3 Electrical network . . . 34
4.4 Energy network representation of the electrical circuit . . . 34
4.5 *Flownex*® network . . . 36
4.6 Notation used to define the structure of a *Flownex*® network [11] . . . 36
4.7 Relationship between the incidence matrix and the element connectivity matrix . . . 37
4.8 Relationship between the incidence matrix and the node connectivity matrix . . . 37
4.9 Energy network used for tree and co-tree analysis . . . 38
4.10 A normal tree of the network . . . 39

5.1 Network representation of thermohydraulic systems . . . 46
5.2 A pipe section discretised into control volumes . . . 47
5.3 Two types of control volumes . . . 47
5.4 Hydraulic network of a pipe section . . . 49
5.5 Thermal network of a pipe section . . . 52
5.6 Pressure ratio curve maps: (a) Turbine (b) Compressor [12] . . . 53
5.7 Efficiency curve maps: (a) Turbine (b) Compressor [12] . . . 53
5.8 Generalised element modelling of turbomachines . . . 55
5.9 Compressor-turbine combination . . . 56
5.10 Mechanical network representation of a shaft . . . 57
5.11 RCCS pipe network surrounding the RPV [13] . . . 58
5.12 Two standpipes of the RCCS [13] . . . 59
5.13 Representation of the U-tube and a conceptual view of the control volumes . . . 59
5.14 Hydraulic network of the U-tube . . . 60
5.15 Thermal network of the U-tube . . . 62
5.16 Information flow between domains . . . 63
5.17 Methodology for reduced order model extraction and validation (U-tube) . . . 63
5.18 Downcomer and riser densities . . . 64

5.19 Temperature in the riser pipe . . . 65
5.20 Mass flow rate due to natural convection . . . 65
5.21 Concentric tube heat exchangers. (a) Parallel-flow. (b) Counterflow [14] . . . 66
5.22 Structural representation of heat exchanger units . . . 67
5.23 General network representation of a heat exchanger . . . 67
5.24 Heat exchanger component in *Flownex*® . . . 71
5.25 Result comparison in Simulink® environment . . . 71
5.26 Primary and secondary temperature inputs . . . 72
5.27 (a) Primary output temperature (b) Secondary output temperature . . . 72
5.28 Thermohydraulic system: PBMR PCU . . . 73
5.29 Conceptual model of the PCU . . . 74
5.30 *Flownex*® network of the PCU . . . 74
5.31 Hydraulic network of the PCU . . . 75
5.32 Thermal network of the PCU . . . 77
5.33 Mechanical network of the PCU . . . 78
5.34 Methodology for reduced order model extraction and validation (PBMR PCU) . . . 78
5.35 Helium injection: Mass flow rate comparison . . . 80
5.36 Helium injection: Pressure comparison . . . 80
5.37 Helium injection: Temperature comparison (compressors and reactor) . . . 81
5.38 Helium injection: Temperature comparison (turbines) . . . 81
5.39 Helium injection: Shaft speed . . . 81
5.40 Helium extraction: Mass flow rate comparison . . . 82
5.41 Helium extraction: Pressure comparison . . . 82
5.42 Helium extraction: Temperature comparison (compressors and reactor) . . . 83
5.43 Helium extraction: Temperature comparison (turbines) . . . 83
5.44 Helium extraction: Shaft speed . . . 83
5.45 Helium bypass: Mass flow rate comparison . . . 84

5.46 Helium bypass: Pressure comparison 84
5.47 Helium bypass: Temperature comparison (compressors and reactor) 85
5.48 Helium bypass: Temperature comparison (turbines) 85
5.49 Helium bypass: Shaft speed 85

6.1 Simplified schematic drawing of the PBMR power conversion unit 88
6.2 Simplified Flownet model of the PBMR PCU used for model validation [12] . . . 89
6.3 Schematic diagram of the conceptual model of the PCU [12] 90
6.4 Perturbations in pressures predicted by the linear model and Flownet [12] 91
6.5 Perturbations in shaft speed predicted by the linear model and Flownet [12] . . . 91
6.6 Linear *Simulink*® model of the PCU [15] 92
6.7 Comparison between *Simulink*® and Flownet models [15] 93
6.8 Hydraulic and mechanical network representation of the PCU 94
6.9 Helium injection: A comparison between perturbations in power output 101
6.10 Helium extraction: A comparison between perturbations in power output 101
6.11 Helium bypass: A comparison between perturbations in power output 102
6.12 Helium boost: A comparison between perturbations in power output 102
6.13 Model predictive control scheme 104
6.14 Conceptual diagram of the optimal PID and Fuzzy control strategies 104
6.15 Optimal PID control [16] 105
6.16 Performance of the optimal PID control strategy (ITAE = 43.9) [16] 105
6.17 Optimal Fuzzy PID control [16] 106
6.18 Performance of the optimal Fuzzy PID control strategy (ITAE = 24.62) [16] 106
6.19 Conceptual diagram of the Model-predictive control strategy 107
6.20 Model predictive control 107
6.21 Performance of the model-predictive controller (ITAE = 0.3169) 107
6.22 Perturbation in helium mass flow rate at high pressure side 108
6.23 Perturbation in helium mass flow rate at the low pressure side 108

7.1 Unique contribution: Thermohydraulic state space model extraction method . . 112

A.1 Königsberg bridge problem 121

A.2 Graph of the Königsberg bridge problem 121

A.3 Directed graph 122

A.4 Disconnected graph 122

A.5 Original graph and one possible sub-graph 123

A.6 A graph with one possible tree and co-tree 123

A.7 Fundamental cut-sets and loop-sets 125

A.8 Connected graph with a specific tree indicated in bold 126

C.1 Incidence matrix representing the hydraulic graph of the U-tube 130

C.2 Incidence matrix representing the thermal graph of the U-tube 130

C.3 Element matrices: (a) Hydraulic (b) Thermal 131

C.4 Hydraulic sources and state variables 131

C.5 Thermal sources and state variables 131

C.6 Extracted hydraulic **A**-matrix 132

C.7 Extracted thermal **A**-matrix 132

C.8 Extracted hydraulic **B**-matrix 132

C.9 Extracted thermal **B**-matrix 132

LIST OF TABLES

4.1 Examples of generalised variables 31

4.2 The five generalised system elements [17, 18] 33

5.1 Summary of generalised hydraulic elements 50

5.2 Summary of generalised thermal elements 52

5.3 Summary of generalised elements of rotating masses 57

5.4 Calculated internal pressures 64

6.1 Operating points of the turbomachines 99

NOMENCLATURE

Roman lettering (lower case)

Symbol	Unit	Description
c_p	kJ/(kg · K)	Specific heat at constant pressure
c_v	kJ/(kg · K)	Specific heat at constant volume
d	-	Disturbance vector
e	kJ	Energy
e	-	Effort vector
e	-	Generalised effort variable
f	-	Generalised flow variable
f	-	Flow vector
f	-	Darcy-Weisbach friction factor
g	9.83 m/s^2	Gravitational constant
h_N	W/(m^2 · K)	Convection heat transfer coefficient
h	kJ/kg	Specific enthalpy
i	-	Node index
i	A	Electrical current
j	-	Link index
K	-	Secondary loss factor
k_c	W/(m · K)	Conduction heat transfer coefficient
ℓ	m	Length
$\dot{m}$	kg/s	Mass flow rate
$\hat{\mathbf{n}}$	-	Normal component
p	W	Instantaneous power
t	s	Seconds
u	-	Input variable
v	m/s	Velocity
v	V	Voltage

Continued on next page

Symbol	Unit	Description
v	-	Disturbance variable
$\mathbf{v}$	m/s	Velocity vector
$\dot{w}$	kJ/s or kW	Energy flow rate
x	-	State variable
y	-	Output variable
z	m	Height

Roman lettering (upper case)

Symbol	Unit	Description
A	m^2	Area
$\mathbf{A}$	-	State matrix
$\mathbf{A}_I$	-	Incidence matrix
B	Pa	Bulk modulus
$\mathbf{B}$	-	Input matrix
C	-	Capacitive element
C_h	-	Hydraulic capacitance element
$\mathbf{C}$	-	Output matrix
D	m	Diameter
$\mathbf{D}$	-	Feed-forward matrix
$\mathbf{E}$	-	Element connectivity matrix
$\hat{\mathbf{E}}$	-	Random variable sequence
F	N	Force
$\mathbf{F}_c$	-	Fundamental cut-set matrix
$\mathbf{F}_l$	-	Fundamental loop-set matrix
$\mathbf{G}$	-	Transfer function matrix
J	$\mathrm{kg} \cdot \mathrm{m}^2$	Inertia
K	-	Friction factor
L	-	Inductive element
M	kg	Mass
$\mathbf{N}$	-	Node connectivity matrix
N'	$(\mathrm{rev/s})/\sqrt{\mathrm{K}}$	Non-dimensional speed
N	rev/s	Speed of a turbomachine
P	Pa	Pressure
P_r	-	Machine pressure ratio
P_{rc}	-	Compressor pressure ratio
P_{rt}	-	Turbine pressure ratio
$\dot{Q}$	kW	Heat transfer rate
Q'	$(\mathrm{kg/s} \times \sqrt{\mathrm{K}})/\mathrm{Bar}$	Non-dimensional mass flow rate
R	-	Resistive element
S	-	Source element
T	K	Temperature

Continued on next page

Symbol	Unit	Description
U	kW/K	Heat transfer coefficient
$\mathbf{U}$	-	Input vector
$\mathbf{U}_m$	-	Control vector of the advanced controller
V	m^3	Volume
W	kJ	Work
$\hat{\mathbf{W}}$	-	Random variable sequence
$\dot{W}$	kJ/s or kW	Power output of a turbomachine
$\mathbf{X}$	-	State vector
$\mathbf{Y}$	-	Output vector
$\mathbf{Y}_{ref}$	-	Reference vector

Subscripts

01	Turbomachine inlet
02	Turbomachine outlet
c	Compressor
cond	Conduction heat transfer
conv	Convection heat transfer
e	Effort
f	Flow
gen	Heat generation
h	Hydraulic domain
k	Source index
m	Mechanical domain
p	Primary side of a heat exchanger
rad	Radiation heat transfer
s	Secondary side of a heat exchanger
t	Thermal domain
t	Turbine

Greek letters

Symbol	Unit	Description/Quantity
$\bar{\beta}$	-	Body force distribution
η	-	Machine isentropic efficiency
η_c	-	Isentropic efficiency of a compressor
η_t	-	Isentropic efficiency of a turbine
$\boldsymbol{\theta}$	-	Parameter vector
ε	-	Emissivity
γ	-	Specific heat ratio
κ	-	Friction factor

Continued on next page

Symbol	Description	Units
ω	rev/s or Hz	Angular velocity
Ω	-	Turbomachine variable mapping
ρ	kg/m^3	Density
σ	5.67×10^{-8} W/m$^2 \cdot$ K^4	Stefan-Boltzmann constant
$\bar{\tau}$	-	Surface force distribution
τ	N $\cdot$ m	Torque
ϕ	-	Lagged input-output vector
Ψ	-	System operator

Abbreviations

AC	Adaptive Control
ACSL	Advanced Continuous Simulation Language
AI	Artificial Intelligent
ARMAX	AutoRegressive Moving Average with eXogenous input
CAC	Control Action Correction
CFD	Computational Fluid Dynamics
CRV	Controlled Reference Value
CS	Control Surface
CV	Control Volume
DAE	Differential Algebraic Equation
ESC	Expert Systems based Control
GA	Genetic Algorithm
HICS	Helium Inventory Control System
HPC	High Pressure Compressor
HPT	High Pressure Turbine
HTR	High Temperature Gas-cooled Reactor
IAE	Integral of the Absolute magnitude of the Error
IAEA	International Atomic Energy Agency
ITAE	Integral of Time multiplied by Absolute Error
LOFA	Loss of Flow Accident
LPC	Low Pressure Compressor
LPT	Low Pressure Turbine
LTI	Linear Time Invariant
LTV	Linear Time Varying
LQG	Linear Quadratic Gaussian control
LQR	Linear Quadratic Regulator
ME	Model Extraction
MIMO	Multi-Input Multi-Output
MPC	Model Predictive Control
NL	Nonlinear
OC	Optimal Control
ODE	Ordinary Differential Equation

Continued on next page

OOM	Object Oriented Modelling
OOP	Object Oriented Programming
PBMR	Pebble Bed Modular Reactor
PCU	Power Conversion Unit
PDE	Partial Differential Equation
PID	Propostional-Integral-Derivative
PT	Power Turbine
QTF	Qualitative Transfer Function
RCCS	Reactor Cavity Cooling System
RPV	Reactor Pressure Vessel
SI	System Identification
SISO	Single-Input Single-Output
SSR	State Space Representation
SSM	State Space Model
SSME	State Space Model Extraction

CHAPTER 1

INTRODUCTION

1.1 Introduction

The birth of the modern modelling and simulation discipline can reasonably be traced back to the first flight training simulator, the Link Trainer, by Edward Link in the 1920s. With the arrival of the modern computer in the 1950s, the flight training simulators soon incorporated computer technology. Although it was the simulator that initiated the modern field of modelling and simulation, it was the advances in computer technology that gave the modelling and simulation discipline its computing platform [19]. In the 1960s the speed and the software support of computers increased, leading to crucial spin-offs in modelling and simulation. In the next two decades a variety of software applications were developed specifically for modelling and simulation applications. This allowed the handling of more ambitious modelling endeavours typically found in engineering design activities.

The modelling and simulation discipline evolved from flight training simulators to many other domains [10, 20, 21]. One particular engineering domain that became extremely important through the years is the modelling and simulation of power plants (both fossil and nuclear). In this domain modelling and simulation tools assist in the investigation of design alternatives and to have a good estimate of the operating characteristics of the plant. The rapid development of modelling and simulation tools for power plants can be reasonably linked to the worldwide increase in energy demand which created a need for developing more efficient, economical and environmentally safe power plants. Unfortunately fossil fuel power plants has a very negative impact on the environment due to their large amount of CO_2 emission. This turned the world's attention towards nuclear power for future generation [22].

A promising reactor technology today is the High Temperature Gas-cooled Reactor (HTR) which fulfills the requirements of fourth generation nuclear reactors [23]. This type of reactor offers advantages such as inherent safety and improved economics. Research on HTR technology are underway in many countries around the world of which South Africa is one.

The South African company, PBMR (Pty) Ltd is developing a Pebble Bed Modular Reactor (PBMR) which is based on HTR technology. This project has made significant commercial progress [22].

To gain advantages such as improved safety, optimal performance, increased capacity, increased responsiveness and improved economics of power plants, advanced control techniques are essential. Over the past 30 years much have been written on advanced control. During the 1960s it was considered to be any algorithm or technique that differed from the classical Proportional-Integral-Derivative (PID) controller. The advances in computer technology made the implementation of advanced techniques such as multi-variable control and optimal control possible in the 1970's [24]. Today, advanced control is synonymous with the implementation of computer based technologies. However, it should be mentioned that PID control is still the most widely used control algorithm due to its operator friendliness.

Depending on an individual's background, advanced control may mean different things. It can range from self-tuning or adaptive algorithms and optimisation strategies up to Artificial Intelligent (AI) systems [25]. A general view adopted by the control research community is to regard advanced control as more than just high speed computers and state-of-the-art software [4]. Advanced control is a practice that utilises different disciplines as shown in Fig. 1.1. At the centre of this practice is the system model. This means that it is essential for the engineer to understand the system completely in order to implement advanced control.

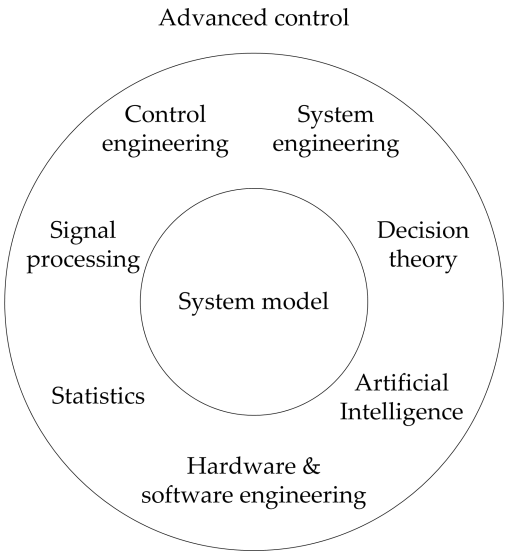

Figure 1.1: Schematic description of advanced control

System models have the capability to capture dynamic information about the physical system and allow effects such as time and space to be scaled. More importantly models allow the extraction of properties and hence simplification (abstraction), to retain only details relevant to the problem. This reduces the need for actual experiments and therefore reduces cost, risk and time [4].

Current approaches in the area of advanced control rely heavily upon a study of the system

behaviour and the use of system models [8, 26]. Therefore, this study will focus on the development of a structured methodology to derive system models of thermohydraulic systems that can be used for advanced model-based control strategies.

1.2 Models of thermohydraulic systems for control purposes

Obtaining a model of a thermohydraulic system is a challenging task since it is characterised by the coupling of several phenomena of different natures, as opposed to, e.g. a purely electrical or mechanical system [6]. In terms of control requirements, the model should be able to describe the dynamic (transient) behaviour of the system. In this context the model can be a mathematical or a qualitative description of the system behaviour. This classification can be subdivided into different model types used for control purposes as shown in Fig. 1.2.

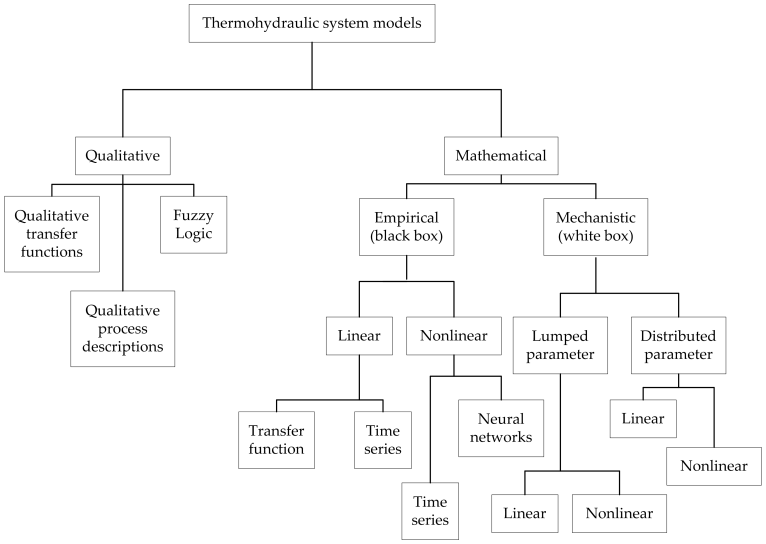

Figure 1.2: Model types for control [4]

These model types will now be discussed in the context of thermohydraulic systems in the following sections.

1.2.1 Mechanistic models

If information is available about the thermohydraulic system and its characteristics, the dynamic behaviour of the system can be described by a set of differential equations. Such a model is called a mechanistic model [3]. A thermohydraulic system is discretised into control volumes and a mechanistic model is derived by applying laws for the conservation of mass, energy and momentum transfer to the control volumes. The structure of the mechanistic model may either be a lumped parameter or a distributed parameter representation. Lumped parameter models are described by Ordinary Differential Equations (ODEs) and distributed parameter models by partial differential equations (PDEs). ODEs describe a thermohydraulic

system in one dimension, normally time. A lumped parameter model can for example describe the pressure in a tank at a specific time. PDE models have a dependence on spatial locations. A distributed model can for example describe the temperature profile of a nuclear reactor core.

It is clear that distributed parameter models are much more complex than lumped parameter models. The solution of these models is also not a straight forward task. It is possible to approximate the PDEs with ODEs, given certain assumptions [27]. Both these models can further be classified as linear or nonlinear. Usually the nonlinear differential equations are linearised around an operating point to make the analysis more tractable.

Mechanistic models are very expensive and time consuming to develop. This might cause them to be practically infeasible, especially when there is not much information available about the system. The system might also be too complex, meaning that the resulting equations cannot be solved. In such cases empirical or black-box models can be used.

1.2.2 Empirical models

Empirical (black-box) models functionally map the input variables to output variables of a system. These models have a lumped parameter structure by implication, but the parameters do not have any physical meaning. For example one cannot identify system parameters such as heat or mass transfer coefficients. This is a major drawback of empirical models. However, if some trends in the system need to be presented accurately, this approach is effective. The cost of developing an empirical model is much less in terms of time and effort compared to mechanistic models.

Empirical models may further be classified as linear and nonlinear. In the linear category, the transfer function and time series models are the most popular. A variety of linear black-box techniques can be found in Eykhoff [28]. In the nonlinear category, the time-series technique features again together with neural network techniques. These techniques use combinations of weighted products and powers of variables to represent the behaviour of a system. Due to the increasing power of computers, neural network techniques have become a feasible method for building models of dynamic systems for control applications [29, 30].

1.2.3 Qualitative models

There may be cases when a system cannot be effectively represented by a mathematical description. Such cases result due to discontinuities in the system. These systems are usually operated at distinct operating regions. In such cases qualitative models can be formulated. A good example of a qualitative model is the ”rule-based” model that makes use of ”If-then” structures to describe system behaviour. These models are also known as fuzzy logic models. The rules can be formulated using knowledge supplied by human experts. Alternatively, the rules can be generated automatically by optimisation techniques such as Genetic Algorithms (GA). These models are suitable for system monitoring and control applications.

A Qualitative Transfer Function (QTF) is another qualitative modelling method that retain most

of the qualities of a quantitative transfer function. This technique can be cast into and object or network framework where models can be connected to form a directed graph. The nodes represent variables and the links that connect the nodes describe the relationship between the nodes. The overall system behaviour (qualitative process description) can be derived by working through the graph [3].

1.3 Model-based control

Classical control is essentially limited to Single-Input Single-Output (SISO) systems described by linear differential equations with constant coefficients (or their corresponding Laplace transforms). However, the so-called modern control theory has developed to a point where Multi-Input Multi-Output (MIMO) systems are considered, described by systems of ordinary differential equations, variable-coefficient differential equations and nonlinear differential equations. At present, there are a number of advanced control techniques being researched capable of controlling processes such as power plants [31]:

- **Model Predictive Control (MPC)**: Model predictive control can be expressed as a control problem of minimising an objective function (or cost function) subject to system constraints. An embedded mathematical model of the system to be controlled, allows the controller to predict the future effects of control actions taken at present. Hence the controller chooses the best possible actions to meet the control objective. This optimisation process is solved at each time step and allows the controller to correct any new disturbances as well as to account for modelling errors.
- **Optimal Control (OC)**: An optimal control system can be obtained when the parameters of the control system are adjusted so that a performance index (or cost function) reaches an extremum, commonly a minimum value.
- **Adaptive Control (AC)**: Adaptive control systems combine parameter estimation methods and control design algorithms to determine mathematical models and perform control system design on-line.
- **Expert Systems based Control (ESC)**: Expert systems based control provide intelligent control decisions based on expert knowledge (in the form of a mathematical or qualitative model) incorporated in the algorithm.

All these algorithms have a common feature: all are based on a system model as shown in Fig. 1.3. Fig. 1.3 shows a generic form of a model-based control strategy. There are basically three distinct features associated with model-based control systems [5]:

1. **The dynamic system model**: The system model is used to compute the predicted values of the process measurements.

2. **Disturbance estimation / model parameter adaption**: Adjustments are made to the disturbance estimate or model parameters to minimise the error between the predicted values and the actual measurements.

3. **Controller**: The controller computes the actions needed so that the selected outputs of the process will be driven to their desired or optimum set points, while respecting constraints on the system variables.

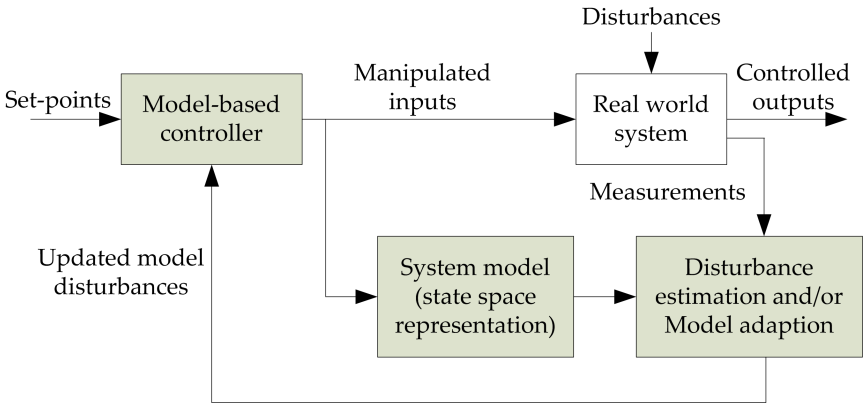

Figure 1.3: Model-based advanced control strategy [5]

The most popular model form used in these algorithms is the state space representation [2]. The state space representation of a system is shown in Fig. 1.4. The input of the state space model is represented by a input vector $\mathbf{U} = \begin{bmatrix} u_1 & u_2 & \cdots & u_k \end{bmatrix}'$; the output is represented by an output vector $\mathbf{Y} = \begin{bmatrix} y_1 & y_2 & \cdots & y_l \end{bmatrix}'$. The states of the system are contained in the state vector, $\mathbf{X} = \begin{bmatrix} x_1 & x_2 & \cdots & x_n \end{bmatrix}'$. The state variable representation is a mathematical description of the system consisting of a state equation and an output equation.

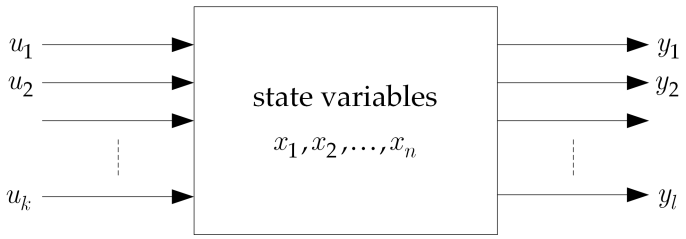

Figure 1.4: State space representation of a system

The general state space representation in matrix notation is given as

$$\begin{aligned} \dot{\mathbf{X}}(t) &= \mathbf{A}\mathbf{X}(t) + \mathbf{B}\mathbf{U}(t) \text{ (State equation)} \\ \mathbf{Y}(t) &= \mathbf{C}\mathbf{X}(t) + \mathbf{D}\mathbf{U}(t) \text{ (Output equation)}, \end{aligned} \tag{1.1}$$

where **A** is the state matrix, **B** the input matrix, **C** the output matrix and **D** the feed-forward matrix.

1.4 Conclusion on modelling methods for control

Considering the modelling techniques available for control system design a decision needs to be made as to which technique can be used to derive state space models of thermohydraulic systems. Since state space models are mathematical models, only two directions can be followed: Mechanistic or empirical modelling. In the industry mechanistic models are preferred since they can be used for design and control purposes [12]. The drawback is that these models take time and effort to develop. Empirical models are less expensive to develop, but their parameters do not have any physical meaning, unless these were derived through expert knowledge of the plant. They are also only reliable for normal operating conditions and less reliable for abnormal conditions [30].

The challenge is to develop a modelling technique that reduces the amount of time and effort, but still deliver models that has physical meaning. Research in this area also needs to focus on computer-aided design of control systems that has a symbolic and numerical computation interface [32]. A research area, that is still relatively new, that can cope with the mentioned challenges is called Model Extraction (ME). The field of model extraction focuses on developing architectural models (graphical representations) of systems using a generic database of components through a computer interface, and on model extraction algorithms. The extraction algorithms automatically generate a dynamic model from the graphical presentation of a physical system in the desired form, e.g. in state space form. *Symbols 2000*® is a simulation and control analysis code, based on a bond graph approach, capable of extracting models of graphical representations as shown in Fig. 1.5. A considerable amount of work has been done on model extraction methods for thermohydraulic systems represented by bond graphs [6, 33]. However, the main thermohydraulic simulation codes such as *Relap*®, *MacroFlow*®, *Sinda/Fluint*® and *Flownex*® are based on the network approach. Not much attention has been given to developing state space model extraction methods for thermohydraulic simulation codes based on the network approach.

In the network approach, a thermohydraulic system is represented by a network of nodes and elements, as shown in Fig. 1.6. The elements are components such as pipes, valves, turbines and heat exchangers, while nodes are the end points of the elements. Nodes can also be used to represent reservoirs with specified volumes. The elements are connected according to the design of plant to form a network representation.

1.5 Problem statement

At present well developed thermohydraulic simulation packages are available for simulating transients of power plants. These codes provide accurate results, but it may be difficult to interpret their results and make simple predictions necessary for control and system engineering. It is also not always clear from these simulations what the important parameters are that drive a system's dynamics. A simplified linear or nonlinear state space model is needed that captures the interdependence of system components in order to make sound control and system design decisions [12]. Many hours are spent on writing equations from first principles

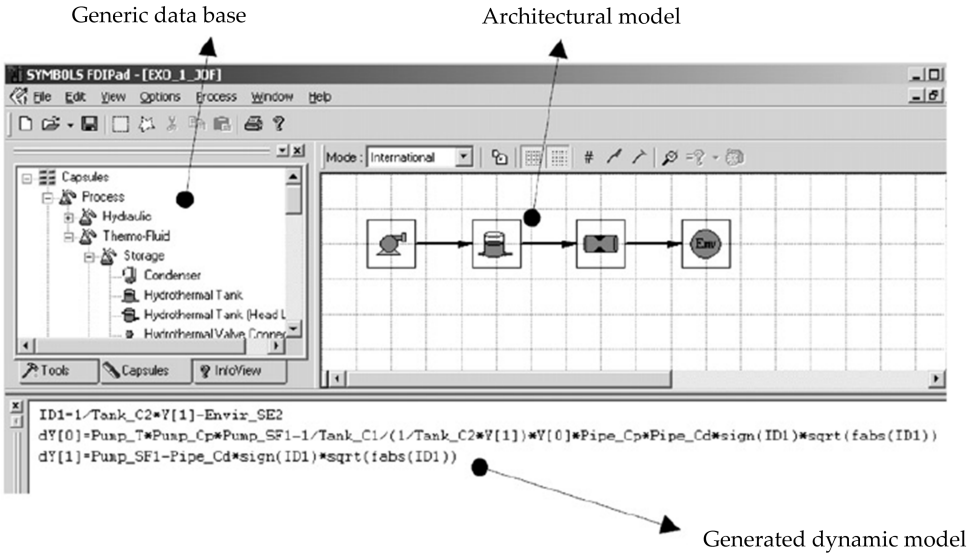

Figure 1.5: Automatic model generation using *Symbols 2000*® [6]

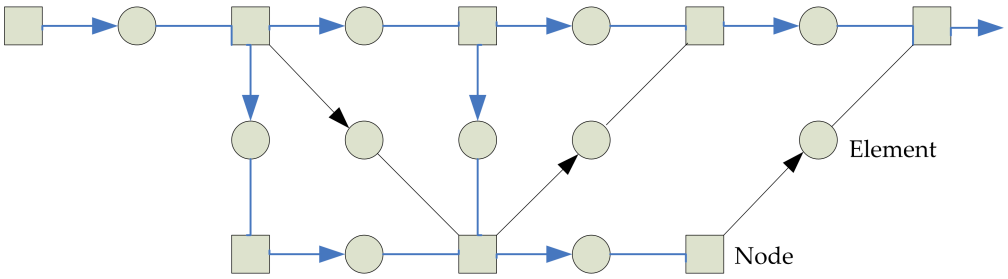

Figure 1.6: Thermohydraulic network [7]

in order to develop reduced order state space models that can be used for control and systems engineering. A need is therefore recognised among the engineering community for a model extraction tool that automates the model generation process in a structured and systematic way.

1.6 Objective of this study

The objective of this study is to develop a method for extracting state space models of thermohydraulic systems, intended for use in thermohydraulic software codes based on the network approach. The extracted state space models can then be used for control and system engineering purposes.

The aim is to take mechanical, flow and heat transfer mechanisms into account when developing the extraction algorithm. State space models will be derived ranging from elementary systems up to large and complex systems such as the PBMR Power Conversion Unit (PCU). The extraction algorithm will be developed in the *Matlab*® environment. The code

will however be developed in such a way that it can easily be embedded in a network based thermohydraulic code such as *Flownex*® to form a unified simulation and control analysis code as shown in Fig. 1.7.

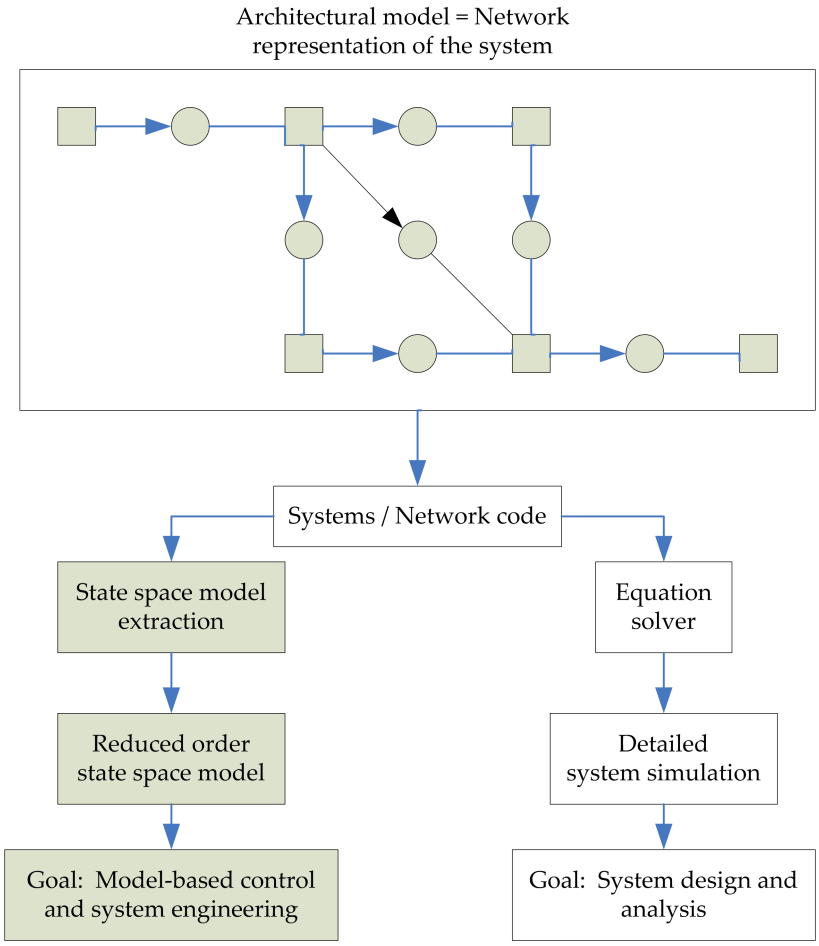

Figure 1.7: Simulation and control analysis code based on the network approach

The highlighted blocks indicate the focus of this study. The study does not focus on detailed system modelling and simulation. It also does not focus on a methodology for control system design. The study focuses on an automated state space model extraction methodology for control purposes. This methodology will help control engineers by reducing the time and effort spent on developing reduced order models. Such models are usually derived manually (hand calculation) and are then coded in an environment such as *Matlab*®. The methodology to be developed automates this process by means of an extraction algorithm.

1.7 Outline of the thesis

Chapter 2 presents a literature survey of previous work on state space modelling of thermohydraulic systems. The chapter also discusses dedicated codes available for control

system development. The necessity of state space models along with existing state space extraction methods are discussed. The strengths and limitations of the methods discussed are highlighted.

Chapter 3 provides background on state space model representations. The chapter introduces the concept of a system and its importance in state space modelling. State space models are placed into context by discussing the three system modelling domains: Time domain, frequency domain and operator domain. The basic structure and properties of state space representations are discussed followed by two electrical network examples. These examples illustrate how state space models are derived manually. These examples also illustrate similarities between electrical and thermohydraulic network representations.

In Chapter 4 the state space model extraction methodology is described. The methodology is based on a unified approach to system modelling which considers systems as energy manipulators. This concept of perceiving thermohydraulic systems as energy handling systems is abstracted in terms of generalised system variables and elements. A state space extraction algorithm is derived based on this energy handling concept following a network approach. The automatic state space extraction algorithm is evaluated on an electrical network considered in Chapter 3 to illustrate the power of the algorithm.

Chapter 5 describes the network approach for discretising a thermohydraulic system. From this follows the development of generalised elements that can be used to develop reduced order state space models suitable for control purposes. The generalised components are used to construct network representations of small scale thermohydraulic systems such as a U-tube and a heat exchanger up to larger and more complex systems such as a PBMR PCU. The state space extraction algorithm uses these network representations to extract state space models. The state space models are solved and the results are compared with results obtained from *Flownex*®. Chapter 4 and Chapter 5 represents the main contribution of this study, namely the development of a state space extraction methodology for thermohydraulic systems.

Chapter 6 describes the extraction of a reduced order linearised state space model of the PBMR power conversion unit. The state space model is then imbedded in a model-predictive control scheme to control the power output of the system. The controller showed superior performance compared to optimised PID and Fuzzy PID control schemes. Chapters 5 and 6 illustrate the value of the state space model extraction methodology.

In Chapter 7 conclusions are made regarding the study on state space model extraction methods. The uniqueness of the study is discussed since a whole new thermohydraulic state space model extraction methodology based on a network approach is developed. Previous work in this research area focused only on bond graph approaches. The limitations of the current approach are highlighted and recommendations for future work on state space model extraction of thermohydraulic systems are made.

CHAPTER 2

LITERATURE SURVEY

2.1 Introduction

This chapter will focus on previous work on state space modelling of thermohydraulic systems. Its place in control system design, as well as the context and necessity of state space modelling will be discussed. The approaches followed by previous researchers to derive state space models will also be considered. The limitations of current approaches are pointed out at the end of this chapter.

2.2 State space models of thermohydraulic systems

2.2.1 The scope of modelling methods and structures for control

In the last decade there has been a considerable amount of change in the electric power generation industry. Larger and faster operating plants have been constructed to operate in a much more dynamic environment. At the same time information technology has also improved significantly. New power plants have modern digital control systems and advanced man-machine interface tools. This sets the scene for control engineers to develop advanced control algorithms. Advanced control is not the digital implementation of traditional controllers such as PIDs, but incorporates system knowledge in terms of system models to gain greater performance in terms of set-point tracking and robustness. Modelling techniques and structures for control of thermohydraulic systems such as power plants have also changed over the years and will be discussed shortly.

Traditionally models for power plant engineering studies were either derived experimentally, using step and frequency response techniques, or from first principles using mass, energy and momentum balances and phenomenological correlations [34, 35, 36, 37]. Today, the derived

models look much the same, but the techniques used for deriving them are much more sophisticated due to the advances in computer technology.

Two kinds of modelling methods exist that are based on first principles namely, *interpretation* models and *knowledge* models [38]. These methods differ only in how coarse or fine the lumping of the distributed effects are done. The models derived by these methods serve different purposes. Interpretation (lumped parameter) models are derived using a coarse lumping approach. Such models are extremely important for control system design. One of the first power plant models based on this approach was the one developed by Chien *et al.* [39]. The model described the dynamics of a naval boiler. The equations describing the boiler-turbine system was linearised and used for developing transfer functions for control system development. This work lead to the development of many similar models of power plants. Knowledge models (distributed parameter) have fine lumping of the balance equations and require sophisticated solution techniques. These models give accurate prediction of plant behaviour and are used for power plant design.

A third modelling method is called *System Identification* (SI). This technique uses input-output data to derive models of systems such as power plants. This technique became very popular in the 1970s when it was in its developing stages. The resulting models do not have a physical basis (black-box) and can therefore not be used for design purposes. Black-box models can be used very successfully for control system design.

Moving on to control structures, transfer functions and state space representations are the two main modelling structures used for control system design [38]. The transfer function equations for a Multi-Input Multi-Output (MIMO) continuous time system are

$$\mathbf{Y}(s) = \mathbf{G}(s)\mathbf{U}(s), \tag{2.1}$$

where $\mathbf{Y}(s)$ is a $m \times 1$ output vector, $\mathbf{U}(s)$ is a $r \times 1$ input vector and $\mathbf{G}(s)$ is the $m \times r$ transfer function matrix. In the Single-Input Single Output (SISO) case, $m = r = 1$.

The state space equations may be written as

$$\begin{aligned} \dot{\mathbf{X}}(t) &= \mathbf{A}\mathbf{X}(t) + \mathbf{B}\mathbf{U}(t) \\ \mathbf{Y}(t) &= \mathbf{C}\mathbf{X}(t) + \mathbf{D}\mathbf{U}(t), \end{aligned} \tag{2.2}$$

where $\mathbf{Y}(t)$ and $\mathbf{U}(t)$ are the output and input vectors, $\mathbf{X}(t)$ is the $n \times 1$ state vector. **A** is the state matrix, **B** the input matrix, **C** the output matrix and **D** the feed-forward matrix. Eq. (2.2) is the linear and time-invariant form. The state space representation may take nonlinear and time-variant forms.

System identification models are written in terms of difference equations. These models always contain a random disturbance term. Considering a SISO system the difference equation has the following form

$$y(t) + a_1 y(t-1) + \ldots + a_n y(t-n) = b_1 u(t-1) + \ldots + b_m u(t-m) + v(t), \tag{2.3}$$

where $y(t)$ and $u(t)$ are the discrete input and output sequences, and $v(t)$ is a disturbance. Eq. (2.3) may be written as

$$y(t) = \boldsymbol{\theta}'\boldsymbol{\phi}(t) + v(t), \tag{2.4}$$

where

$$\boldsymbol{\theta}' = [a_1 \dots a_n \; b_1 \dots b_m] \tag{2.5}$$

$$\boldsymbol{\phi}' = [-y(t-1) \dots -y(t-n) \; u(t-1) \dots u(t-m)] \tag{2.6}$$

In Eq. (2.5), $\boldsymbol{\theta}$ is the parameter vector and in Eq. (2.6), $\boldsymbol{\phi}$ is the lagged input-output vector (The accent represents the transpose of a vector). Eq. (2.4) is known as an AutoregRessive Moving Average with eXogenous input (ARMAX) model and can be transformed into the following state space format

$$\begin{aligned} \mathbf{X}(t+1) &= \mathbf{A}\mathbf{X}(t) + \mathbf{B}\mathbf{U}(t) + \hat{\mathbf{W}}(t) \\ \mathbf{Y}(t) &= \mathbf{C}\mathbf{X}(t) + \hat{\mathbf{E}}(t) \end{aligned} \tag{2.7}$$

where $\hat{\mathbf{W}}(t)$ and $\hat{\mathbf{E}}(t)$ are sequences of independent random vectors. MIMO formats of system identification models also exist.

Traditional or classical control design relies on the transfer function representation. Methods such as Ziegler-Nichols, root-locus and lag-lead designs can be used to tune these classical controllers. SISO systems are modelled quite comfortably with transfer function representations. However in the MIMO case, using transfer function matrices is not a straight forward case. Specialised decoupling techniques must be used in order to complete the design. Frequency response techniques and decoupling controllers are often supplemented by feedforward control. Modern control techniques on the other hand rely on state space representations. This representation is ideal for SISO and MIMO systems and can be used for the design of sophisticated control algorithms. In the next section some recent applications of state space models in control system design of thermohydraulic systems will be considered.

2.2.2 Previous state space model applications

Recent advances in computer technology allow the modelling and simulation of complex dynamic systems such as fossil and nuclear power plants. These simulations are carried out with sufficient accuracy by well developed modelling and simulation codes for performance analysis, optimisation studies, accident scenarios and control system evaluation. Many of these codes follow a Computational Fluid Dynamic (CFD) approach for detailed analysis of physical phenomena. The models derived by these codes are too complex for control system design. For control system design a dynamic model of the plant needs to be represented as an initial value problem having a state space form.

Weng *et al.* [40] developed a nonlinear state space model based on fundamental laws of physics and lumped-parameter approximation for a fossil fuelled generating unit with a load capacity of 525 MW. The goal of the model was to evaluate the overall plant performance and component interactions rather than to investigate microscopic details occurring inside the plant components. The model was used to derive a robust controller that can control the power output over a wide range of operating points. The results of the simulations demonstrated that the robust controller derived from the state space model satisfied the performance requirements of power variation in the range of 40 - 100 %.

Weng *et al.* stated advantages of physics-based state space models relative to empirical (black-box) state space models. Dynamic variables such as temperature, pressure and mass flow in a physics-based state space model can be related to the actual system variables. In empirical state space models the variables have no physical meaning since the data is fitted using system identification methods. Nonlinear state space models can predict the plant dynamics under different operating conditions. State space models derived by identification techniques may not predict the system behaviour correctly outside the range of the data set. Finally Weng *et al.* stated that the state space modelling approach proved to be very effective in control system design of power generation processes such as the Cromby Unit I and II of the Philadelphia Electric Company and New Boston Units I and II of the Boston Edison Company.

Åström and Bell [41] developed a physics-based fourth order nonlinear state space model of a natural circulation drum-boiler from first principles. The model describes the dynamics of the drum, downcomer and riser components. The goal of the state space model is to capture key dynamics of the steam generation system which is a crucial part of most power plants. According to Åström and Bell there is an increasing demand for power plants that can change their power output rapidly. This lead to a challenging task for control engineers to develop controllers that can cope with large changes in operating conditions. A possible way to solve the problem is to incorporate system knowledge in controllers. This led to significant development of methods for model-based control. For a detailed description of current developments in model-based control see Qin and Badgwell [42].

Fazekas *et al.* [43] developed a nonlinear state space model of the primary circuit in a VVER-type nuclear power plant from first principles. The main goal of the state space model was for the development of a pressure control loop in the primary circuits of units 1, 3 and 4 of the Parks Nuclear plant. A model-based approach was followed which contributed to a more efficient system. According to Fazekas *et al.* good dynamic models of pressurised water reactors are available. The systems were simulated using *APROS*® software coupled with neutronic kinetic/thermal codes. However these models contained too many state variables. The model structure did not allow model-based control system design, meaning it is not in state space form. The problem can be solved in two different ways: The complex model can be simplified using model-reduction techniques or by constructing composite models from minimal elements. Fazekas *et al.* followed the second approach since the model is more transparent and easy to understand.

Pritchard and Rubin [12, 15] developed a linear state space model of the PBMR power conversion unit from first principles. The goal of the model was to gain insight on the dominant dynamic behaviour of the power system. Linear models of the turbines and compressors were first developed followed by models for the shafts and the volumes inside the circuit. The system equations were then derived from these component models and put into state space form. The model can be used for systems engineering and control applications.

Li *et al.* [44] derived a state space model of the HTR-10 high temperature gas-cooled reactor based upon the conservation of fluid mass, momentum and energy. The model describes the reactor neutron kinetics with reactivity feedback and reactor thermohydraulics. The reactor was nodalised to employ a lumped parameter modelling approach. The transient results showed that the model was capable of predicting key dynamics of the reactor that can serve as

a basis for model-based control algorithms. Qaiser *et al.* used a fifth order state space model of a 10 MW swimming pool type research reactor, PARR-1, for the development of a sliding-mode controller. The controller controls the output power by manipulating the control rod position. The sliding-mode controller showed improved performance as compared to a classical PID controller.

Kazeminejad [45] derived a state space model which incorporates point neutron kinetics, one-dimensional flow, single-phase thermohydraulics and heat conduction based on a lumped parameter approach. The goal of the model is to study the safety aspects of a 10 MW IAEA research reactor during a Loss of Flow Accident (LOFA). Kazeminejad states that over the past 30 years there has been great effort on the part of the power utilities to develop simpler models and modelling tools for thermohydraulic simulation of reactor dynamics. The use of reduced models for the study of dynamic behaviour of nuclear reactors is widespread since they allow faster calculation speeds and qualitative understanding of the physical phenomena involved. He highlights however that these models are ideal for operational transients, but complex transients and safety-critical transients still need to be simulated by detailed models that capture more accurately the phenomena involved. A similar approach was also used by Ying *et al.* [46] to analyse natural circulation flow in solid breeder designs with poloidal coolant channels under a LOFA condition. A state space model was derived which couples the flow transient behaviours with transient heat transport. The model provided approximate estimates, yet accurate enough to understand the various phenomena involved.

State space models can also be derived for specific thermohydraulic system components. Bonivento *et al.* [47] developed a state space model of a heat exchanger. Modelling a heat exchanger is a difficult task since it has complex dynamics characterised by distributed parameters and non-linearity. The state space model was derived by using a lumping approach. The thermal exchange surface was divided in sections (lumps) so that the state vector is defined by the temperature of the sections. A PID and Model-Predictive Controller (MPC) were designed using the derived state space model. The simulation results showed better performance concerning set-point tracking and disturbance robustness for the predictive controller. Varga *et al.* [48] also used state space models for analysing the controllability and observability of heat exchanger networks in the time-varying parameter case. This kind of analysis assists in evaluating the control properties of a heat exchanger network, even in the early stages of design. It is recommended that such a tool be combined with a design tool to integrate process design with process control design.

2.2.3 The necessity of state space models

With today's increasing demands with respect to performance, operating costs and environmental issues there is an increasing need for the development of advanced control systems for power plants. Two factors support the development of advanced control systems namely the rapid increase in computing power and the development of modern control theory (multi-variable techniques based on predictive control theory). However it seems difficult to introduce new technologies and new control concepts in thermal power plants today mainly because of the diffidence towards systems that will revolutionise well-assessed technologies

(classical multi-SISO configuration) and design procedures [38].

Modern thermal power plants must be able to adjust the power load in response to instantaneous requests of the grid with highest possible thermodynamic efficiency. Classical control systems do not compensate for plant interaction when sudden and significant changes of the power demand are observed. Significant oscillations of thermal variables occur which cause stresses on the system components. Current research focuses on multi-variable techniques based on predictive control theory. A valuable feature of these techniques is the fact that they can incorporate system constraints and measurable disturbances in their algorithms. These techniques also incorporate system knowledge by means of state space models. Implementations of these techniques showed significant improvements of plant performance in extreme situations, where sudden changes of the power load occurred [8, 49, 50, 51].

Since the replacement of the classical multi-SISO configuration by modern MIMO controllers have not found application in the industrial realm, the attention in research was devoted to structures where the classical regulation is kept, and a multi-variable solution corrects it. This approach greatly improves the trajectories of thermodynamic variables. Two architectures namely Controlled Reference Value (CRV) and Control Action Correction (CAC) exist as shown in Figs. 2.1 and 2.2. The vectors $\mathbf{Y}$ and $\mathbf{Y}_{ref}$ represent the controlled output and reference variables respectively. The vector, $\mathbf{U}$ represents the controlled variables, and $\mathbf{U}_m$ represents the control variables of the advanced controller. Finally $\mathbf{d}$ represents the disturbance variables.

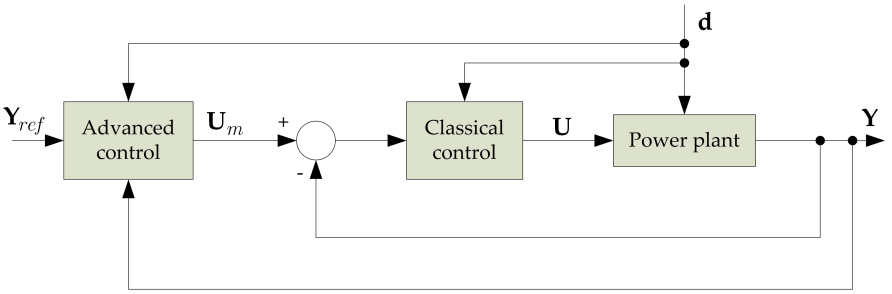

Figure 2.1: Controlled Reference Value (CRV) approach [8]

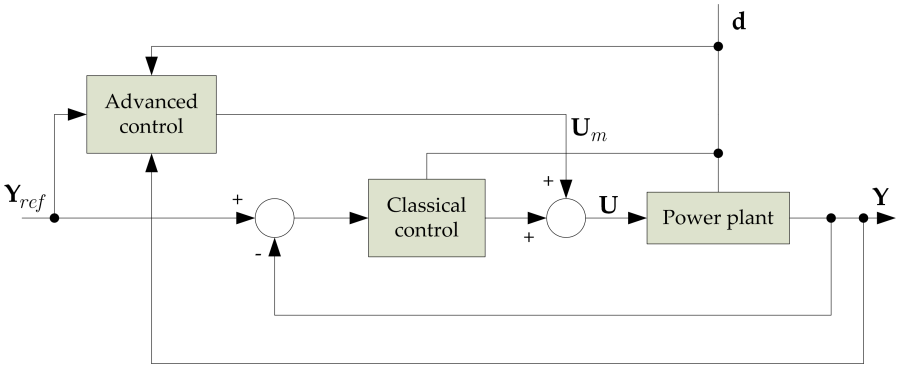

Figure 2.2: Control Action Control (CAC) approach [8]

Modern control architectures such as these has the ability to include constraints on thermohydraulic variables to keep them in admissible ranges which guarantees safe operation. They can deal with disturbances such as power needs of the grid and they can improve the system performance and efficiency. However to gain these advantages these advanced control systems are dependent on well developed state space models that are incorporated in their control algorithms.

2.3 Dedicated codes for control system development

In the following sections dedicated codes used for control purposes are discussed in terms of their approaches and capabilities.

2.3.1 Object-oriented approach

Modelica®

Modelica® is a modelling language developed in an international effort. The two main objectives of the language is to facilitate model exchange and model libraries, and to use a object-oriented approach to allow the reuse of modelling knowledge. *Modelica®* has a number of libraries. The thermohydraulic library has a flexible model for fluid control volumes, which are the basic building blocks of the library [52]. It incorporates a state space formulation for the transport of mass, momentum and energy and a correlation database (e.g. heat transfer coefficients). The library is excellent for application specific models. The library is currently being expanded to realise models of heat exchangers, pumps, turbines and valves.

Dymola®

Dymola® is a multi-domain, object-oriented modelling and simulation environment that uses the *Modelica®* language. It has component libraries ranging from electrical components up hydraulic and thermodynamic components. Models can be constructed by dragging components from the library and connecting them in a graphical editor. *Dymola®* has a unique solver for Differential Algebraic Equations (DAEs) which give high performance and robustness to symbolic manipulation. *Dymola®* is also open in the sense that users can define their own components for their unique needs.

2.3.2 Bond graph approach

20-Sim®

20-Sim® follows a bond graph approach and allows the user to simulate dynamic systems in the hydraulic, mechanical and electric domains or in combinations of these domains. It supports graphical modelling, allowing users to build models in a user friendly way such as entering a model by means of an engineering sketch. It allows the generation of C-code or *Matlab®* code for further analysis and control applications. *20-Sim®* supports model parameter optimisation, linearisation and 3D animation.

SimECS®

SimECS® is a software package that focuses on the dynamic modelling of energy conversion systems [53, 54]. It is currently developed at the Delft University of Technology. A causal, modular and lumped parameter approach is followed where system models are generated by connecting components. Applications of *SimECS®* for control and system design include simulations of biomass fired steam power plants, rankine cycle power plants and refrigeration plants. Future applications may include the combination of control and electro-mechanic libraries to obtain complete simulators of power generation plants.

Symbols 2000®

Symbols 2000® is a hierarchical hybrid modelling, simulation and control analysis software package [6, 33]. It follows a bond graph approach which is a multidisciplinary and unified graphical modelling language. It has a generic component database consisting of predefined process, control and sensor classes. The thermohydraulic process class can be used for developing models of most thermohydraulic processes. *Symbols 2000®* has the ability to extract symbolic state space models of an architectural model created by the user by means of a graphical user interface. The powerful symbolic solution engine can solve differential causalities and algebraic loops.

2.3.3 Block diagram approach

Simulink®

Simulink® forms part of the *Matlab®* environment and follows an interactive block diagram approach to dynamic system modelling. Linear and nonlinear models of systems are supported. The user is allowed to define the mathematical properties of each block. It has a library of components that can be connected to form system models. Code from other simulation software can be incorporated in *Simulink®*. It also has a powerful solver that supports differential algebraic equations with algebraic loops.

ACSL® (Advanced Continuous Simulation Language)

ACSL® can model systems that range from oil and natural gas processing up to nuclear power plants. Models can be ported to other applications such as operator trainers and control systems. The software focuses on modelling and simulation of dynamic systems by allowing the user to build object-oriented graphical block diagrams. *ACSL*® constitutes a mathematical analysis package for visual presentation of the data and an optimiser for optimisation of critical parameters in simulations.

2.3.4 Analytical approach

Matlab®

Matlab® is a technical computing environment which merges computation, visualisation and programming to express problems and solutions in mathematical notation [55]. *Matlab*® specialises in solving problems formulated in terms of matrices and vectors. A strong feature is the number of ad-on toolboxes which focus on application-specific solutions. The number of control system toolboxes provide a comprehensive set of tools for classical and modern control system design.

2.4 State space model extraction methods

Another approach for modelling dynamic systems in a fundamental principle paradigm is Model Extraction (ME). This approach focuses on generating dynamic models automatically from graphical representations of physical systems [10]. These models can be linear or nonlinear and are presented in state space form. Two kinds of state space model extraction methods currently exist namely, the *bond graph approach* and the *network approach*. These two approaches along with the block diagram approaches fall in the graph-based modelling paradigm. Graph-based refers to the fact that these approaches use graphical presentations of system components and their interconnections to derive mathematical models.

Bond graphs were first developed by Paynter and further refined by Karnopp, Rosenberg and Thoma [56, 57]. A systematic state space model extraction method for bond graph representations of dynamic systems were derived by Rosenberg, Granda and Minten [58, 59, 60]. Their work focused mainly on mechanical and electrical systems. Pseudo bond graphs developed by Karnopp [56] enabled bond graph modelling of thermohydraulic systems.

The network approach originated from the field of electronic circuit analysis. State space models can also be extracted automatically from network representations. This method of model generation extended to other domains such as mechanical and fluid systems. Filho and Conçalves [61] derived a systematic procedure for obtaining a state space model from a network representation of a lumped parameter system. Their application examples included mechanical and fluid systems. They also implemented their procedure in a modelling

software package called *MASD*®. *MASD*® constitutes *Pascal*® routines which implement a user interface and the system network characterisation. Code written in *Mathematica*® allow symbolic manipulations to obtain symbolic state space equations.

Altun *et al.* [62, 63] also derived a systematic procedure for finding the energy based state variable representations of electrical networks using a network approach. They have developed a software package with a graphical user interface where the user can set up a network representation of a system. A state space model can then be generated automatically from the representation. Their extraction algorithm can also reduce the order of the model by eliminating dependent energy storage elements.

2.5 Limitations of current approaches

According to the literature, modern control system design methods require system knowledge in the form of a low order state space models. Researchers in this area prefer to derive these state space models from first principles, due to their clarity. A drawback of developing models following this approach is the significant cost in terms of time and money. A need therefore exists to develop modelling tools that can derive state space models in a systematic and automated way, based on first principles.

Detailed simulation codes, based on first principles, are available for modelling thermohydraulic systems. One approach would be to reduce detailed models to lower order state space models using model reduction techniques. However, the models derived in this way lose their transparency and therefore their physical meaning. Another first principle approach would be to use state space model extraction methods. Two state space extraction approaches exist namely the bond graph approach and the network approach. Bond graph extraction methods and codes are available for extracting state space models of thermohydraulic systems. State space extraction based on the network approach were used for single domain applications, but not much attention has been given to thermohydraulic (multi-domain) systems. Therefore, there is an opportunity to investigate the possibility of using a network approach for extracting state space models of thermohydraulic systems.

2.6 Conclusion

In this chapter the need for state space models of thermohydraulic systems was discussed by considering previous applications and control software tools. A significant need for a modelling tool that can extract state space models of thermohydraulic systems was identified. It was also found that not much work has been done on state space extraction methods for thermohydraulic systems, based on a network approach. As an introduction to such a study, the next chapter will focus on state space models.

CHAPTER 3

STATE SPACE MODELS

3.1 Introduction

In this chapter an in-depth overview will be given on state space model representations. The concept of a system will first be explained since it is central to the development of state space models. System models are then discussed in terms of the three system modelling domains to point out the relevance of state space representation. Finally the basic structure and properties of state space representations are discussed followed by two electrical network examples. These examples illustrate how state space models are derived manually. The similarities between electrical and thermohydraulic network representations are also illustrated.

3.2 The notion of a system

The word 'system' is very often used loosely to describe a variety of concepts. It is therefore necessary to give a formal definition of the word as it will be used in this study. A system is an entity separable from the rest of the universe (the environment of the system) by means of a physical or conceptual boundary [56]. A system interacts only through this boundary with its environment. A system can be broken up into subsystems, and subsystems can be broken up into components. Components can finally be broken up into primitive elements. For example, the PBMR power conversion unit can be seen as a system. This system consists of components such as heat exchangers, turbines, compressors, pipes, valves and the reactor. These components consist of elements or mechanisms that describe the physical phenomena inside these components.

Any influences of the environment affecting the system are represented by an input vector $\mathbf{U}(t)$ consisting of input variables $u_1(t), \ldots, u_k(t)$. The affects of the system on the environment are represented by an output vector $\mathbf{Y}(t)$ consisting of output variables $y_1(t), \ldots, y_l(t)$. A system

can mathematically be described as an operator Ψ which maps inputs $\mathbf{U}(t)$ to outputs $\mathbf{Y}(t)$ as shown conceptually in Fig. 3.1. The operator of a system is mathematically given by

$$\mathbf{Y}(t) = \Psi(\mathbf{U}(t)). \tag{3.1}$$

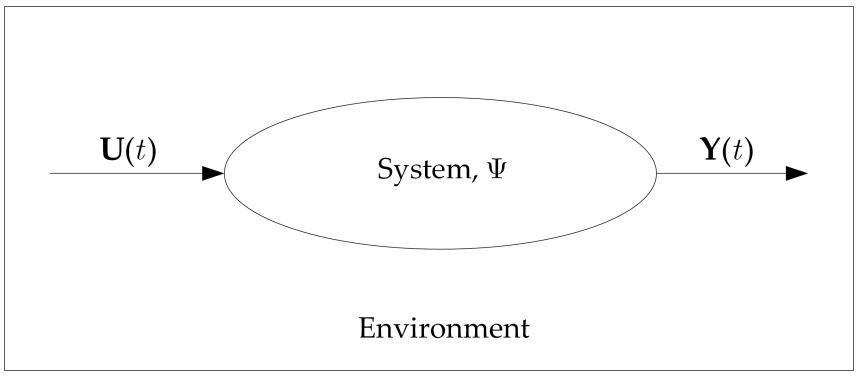

Figure 3.1: System mapping input functions to output functions [3]

The system Ψ can be described in terms of three domains as shown in Fig. 3.2. The frequency and operator domains are only used for describing linear systems. These descriptions are obtained by applying Laplace and Fourier transforms respectively. Thermohydraulic system models are preferably set up in the time domain. In the time domain models can be represented either in input-output model form or in state space model form. A detailed description of input-output models can be found in Hangos [3]. In the next section state space models will be described in more detail.

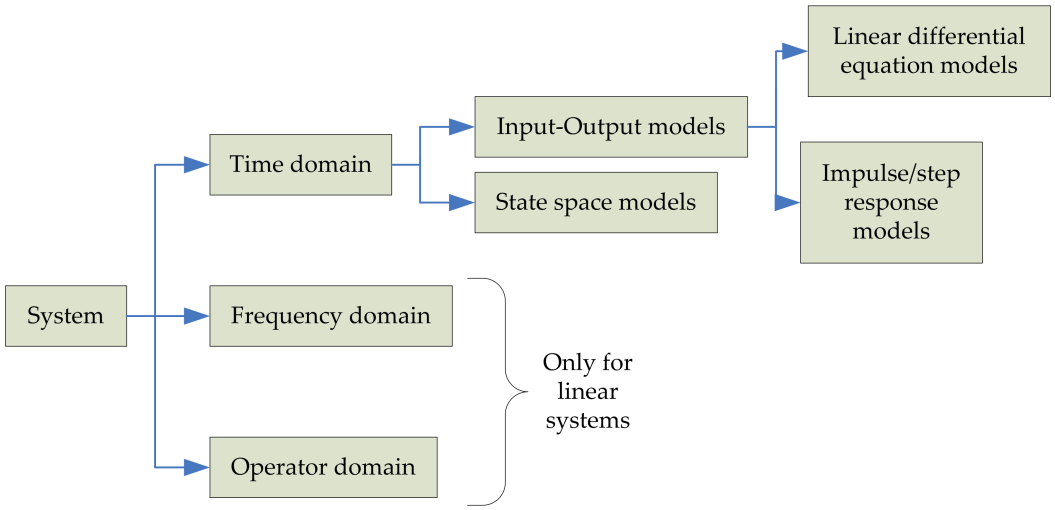

Figure 3.2: System descriptions

3.3 State space representation

In the previous section a system was considered as an operator mapping from an input vector space to an output vector space. If this concept is used, the entire input and output history of the system together with the planned inputs are needed to compute future output values, $\mathbf{Y}(t)$.

Alternatively one can use a concept called the *state* of the system. The state of the system at t_0 (a given time instant) contains all the past information on the system up to time t_0, including the initial conditions for the outputs and its derivatives as well as the past input history. To compute the outputs, $\mathbf{Y}(t)$, for $t \geq t_0$ (all future values) one need only $\mathbf{U}(t)$, $t \geq t_0$ and the state $\mathbf{X}(t)$ at $t = t_0$. The state variables, $[x_1(t), x_2(t), \ldots, x_n(t)]' = \mathbf{X}(t)$, therefore describe the future response of a system. A simple example of a state variable is the state of a light switch. The switch can either be in a on or off state. Thus, if we know the present state (position) of the switch at t_0 and if an input is applied, it is possible to determine the future value of the state of the system.

A conceptual diagram of the state space representation is given in Fig. 3.3.

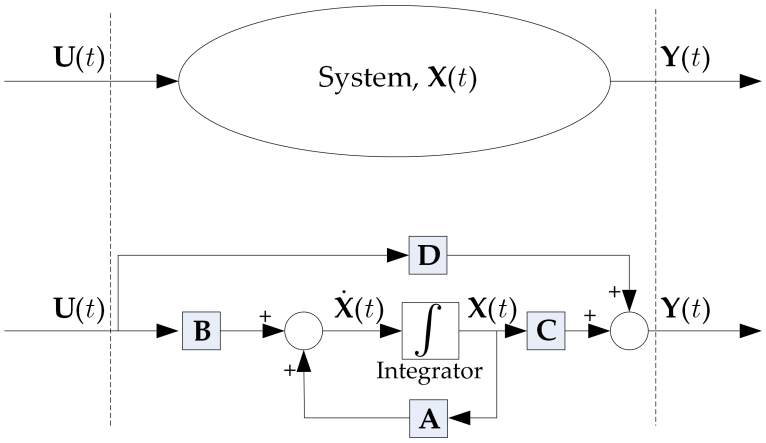

Figure 3.3: Conceptual diagram of the state space representation

The State Space Representation (SSR) consists of two sets of equations. The first equation set comprises state equations which describe the evolution of the states as a function of the state and input variables. These equations are **ordinary differential equations**. The second set comprises output equations which relate the output variables to the state and input variables. These equations are **algebraic equations**. The variables are expressed as vectors and the differential equations are cast into matrix form. In general the state space representation of a system with k inputs and l outputs and n state variables is written in the following form:

$$\begin{aligned} \dot{\mathbf{X}}(t) &= \mathbf{A}\mathbf{X}(t) + \mathbf{B}\mathbf{U}(t) \text{ (State equations)} \\ \mathbf{Y}(t) &= \mathbf{C}\mathbf{X}(t) + \mathbf{D}\mathbf{U}(t) \text{ (Output equations)}, \end{aligned} \tag{3.2}$$

where

$$\begin{aligned}&\mathbf{X}(t) \in \mathbb{R}^n,\ \mathbf{Y}(t) \in \mathbb{R}^l,\ \mathbf{U}(t) \in \mathbb{R}^k\\ &\dim[\mathbf{A}] = n \times n\\ &\dim[\mathbf{B}] = n \times k\\ &\dim[\mathbf{C}] = l \times n\\ &\dim[\mathbf{D}] = l \times k\end{aligned}$$

$\mathbf{X}(t)$ is called the state vector, $\mathbf{Y}(t)$ is called the output vector and $\mathbf{U}(t)$ the input vector or control vector. **A** is the state matrix, **B** the input matrix, **C** the output matrix and **D** the feed-forward matrix.

The state space representation can be adapted according to the properties of the system. It can represent time-invariant or time-varying systems. A system is time-invariant if its response to a given input is invariant under time shifting. As shown in Fig. 3.4 this means that the system does not change its properties over time.

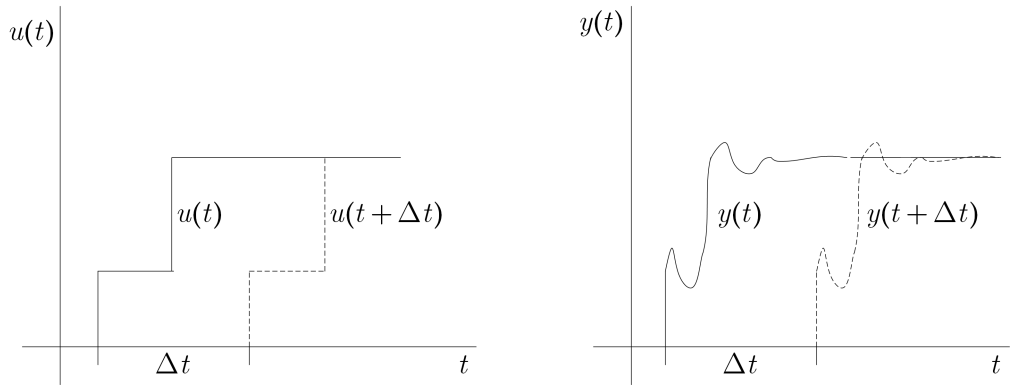

Figure 3.4: Illustration of time invariance [9]

Eq. (3.2) represents a linear time-invariant system. For a time-varying system the state space representation is written as follows:

$$\begin{aligned}\dot{\mathbf{X}}(t) &= \mathbf{A}(t)\mathbf{X}(t) + \mathbf{B}(t)\mathbf{U}(t)\\ \mathbf{Y}(t) &= \mathbf{C}(t)\mathbf{X}(t) + \mathbf{D}(t)\mathbf{U}(t).\end{aligned} \tag{3.3}$$

Finally a system can be linear or nonlinear. A system is called linear if it responds to a linear combination of its possible inputs with the same linear combination of the corresponding outputs. For a linear system it can be written that:

$$\Psi[a_1u_1 + a_2u_2] = a_1\Psi[u_1] + a_2\Psi[u_2] \tag{3.4}$$

where

$$a_1, a_2 \in \mathbb{R} \text{ and } \Psi[u_1] = y_1,\ \Psi[u_2] = y_2.$$

Eqs. (3.2) and (3.3) can be used to represent linear systems. For nonlinear systems the state space representation has the following form:

$$\begin{aligned}\dot{\mathbf{X}}(t) &= \boldsymbol{f}(\mathbf{X}(t), \mathbf{U}(t))\\ \mathbf{Y}(t) &= \boldsymbol{g}(\mathbf{X}(t), \mathbf{U}(t)),\end{aligned} \tag{3.5}$$

where the nonlinear vector functions $\boldsymbol{f}$ and $\boldsymbol{g}$ characterise the nonlinear system. Their parameters constitute the system parameters.

3.4 State space modelling of networks

A thermal network is defined by a set of nodes and conductances, and is analogues to an electrical network [64]. The network is derived from energy balance equations and is equivalent to a particular finite difference discretisation of the underlying heat-transfer equation [65]. This network method has evolved into a more advanced variant called the thermohydraulic network approach [11]. Due to this connection between thermohydraulic networks and electrical networks, the state space modelling process will be discussed by means of two electrical networks. The reason for this is to first give the reader an overview of how state space models are derived manually (writing the equations from first principles). The following chapters will build on the background given in this section.

Equations describing an electrical circuit can be classified as **elemental equations** and **structural equations**. The elemental equations are the equations representing the dynamic behaviour of individual elements of the system. These equations are first order differential equations of energy storage elements (inductors and capacitors) and algebraic equations for dissipative elements (resistors). Structural equations are algebraic equations and represent the interconnection of individual elements in the system. These two types of equations can be used to derive state space representations of electrical networks.

Starting with the elemental equations, the elemental equation for a capacitor is

$$i = C\frac{dv}{dt}, \tag{3.6}$$

for and inductor

$$v = L\frac{di}{dt}, \tag{3.7}$$

and for a resistor

$$v = iR, \tag{3.8}$$

where i is the current, v the voltage, C the capacitance, L the inductance and R the resistance.

The structural equations are given in terms of Kirchhoff's current and voltage laws. Kirchhoff's current law states that the algebraic sum of all the currents at any node in a circuit equals zero. Kirchhoff's voltage law states that the algebraic sum of all the voltages around any closed path in a circuit equals zero. The current and voltage laws can be stated analytically:

$$\sum_{j=1}^{m} i_j = 0 \tag{3.9}$$

$$\sum_{j=1}^{m} v_j = 0 \tag{3.10}$$

Kirchhoff's current and voltage laws are also called **continuity** and **compatibility** equations. The state space description forms a so-called internal model of the system, in that the system response is specified via the system variables which indicate the energies stored within the system stores [10]. In an electrical circuit the capacitors and inductors represent the energy stores of the system. The system variable that indicates the energy stored in a capacitor is voltage v_C and the system variable that indicates the energy stored in an inductor is current i_L [66]. Due to the fact that these variables specify the system response, they are chosen as the state variables. Considering Fig. 3.5 it can be seen that the system has two storage elements.

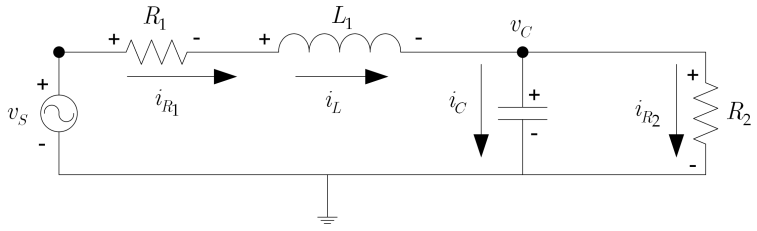

Figure 3.5: Electrical network: Example 1

The state space modelling process starts by first writing down the structural equations. According to Kirchhoff's current law

$$i_L - i_C - i_{R_2} = 0, \tag{3.11}$$

and according to Kirchhoff's voltage law

$$-v_S + v_{R_1} + v_L + v_C = 0. \tag{3.12}$$

Next the storage elemental equations can be written as follows:

$$i_C = C\frac{dv_C}{dt} \tag{3.13}$$

$$v_L = L\frac{di_L}{dt} \tag{3.14}$$

and for the dissipative elements

$$v_{R_1} = R_1 \cdot i_{R_1} \tag{3.15}$$

$$v_{R_2} = R_2 \cdot i_{R_2}. \tag{3.16}$$

Eqs. (3.11) - (3.16) can now be combined into a state space representation of the following form

$$\begin{aligned} \dot{\mathbf{X}}(t) &= \mathbf{A}\mathbf{X}(t) + \mathbf{B}\mathbf{U}(t) \\ \mathbf{Y}(t) &= \mathbf{C}\mathbf{X}(t) + \mathbf{D}\mathbf{U}(t), \end{aligned} \tag{3.17}$$

where the state vector and input scalar are given by

$$\mathbf{X}(t) = \begin{bmatrix} v_C \\ i_L \end{bmatrix}, \; u(t) = v_S. \tag{3.18}$$

Substituting Eqs. (3.13) and (3.16) into Eq. (3.11) gives

$$i_L - C\frac{dv_C}{dt} - \frac{v_{R_2}}{R_2} = 0. \tag{3.19}$$

Rewriting Eq. (3.19) and substituting v_{R_2} with v_c results in

$$\frac{dv_C}{dt} = -\frac{1}{R_2 C}v_C + \frac{1}{C}i_L. \tag{3.20}$$

Eq. (3.20) is now written in terms of state variables only. Substituting Eqs. (3.14) and (3.15) into Eq.(3.12) gives

$$-v_S + R_1 \cdot i_{R_1} + L\frac{di_L}{dt} + v_C = 0. \tag{3.21}$$

Rewriting Eq.(3.21) and substituting i_{R_1} with i_L results in

$$\frac{di_L}{dt} = -\frac{1}{L}v_C - \frac{R_1}{L}i_L + \frac{1}{L}v_S. \tag{3.22}$$

Eqs. (3.20) and (3.22) can now be cast into matrix form

$$\begin{bmatrix} dv_C/dt \\ di_L/dt \end{bmatrix} = \begin{bmatrix} -1/R_2C & 1/C \\ -1/L & -R_1/L \end{bmatrix} \begin{bmatrix} v_C \\ i_L \end{bmatrix} + \begin{bmatrix} 0 \\ \frac{1}{L} \end{bmatrix} v_S \tag{3.23}$$

where

$$\mathbf{A} = \begin{bmatrix} -1/R_2C & 1/C \\ -1/L & -R_1/L \end{bmatrix}, \ \mathbf{B} = \begin{bmatrix} 0 \\ 1/L \end{bmatrix}.$$

If v_C is chosen as the output variable, then the output equations can be written as follows

$$y = \begin{bmatrix} 1 & 0 \end{bmatrix} \begin{bmatrix} v_C \\ i_L \end{bmatrix} + \begin{bmatrix} 0 \end{bmatrix} v_S \tag{3.24}$$

where

$$\mathbf{C} = \begin{bmatrix} 1 & 0 \end{bmatrix}, \ \mathbf{D} = \begin{bmatrix} 0 \end{bmatrix}.$$

Eqs. (3.23) and (3.24) therefore form the state space representation of the electrical network in Fig. 3.5.

As stated previously, there is a relation between electrical and thermohydraulic networks. The following electrical network closely resembles a typical pipe network. The voltage sources can be interpreted as pressure sources, the capacitances as volumes and the resistances as flow resistances. Consider the electrical network in Fig. 3.6. The circuit contains two storage elements (C_1 and C_2), resistances ($R_1, \ldots, R_7$) and two voltage sources (v_{s_1} and v_{s_2}). The direction of the current flow through the circuit is indicated by the arrows.

The state and input vectors of the state space representation of this network are given by

$$\mathbf{X}(t) = \begin{bmatrix} v_{C_1} \\ v_{C_2} \end{bmatrix}, \ \mathbf{U}(t) = \begin{bmatrix} v_{S_1} \\ v_{S_2} \end{bmatrix}. \tag{3.25}$$

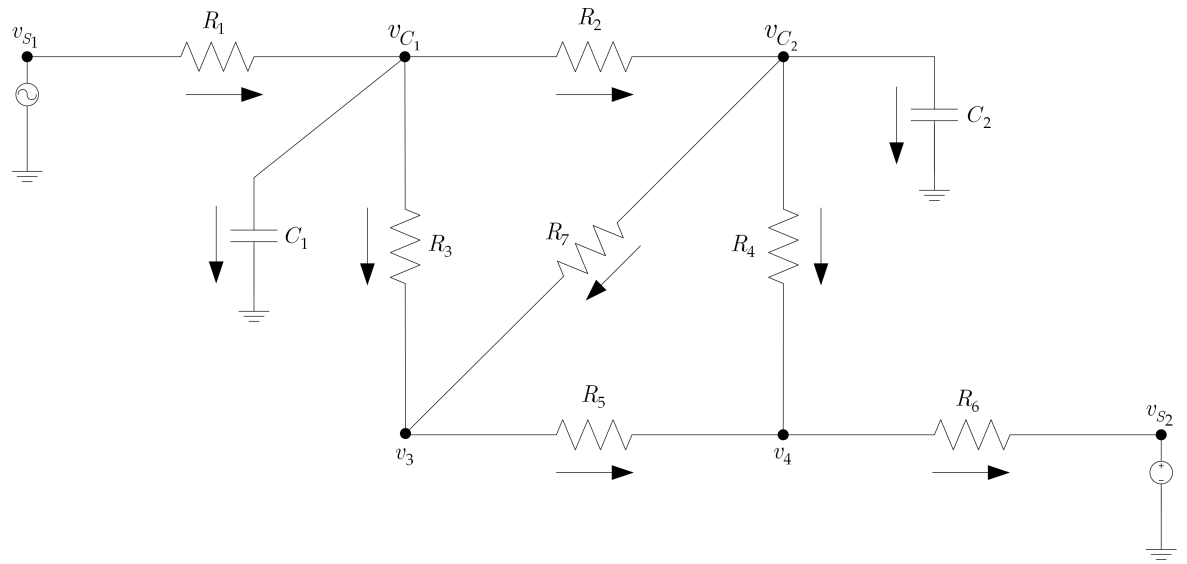

Figure 3.6: Electrical network: Example 2

Again the state space modelling process is initiated by writing down Kirchhoff's laws for the network. In this example only Kirchhoff's current law is needed to describe the structural equations completely. The structural equations are given by

$$\begin{aligned} i_{R_1} - i_{C_1} - i_{R_3} - i_{R_2} &= 0 && (3.26)\\ i_{R_2} - i_{R_7} - i_{R_4} - i_{C_2} &= 0 && (3.27)\\ i_{R_3} + i_{R_7} - i_{R_5} &= 0 && (3.28)\\ i_{R_5} + i_{R_4} - i_{R_6} &= 0. && (3.29) \end{aligned}$$

The elemental equations of the storage elements are given by

$$\begin{aligned} i_{C_1} &= C_1 \frac{dv_{C_1}}{dt} && (3.30)\\ i_{C_2} &= C_2 \frac{dv_{C_2}}{dt} && (3.31) \end{aligned}$$

and the elemental equations for the resistors are given by

$$v_{R_j} = R_j \cdot i_{R_j}, \text{ where } j = 1, \ldots, 7. \quad (3.32)$$

Eqs. (3.30) - (3.32) are substituted into Eqs. (3.26) - (3.29) to give

$$\begin{aligned} \frac{v_{S_1} - v_{C_1}}{R_1} - C_1 \frac{dv_{C_1}}{dt} - \frac{v_{C_1} - v_3}{R_3} - \frac{v_{C_1} - v_{C_2}}{R_2} &= 0 && (3.33)\\ \frac{v_{C_1} - v_{C_2}}{R_2} - \frac{v_{C_1} - v_3}{R_7} - \frac{v_{C_2} - v_4}{R_4} - C_2 \frac{dv_{C_2}}{dt} &= 0 && (3.34)\\ \frac{v_{C_1} - v_3}{R_3} + \frac{v_{C_2} - v_3}{R_7} - \frac{v_3 - v_4}{R_5} &= 0 && (3.35)\\ \frac{v_3 - v_4}{R_5} + \frac{v_{C_2} - v_4}{R_4} - \frac{v_4 - v_{S_2}}{R_6} &= 0. && (3.36) \end{aligned}$$

Next v_3 and v_4 are solved using Eqs. (3.35) and (3.36) and then substituted into Eqs. (3.33) and (3.34). Eqs. (3.33) - (3.34) are then written in terms of the state variables v_{C_1} and v_{C_2}, and the input variables v_{S_1} and v_{S_2}. In order to ease the presentation of the equations, numeric values are chosen for each element $(C_1, C_2 = 1\ \mu\text{F},\ R_1, \ldots, R_7 = 1\ \text{k}\Omega)$.

Solving for v_3 and v_4 in Eqs. (3.35) and (3.36) gives

$$v_3 = \frac{3}{8}v_{C_1} + \frac{1}{2}v_{C_2} + \frac{1}{8}v_{S_2} \tag{3.37}$$

$$v_4 = \frac{1}{8}v_{C_1} + \frac{1}{2}v_{C_2} + \frac{3}{8}v_{S_2} \tag{3.38}$$

Rearranging Eqs. (3.33) and (3.34) so that the differentials are on the left gives

$$\frac{dv_{C_1}}{dt} = -3000v_{C_1} + 1000v_{C_2} + 1000v_3 + 1000v_{S_1} \tag{3.39}$$

$$\frac{dv_{C_2}}{dt} = 1000v_{C_1} - 3000v_{C_2} + 1000v_3 + 1000v_4. \tag{3.40}$$

Substituting Eqs. (3.37) and (3.38) into Eqs. (3.39) and (3.40) gives

$$\frac{dv_{C_1}}{dt} = -2625v_{C_1} + 1500v_{C_2} + 1000v_{S_1} + 125v_{S_2} \tag{3.41}$$

$$\frac{dv_{C_2}}{dt} = 1500v_{C_1} - 2000v_{C_2} + 500v_{S_2}. \tag{3.42}$$

Eqs. (3.41) and (3.42) can be cast into the state space matrix representation as follows

$$\begin{bmatrix} dv_{C_1}/dt \\ dv_{C_2}/dt \end{bmatrix} = \begin{bmatrix} -2625 & 1500 \\ 1500 & -2000 \end{bmatrix} \begin{bmatrix} v_{C_1} \\ v_{C_2} \end{bmatrix} + \begin{bmatrix} 1000 & 125 \\ 0 & 500 \end{bmatrix} \begin{bmatrix} v_{S_1} \\ v_{S_2} \end{bmatrix} \tag{3.43}$$

where

$$\mathbf{A} = \begin{bmatrix} -2625 & 1500 \\ 1500 & -2000 \end{bmatrix},\ \mathbf{B} = \begin{bmatrix} 1000 & 125 \\ 0 & 500 \end{bmatrix}.$$

If v_{C_1} and v_{C_2} are chosen as the output variables, then

$$\begin{bmatrix} y_1 \\ y_2 \end{bmatrix} = \begin{bmatrix} 1 & 0 \\ 0 & 1 \end{bmatrix} \begin{bmatrix} v_{C_1} \\ v_{C_2} \end{bmatrix} + \begin{bmatrix} 0 & 0 \\ 0 & 0 \end{bmatrix} \begin{bmatrix} v_{S_1} \\ v_{S_2} \end{bmatrix} \tag{3.44}$$

where

$$\mathbf{C} = \begin{bmatrix} 1 & 0 \\ 0 & 1 \end{bmatrix},\ \mathbf{D} = \begin{bmatrix} 0 & 0 \\ 0 & 0 \end{bmatrix}.$$

Eqs. (3.43) and (3.44) form the state space representation of the electrical network in Fig. 3.6.

3.5 Conclusions

In this chapter the reader was introduced to state space models and how they are derived manually. It was also stated that there is a resemblance between electrical and thermohydraulic networks. The connection between these networks will be considered in the following chapter where generalised elements will be introduced. It will also be shown next how networks can be used in an automated model extraction algorithm.

CHAPTER 4

EXTRACTION OF STATE SPACE MODELS

4.1 Introduction

This chapter will focus on deriving a state space model extraction methodology based on a unified approach to system modelling. This unifying approach considers systems as energy manipulators. This means that the dynamic behaviour of a physical system can be perceived as the result of energy exchange within the system. In this way a wide variety of systems can be considered in a common framework, with energy as the main concept. This unifying concept of energy in modelling is not new. It directly flows from the theories of Hamilton and Lagrange.

In this chapter the idea of energy handling systems will be abstracted in terms of generalised system variables and elements. This concept will be linked to certain engineering disciplines to formulate the fundamental rules of system interconnection in an energy-based framework. A network approach will also be adopted where the energy interactions of the system elements are codified into a network representation of the system.

4.2 Generalised system variables and elements

A characteristic of a good modelling method is its ability to generate a mathematical model that describes the dynamic behaviour of a system in terms of physically meaningful variables. Physically meaningful variables used in electrical systems for example are voltage and current, or pressure and mass flow rate in hydraulic systems. Despite the physical difference of the systems considered, some fundamental similarities do exist. The unifying concept that is fundamental to the different engineering disciplines is energy.

A simple example of energy transmission is shown in Fig. 4.1 where an electrical source is connected to a resistor. The battery is the energy source, the resistor is the system and the wire

represents the energy link. The current flows through the wire and is normally called a *through-variable*; voltage is measured across the resistor and is called an *across-variable* [66]. The current and voltage form a pair of system variables and its product is the instantaneous power being transmitted through the energy link, given by

$$p = v \cdot i. \tag{4.1}$$

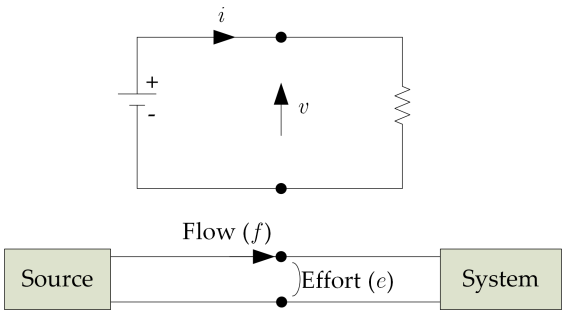

Figure 4.1: Generalised system variables

Energy transmission is associated with one through variable (e.g. current, mass flow) giving the flux of energy flow, and an across-variable (e.g. voltage, pressure) giving the pitch of flow [10]. These two energy variables can in general be seen as an *effort* variable, $e(t)$, and a *flow* variable, $f(t)$, where the energy transferred over the link in a time interval 0 to t is given by

$$E(t) = \int_0^t e(t) \cdot f(t)\, dt. \tag{4.2}$$

Table 4.1 lists the examples of generalised variables in the different engineering disciplines.

Table 4.1: Examples of generalised variables

$e(t)$	$f(t)$	Type of power transfer
Pressure	Mass flow rate	Hydraulic
Temperature	Heat flow rate	Thermal
Rotational speed	Torque	Mechanical (rotational)
Velocity	Force	Mechanical (translational)
Voltage	Current	Electrical

A physical system may therefore be thought of as operating upon a variable set whose product is power or proportional to power. The components in the system are then considered as energy manipulators. When energy is injected into the system it is processed by the components and the result can be observed as a dynamic response. In this study generalised system elements will be associated with energy transfer. The basic system elements can be categorised in terms of energy sources, dissipators and stores. This may seem to be limited, however most physical systems can be modelled in terms of these generalised elements. Although the type of elements are standardised, the performance of individual components of similar types may differ significantly. An example may be the comparison between a resistor and a diode. They

both are energy dissipators, but they behave in completely different ways due to differences in their physical nature.

The physical characteristics of the elements may be specified by an experimental curve (linear or nonlinear) or a physical law. The source element may be represented by any desired mathematical function (e.g. step function, sinusoid function). The resistive element is characterised by an algebraic equation given by

$$f(t) = R \cdot e(t). \tag{4.3}$$

Systems that have no memory do not have the ability to store information considering their history. The behaviour of memoryless systems are determined by their inputs only. Systems that do have memory store information about their history and their response is a function of present and past inputs. In the same way that information is stored, energy can also be stored in the system. Two fundamental energy storage elements exist namely an effort store and a flow store. An effort store can be defined as

$$f(t) = \frac{1}{L}\int_0^t e(t)dt \tag{4.4}$$

and a flow store as

$$e(t) = \frac{1}{C}\int_0^t f(t)dt. \tag{4.5}$$

These are the integral causal formats of the energy stores. Effort and flow stores may also be defined in differential causal format as follows:

$$e(t) = L\frac{df(t)}{dt}, \tag{4.6}$$

$$f(t) = C\frac{de(t)}{dt}. \tag{4.7}$$

The stored energy variables along with the applied efforts and flows represent the time history of energy flux in a system. It is therefore possible to link effort and flow accumulation to the state of a system. The dynamic behaviour of the system can therefore be expressed as a set of first order differential equations of the form [10]:

$$\dot{\mathbf{X}} = \mathbf{f}(\mathbf{X}, \mathbf{U}), \tag{4.8}$$

where **f** can be a linear or nonlinear function, **X** is the state vector, and **U** is the input vector. This implies that the stored energy variables (effort and flow accumulation) form a natural set of state variables of the system and Eq. (4.8) is the state space representation of the system. A summary of the generalised elements is given in Table 4.2.

4.3 State space modelling using a network approach

4.3.1 Algebraic description of a network

A network is basically a set of connected lines. The lines of the network represent the elements of the system. The lines are oriented to indicate the reference directions of the element effort

Table 4.2: The five generalised system elements [17, 18]

Element category	Elements	Symbol
Energy source	Effort source	S_e
	Flow source	S_f
Energy storage	Effort store (inductive element)	L
	Flow store (capacitive element)	C
Energy dissipation	Energy dissipator (resistive element)	R

and flow variables. The convention that will be used in this study is that a line will be oriented in the reference direction of positive flow and decreasing effort. The five generalised elements used in the network approach is shown in Fig. 4.2. The direction of the arrows should not be confused with current flow or mass flow directions, it indicates positive power flow.

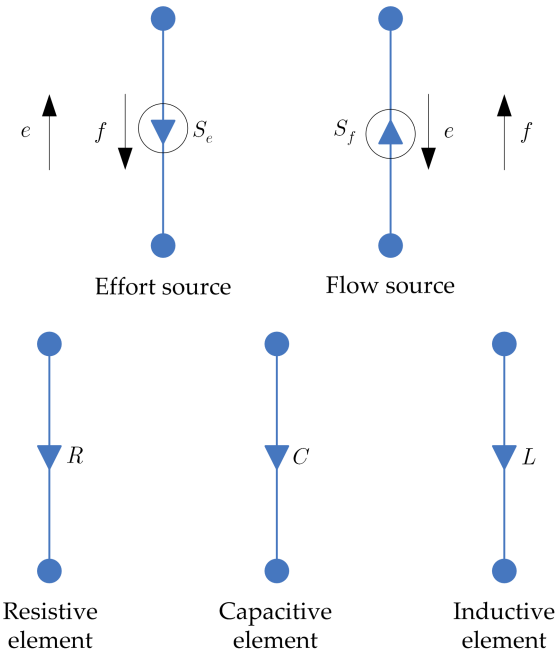

Figure 4.2: Generalised system elements [10]

A state space representation can be obtained automatically by following a network approach. The term "automatically" refers to the fact that the state space model is not obtained by hand calculation, but by means of a computer algorithm. This algorithm takes the network representation as input and generates a symbolic state space representation as output.

In this section the electrical circuit used in Chapter 3 will again be considered. This electrical network, shown again in Fig. 4.3, may also resemble a pipe network. The capacitances represent volumes, the resistances represent flow resistances and the voltage sources may represent pressure sources. This network will therefore be described in terms of generalised elements and variables.

Fig. 4.4 shows the energy network representation of the electrical circuit. The network consists

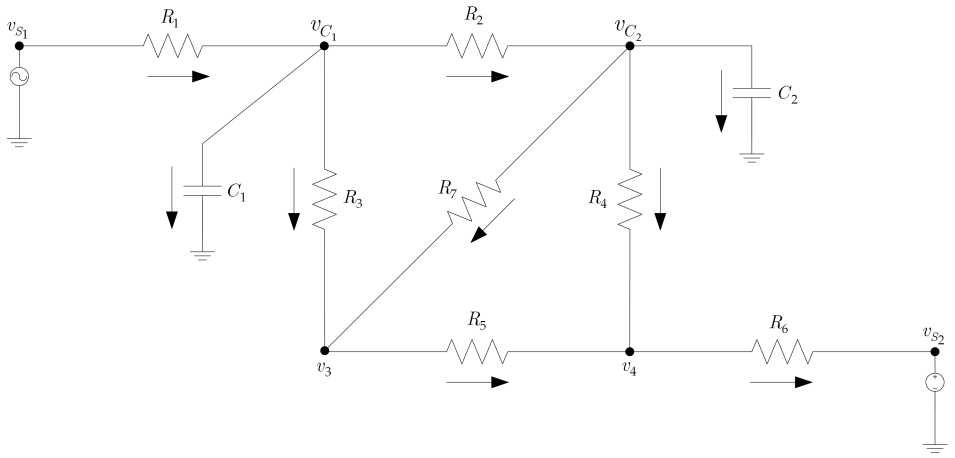

Figure 4.3: Electrical network

of nodes and links. The nodes are labelled with n-symbols and the links or elements with e-symbols. The e-symbol here does not represent an effort variable. The node labelled n_0 is a ground or reference node.

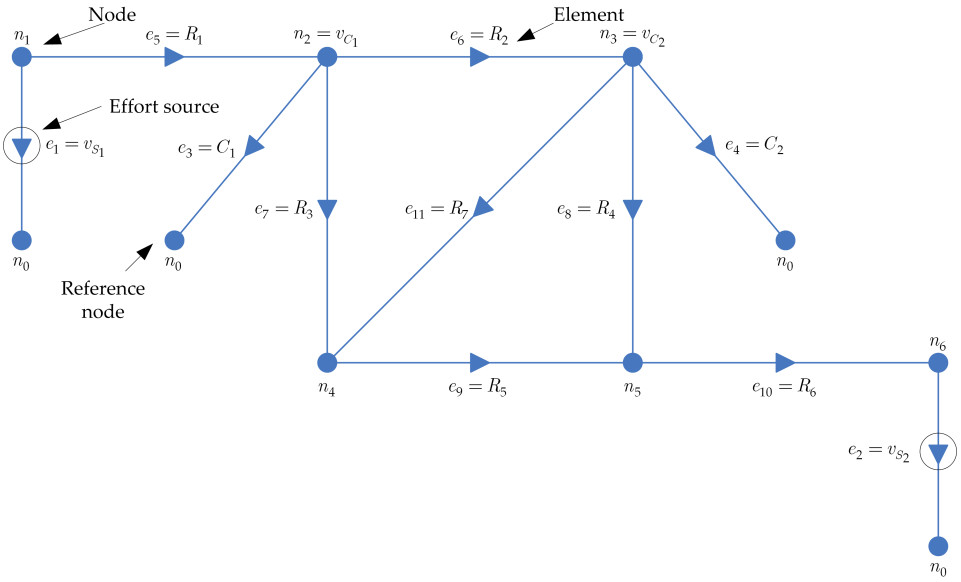

Figure 4.4: Energy network representation of the electrical circuit

The network representation gives the structural information needed to set up the state space model representation. The first step is to cast the network into matrix form that can be used for computer calculation.

Let a network be described by N nodes and E elements. Then an $N \times E$ incidence matrix, $\mathbf{A}_I = [a_{ij}]$, can be defined whose N rows correspond to the N nodes and E columns correspond to E links. Now let each matrix element

a_{ij} = 1, if link j is connected to node i and
the arrow is oriented away from node i,
= -1, if link j is connected to node i and
the arrow is oriented towards node i,
= 0, if no link is connected to node i.

The incidence matrix of the network shown in Fig. 4.4, is given by

$$\mathbf{A}_I = \left[\begin{array}{c|ccccccccccc} & e_1 & e_2 & e_3 & e_4 & e_5 & e_6 & e_7 & e_8 & e_9 & e_{10} & e_{11} \\ \hline n_0 & -1 & -1 & -1 & -1 & 0 & 0 & 0 & 0 & 0 & 0 & 0 \\ n_1 & 1 & 0 & 0 & 0 & 1 & 0 & 0 & 0 & 0 & 0 & 0 \\ n_2 & 0 & 0 & 1 & 0 & -1 & 1 & 1 & 0 & 0 & 0 & 0 \\ n_3 & 0 & 0 & 0 & 1 & 0 & -1 & 0 & 1 & 0 & 0 & 1 \\ n_4 & 0 & 0 & 0 & 0 & 0 & 0 & -1 & 0 & 1 & 0 & -1 \\ n_5 & 0 & 0 & 0 & 0 & 0 & 0 & 0 & -1 & -1 & 1 & 0 \\ n_6 & 0 & 1 & 0 & 0 & 0 & 0 & 0 & 0 & 0 & -1 & 0 \end{array}\right] \tag{4.9}$$

The reference node can be eliminated from the incidence matrix, for it does not contribute any new information. The matrix, $\mathbf{A}_R$, obtained by deleting the corresponding row from the incidence matrix is called a reduced incidence matrix. From now on, this matrix will be called the incidence matrix.

$$\mathbf{A}_R = \left[\begin{array}{c|ccccccccccc} & e_1 & e_2 & e_3 & e_4 & e_5 & e_6 & e_7 & e_8 & e_9 & e_{10} & e_{11} \\ \hline n_1 & 1 & 0 & 0 & 0 & 1 & 0 & 0 & 0 & 0 & 0 & 0 \\ n_2 & 0 & 0 & 1 & 0 & -1 & 1 & 1 & 0 & 0 & 0 & 0 \\ n_3 & 0 & 0 & 0 & 1 & 0 & -1 & 0 & 1 & 0 & 0 & 1 \\ n_4 & 0 & 0 & 0 & 0 & 0 & 0 & -1 & 0 & 1 & 0 & -1 \\ n_5 & 0 & 0 & 0 & 0 & 0 & 0 & 0 & -1 & -1 & 1 & 0 \\ n_6 & 0 & 1 & 0 & 0 & 0 & 0 & 0 & 0 & 0 & -1 & 0 \end{array}\right] \tag{4.10}$$

4.3.2 Comparison with algebraic representation used in *Flownex*®

Flownex®, a thermohydraulic simulation code also implements a network approach. The relationship between the matrices derived from a *Flownex*® network and an energy flow network (Fig. 4.4) will be illustrated shortly. A *Flownex*® network consists of a number of oriented elements (circles) connected with nodes (blocks). An equivalent *Flownex*® network of the network in Fig. 4.4 is shown in Fig. 4.5. The arrows show the positive direction of mass flow.

In *Flownex*® the source elements are not shown, but they are defined at the specific nodes (nodes 1 and 6). The volumes (capacitive elements) are also not shown since they are defined at the nodes (nodes 2 and 3). The network is represented by a node connectivity matrix, **N**, and an element connectivity matrix, **E**.

Considering Fig. 4.6 node i is connected to neighbouring nodes n_{ij} by elements e_{ij}, where $j = 1, 2, \ldots, J$. J represents the number of branches associated with node i. A positive flow

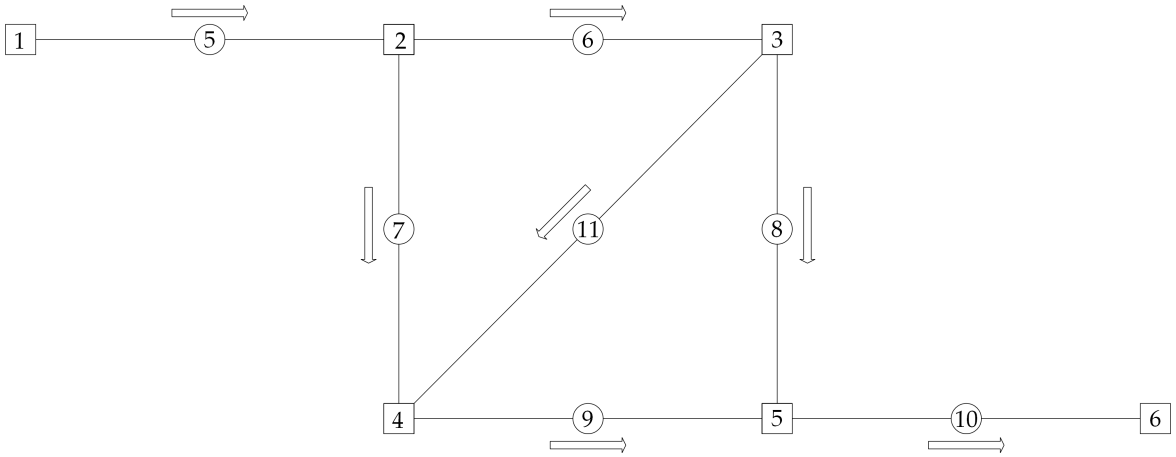

Figure 4.5: *Flownex*® network

direction is assumed towards node i. A positive value is assigned to the element e_{ij} in the element connectivity matrix if the flow is towards i, and a negative value if the flow is away from i.

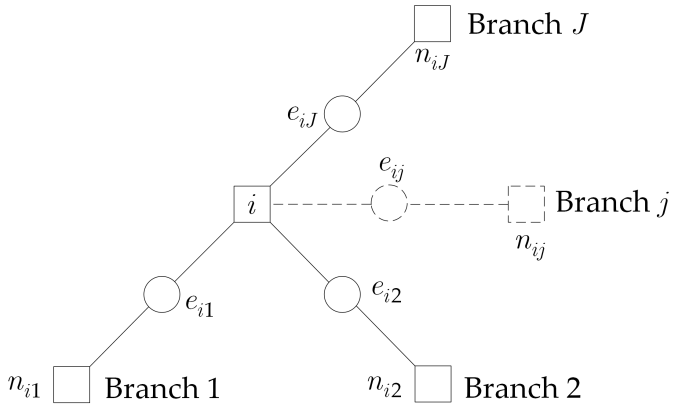

Figure 4.6: Notation used to define the structure of a *Flownex*® network [11]

The element and node connectivity matrices for the network in Fig. 4.5 are as follows:

$$\mathbf{E} = [e_{ij}] = \begin{bmatrix} -5 & 0 & 0 \\ 5 & -6 & -7 \\ 6 & -11 & -8 \\ 7 & 11 & -9 \\ 9 & 8 & -10 \\ 10 & 0 & 0 \end{bmatrix} \tag{4.11}$$

$$\mathbf{N} = [n_{ij}] = \begin{bmatrix} 2 & 0 & 0 \\ 1 & 3 & 4 \\ 2 & 4 & 5 \\ 2 & 3 & 5 \\ 4 & 3 & 6 \\ 5 & 0 & 0 \end{bmatrix} \tag{4.12}$$

The rows of the element and node connectivity matrices correspond to the nodes of the *Flownex*® network. The columns of the element connectivity matrix are populated according to the branches associated with the specific node. The columns of the node connectivity matrix are populated according to the neighbouring nodes of the specific node.

The relationship between the incidence matrix and the element connectivity matrix is shown in Fig. 4.7. Considering the second row in each matrix indicates that elements 5, 6 and 7 are connected to node 2. The encircled element in the second row of the incidence matrix indicates the capacitor element ($e_3 = C_1$).

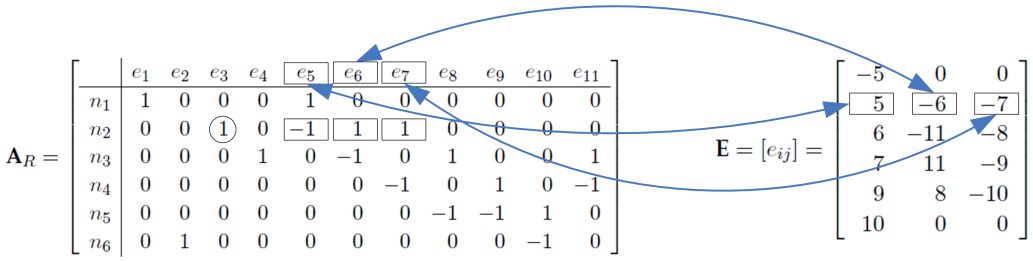

Figure 4.7: Relationship between the incidence matrix and the element connectivity matrix

The relationship between the incidence matrix and the node connectivity matrix is shown in Fig. 4.8. Again, considering the second row in both matrices, node 2 is connected to nodes 1, 3 and 4 by elements 5, 6 and 7 respectively.

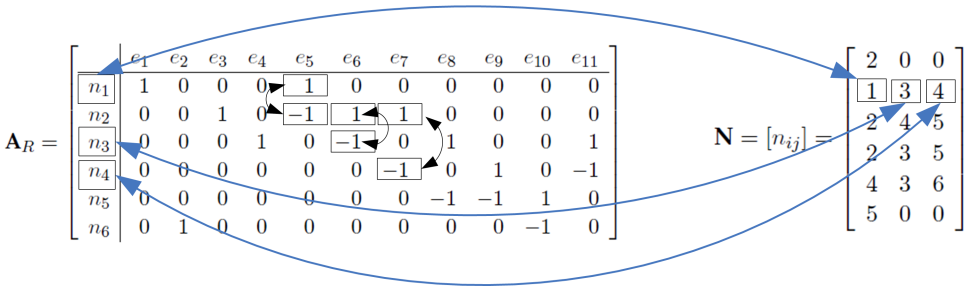

Figure 4.8: Relationship between the incidence matrix and the node connectivity matrix

Considering the relationships, it is possible to derive an energy incidence matrix from the *Flownex*® element and node connectivity matrices or vice versa. To derive the state space representation of the system two kinds of equations are needed: structural equations and elemental equations. The following section will describe how these equations can be derived from the energy network representation.

4.3.3 System structural and elemental equations

The structural equations can be derived using concepts taken from graph theory (see Appendix A). Two graph theoretic concepts are used namely a *tree* and *co-tree*. A tree is a network

containing no loops. The elements that are removed to eliminate the loops are called the co-tree. The network in Fig. 4.4 has a reference node, n_0, therefore the network can be visualised as shown in Fig. 4.9.

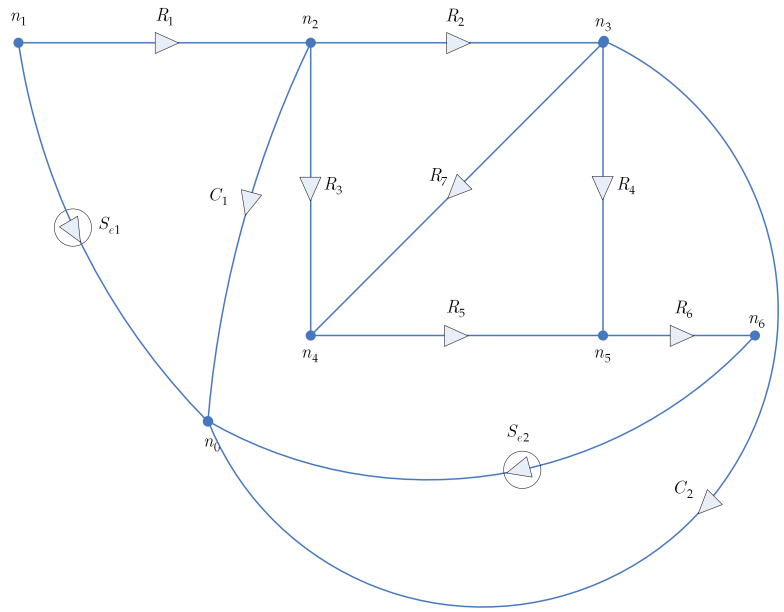

Figure 4.9: Energy network used for tree and co-tree analysis

The elements in the tree and co-tree are defined in a specific way. The tree is defined such that a minimum number of state variables capable of describing the system will be generated. Two generalised storage elements exist namely, flow and effort stores. The capacitive elements are flow stores and the inductive elements are effort stores. As shown in Sec. 4.2, the effort variables of the flow stores and the flow variables of the effort stores are the state variables of the system. In order to eliminate the dependent state variables, the tree of the network is selected such that the tree contains [10]:

1. all the effort sources;
2. the maximum number of flow stores (Capacitive elements);
3. dissipators;
4. the minimum number of effort stores (Inductive elements);

and the co-tree contains:

1. all the flow sources;
2. the maximum number of effort stores (Inductive elements);
3. dissipators;

4. the minimum number of flow stores (Capacitive elements);

A tree selected in this way is called a *normal tree*. In Fig. 4.10 a normal tree is selected. There are algorithms that can automatically select the trees, co-trees and normal trees of networks [62, 63].

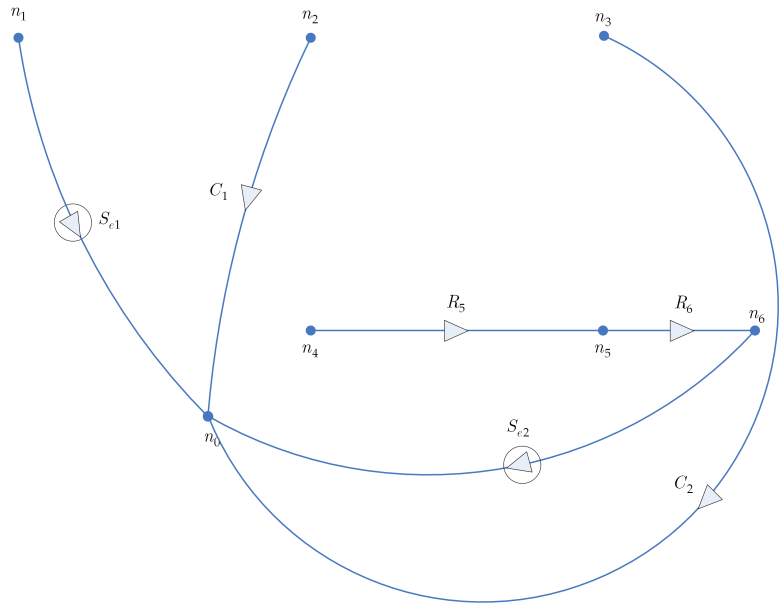

Figure 4.10: A normal tree of the network

The incidence matrix, Eq. (4.10), can be partitioned according to the normal tree into two sub-matrices as follows:

$$\mathbf{A}_R = \left[\begin{array}{c|c} \mathbf{A}_{co} & \mathbf{A}_{tr} \end{array} \right], \tag{4.13}$$

where

$$\mathbf{A}_{co} = \left[\begin{array}{c|ccccc} & e_5 & e_6 & e_7 & e_8 & e_{11} \\ \hline n_1 & 1 & 0 & 0 & 0 & 0 \\ n_2 & -1 & 1 & 1 & 0 & 0 \\ n_3 & 0 & -1 & 0 & 1 & 1 \\ n_4 & 0 & 0 & -1 & 0 & -1 \\ n_5 & 0 & 0 & 0 & -1 & 0 \\ n_6 & 0 & 0 & 0 & 0 & 0 \end{array}\right] \tag{4.14}$$

and

$$\mathbf{A}_{tr} = \left[\begin{array}{c|cccccc} & e_1 & e_2 & e_3 & e_4 & e_9 & e_{10} \\ \hline n_1 & 1 & 0 & 0 & 0 & 0 & 0 \\ n_2 & 0 & 0 & 1 & 0 & 0 & 0 \\ n_3 & 0 & 0 & 0 & 1 & 0 & 0 \\ n_4 & 0 & 0 & 0 & 0 & 1 & 0 \\ n_5 & 0 & 0 & 0 & 0 & -1 & 1 \\ n_6 & 0 & 1 & 0 & 0 & 0 & -1 \end{array}\right]. \tag{4.15}$$

These matrices are used to determine the fundamental cut-set matrix:

$$\mathbf{F}_c = \mathbf{A}_{tr}^{-1}\mathbf{A}_{co} = \left[\begin{array}{cc} \mathbf{H} & \mathbf{I} \end{array}\right], \tag{4.16}$$

where **I** is an identity matrix. The cut-set matrix represents Kirchhoff's laws in matrix form. The fundamental cut-set matrix for the network in Fig. 4.4 is given as

$$\mathbf{F}_c = \left[\begin{array}{cc} \mathbf{H} & \mathbf{I} \end{array}\right] = \left[\begin{array}{ccccc|cccccc} 1 & 0 & 0 & 0 & 0 & 1 & 0 & 0 & 0 & 0 & 0 \\ 0 & 0 & -1 & -1 & -1 & 0 & 1 & 0 & 0 & 0 & 0 \\ -1 & 1 & 1 & 0 & 0 & 0 & 0 & 1 & 0 & 0 & 0 \\ 0 & -1 & 0 & 1 & 1 & 0 & 0 & 0 & 1 & 0 & 0 \\ 0 & 0 & -1 & 0 & -1 & 0 & 0 & 0 & 0 & 1 & 0 \\ 0 & 0 & -1 & -1 & -1 & 0 & 0 & 0 & 0 & 0 & 1 \end{array}\right]. \tag{4.17}$$

The structural equations can then be written in terms of the effort or flow variables. The generalised variables of the network can be written in vector form and partitioned in terms of the tree and co-tree of the network as follows:

$$\mathbf{e} = \begin{bmatrix} \mathbf{e}_{tr} \\ \mathbf{e}_{co} \end{bmatrix}, \ \mathbf{f} = \begin{bmatrix} \mathbf{f}_{tr} \\ \mathbf{f}_{co} \end{bmatrix} \tag{4.18}$$

where **e** and **f** represent the effort and flow variables of the network. The effort and flow vectors in Eq. (4.18) can be partitioned again according to a normal tree as follows:

$$\mathbf{e}_{tr} = \begin{bmatrix} \mathbf{e}_{S,tr} \\ \mathbf{e}_{C,tr} \\ \mathbf{e}_{R,tr} \\ \mathbf{e}_{L,tr} \end{bmatrix}, \ \mathbf{f}_{tr} = \begin{bmatrix} \mathbf{f}_{S,tr} \\ \mathbf{f}_{C,tr} \\ \mathbf{f}_{R,tr} \\ \mathbf{f}_{L,tr} \end{bmatrix} \tag{4.19}$$

and

$$\mathbf{e}_{co} = \begin{bmatrix} \mathbf{e}_{C,co} \\ \mathbf{e}_{R,co} \\ \mathbf{e}_{L,co} \\ \mathbf{e}_{S,co} \end{bmatrix}, \ \mathbf{f}_{co} = \begin{bmatrix} \mathbf{f}_{C,co} \\ \mathbf{f}_{R,co} \\ \mathbf{f}_{L,co} \\ \mathbf{f}_{S,co} \end{bmatrix} \tag{4.20}$$

The structural equations can then be written in terms of the effort or flow variables by using the matrix **H**:

$$\mathbf{e}_{co} = \mathbf{H}'\mathbf{e}_{tr} \tag{4.21}$$

$$\mathbf{f}_{tr} = -\mathbf{H}\mathbf{f}_{co} \tag{4.22}$$

Considering Fig. 4.10

$$\mathbf{e}_{co} = \begin{bmatrix} \mathbf{e}_{C,co} \\ \mathbf{e}_{R,co} \\ \mathbf{e}_{L,co} \\ \mathbf{e}_{S,co} \end{bmatrix} = \begin{bmatrix} e_{R_1} \\ e_{R_2} \\ e_{R_3} \\ e_{R_4} \\ e_{R_7} \end{bmatrix} \tag{4.23}$$

since

$$\mathbf{e}_{R,co} = \begin{bmatrix} e_{R_1} \\ e_{R_2} \\ e_{R_3} \\ e_{R_4} \\ e_{R_7} \end{bmatrix}, \ \mathbf{e}_{C,co} = \mathbf{0}, \ \mathbf{e}_{L,co} = \mathbf{0} \text{ and } \mathbf{e}_{S,co} = \mathbf{0}.$$

The effort vector corresponding to the tree shown in Fig. 4.10 is given by

$$\mathbf{e}_{tr} = \begin{bmatrix} \mathbf{e}_{S,tr} \\ \mathbf{e}_{C,tr} \\ \mathbf{e}_{R,tr} \\ \mathbf{e}_{L,tr} \end{bmatrix} = \begin{bmatrix} e_{S_{e1}} \\ e_{S_{e2}} \\ e_{C_1} \\ e_{C_2} \\ e_{R_5} \\ e_{R_6} \end{bmatrix} \tag{4.24}$$

since

$$\mathbf{e}_{S,tr} = \begin{bmatrix} e_{S_{e1}} \\ e_{S_{e2}} \end{bmatrix}, \ \mathbf{e}_{C,tr} = \begin{bmatrix} e_{C_1} \\ e_{C_2} \end{bmatrix}, \ \mathbf{e}_{R,tr} = \begin{bmatrix} e_{R_5} \\ e_{R_6} \end{bmatrix} \text{ and } \mathbf{e}_{L,tr} = \mathbf{0}.$$

Then Eq. (4.21) can be written as:

$$\begin{bmatrix} e_{R_1} \\ e_{R_2} \\ e_{R_3} \\ e_{R_4} \\ e_{R_7} \end{bmatrix} = \begin{bmatrix} 1 & 0 & -1 & 0 & 0 & 0 \\ 0 & 0 & 1 & -1 & 0 & 0 \\ 0 & -1 & 1 & 0 & -1 & -1 \\ 0 & -1 & 0 & 1 & 0 & -1 \\ 0 & -1 & 0 & 1 & -1 & -1 \end{bmatrix} \begin{bmatrix} e_{S_{e1}} \\ e_{S_{e2}} \\ e_{C_1} \\ e_{C_2} \\ e_{R_5} \\ e_{R_6} \end{bmatrix}. \tag{4.25}$$

Eq. (4.22) can be expanded in the same way. For the electrical network the structural equations in terms of voltages can be derived from Eq. (4.25) as follows:

$$v_{R_1} = v_{S_1} - v_{C_1}, \tag{4.26}$$
$$v_{R_2} = v_{C_1} - v_{C_2}, \tag{4.27}$$
$$v_{R_3} = -v_{S_2} + v_{C_1} - v_{R_5} - v_{R_6}, \tag{4.28}$$
$$v_{R_4} = -v_{S_2} + v_{C_2} - v_{R_6}, \tag{4.29}$$
$$v_{R_7} = -v_{S_2} + v_{C_2} - v_{R_5} - v_{R_6}. \tag{4.30}$$

The matrix $\mathbf{H}$ can also be partitioned in terms of the elements in the tree and co-tree as follows:

$$\mathbf{H} = \begin{bmatrix} \mathbf{H}_{SC} & \mathbf{H}_{SR} & \mathbf{H}_{SL} & \mathbf{H}_{SS} \\ \mathbf{H}_{CC} & \mathbf{H}_{CR} & \mathbf{H}_{CL} & \mathbf{H}_{CS} \\ \mathbf{H}_{RC} & \mathbf{H}_{RR} & \mathbf{H}_{RL} & \mathbf{H}_{RS} \\ \mathbf{H}_{LC} & \mathbf{H}_{LR} & \mathbf{H}_{LL} & \mathbf{H}_{LS} \end{bmatrix}, \tag{4.31}$$

where the first letter in the subscript refers to the element in the tree and the second letter to the element in the co-tree. By inspection the matrices $\mathbf{H}_{RC}, \mathbf{H}_{LC}$ and $\mathbf{H}_{LR}$ are zero matrices since a

normal tree is used for the representation. The elements of **H** can be determined knowing that

$$\mathbf{H}' = \begin{bmatrix} \mathbf{H}'_{SC} & \mathbf{H}'_{CC} & \mathbf{H}'_{RC} & \mathbf{H}'_{LC} \\ \mathbf{H}'_{SR} & \mathbf{H}'_{CR} & \mathbf{H}'_{RR} & \mathbf{H}'_{LR} \\ \mathbf{H}'_{SL} & \mathbf{H}'_{CL} & \mathbf{H}'_{RL} & \mathbf{H}'_{LL} \\ \mathbf{H}'_{SS} & \mathbf{H}'_{CS} & \mathbf{H}'_{RS} & \mathbf{H}'_{LS} \end{bmatrix} = \begin{bmatrix} \mathbf{H}'_{SR} & \mathbf{H}'_{CR} & \mathbf{H}'_{RR} \end{bmatrix}. \tag{4.32}$$

Since there is no capacitances, inductors or sources in the co-tree. Then Eq. (4.32) can be expanded to

$$\begin{bmatrix} \mathbf{H}'_{SR} & \mathbf{H}'_{CR} & \mathbf{H}'_{RR} \end{bmatrix} = \left[\begin{array}{c|cc|cc|cc} & e_{S_1} & e_{S_2} & e_{C_1} & e_{C_2} & e_{R_5} & e_{R_6} \\ \hline e_{R_1} & 1 & 0 & -1 & 0 & 0 & 0 \\ e_{R_2} & 0 & 0 & 1 & -1 & 0 & 0 \\ e_{R_3} & 0 & -1 & 1 & 0 & -1 & -1 \\ e_{R_4} & 0 & -1 & 0 & 1 & 0 & -1 \\ e_{R_7} & 0 & -1 & 0 & 1 & -1 & -1 \end{array}\right], \tag{4.33}$$

where

$$\mathbf{H}'_{SR} = \begin{bmatrix} 1 & 0 \\ 0 & 0 \\ 0 & -1 \\ 0 & -1 \\ 0 & -1 \end{bmatrix}, \ \mathbf{H}'_{CR} = \begin{bmatrix} -1 & 0 \\ 1 & -1 \\ 1 & 0 \\ 0 & 1 \\ 0 & 1 \end{bmatrix} \text{ and } \mathbf{H}'_{RR} = \begin{bmatrix} 0 & 0 \\ 0 & 0 \\ -1 & -1 \\ 0 & -1 \\ -1 & -1 \end{bmatrix}.$$

Moving over from the structural equations to the elemental equations, the elemental equations can be written in matrix form as follows:

$$\begin{bmatrix} \mathbf{f}_{C,tr} \\ \mathbf{f}_{C,co} \end{bmatrix} = \begin{bmatrix} \mathbf{C}_{tr} & \mathbf{0} \\ \mathbf{0} & \mathbf{C}_{co} \end{bmatrix} \frac{d}{dt} \begin{bmatrix} \mathbf{e}_{C,tr} \\ \mathbf{e}_{C,co} \end{bmatrix}, \tag{4.34}$$

$$\begin{bmatrix} \mathbf{e}_{L,co} \\ \mathbf{e}_{L,tr} \end{bmatrix} = \begin{bmatrix} \mathbf{L}_{co} & \mathbf{0} \\ \mathbf{0} & \mathbf{L}_{tr} \end{bmatrix} \frac{d}{dt} \begin{bmatrix} \mathbf{f}_{C,co} \\ \mathbf{f}_{C,tr} \end{bmatrix}, \tag{4.35}$$

$$\begin{aligned} \mathbf{f}_{R,co} &= \mathbf{R}_{co}^{-1} \mathbf{e}_{R,co}, \\ \mathbf{f}_{R,tr} &= \mathbf{R}_{tr}^{-1} \mathbf{e}_{R,tr}. \end{aligned} \tag{4.36}$$

The elements of the network are cast into element matrices given by

$$\mathbf{C}_{tr} = \begin{bmatrix} C_1 & 0 \\ 0 & C_2 \end{bmatrix}, \ \mathbf{C}_{co} = \mathbf{0}, \tag{4.37}$$

$$\mathbf{L}_{tr} = \mathbf{0}, \ \mathbf{L}_{co} = \mathbf{0}, \tag{4.38}$$

$$\mathbf{R}_{tr} = \begin{bmatrix} R_1 & 0 & 0 & 0 & 0 \\ 0 & R_2 & 0 & 0 & 0 \\ 0 & 0 & R_3 & 0 & 0 \\ 0 & 0 & 0 & R_4 & 0 \\ 0 & 0 & 0 & 0 & R_7 \end{bmatrix}, \ \mathbf{R}_{co} = \begin{bmatrix} R_5 & 0 \\ 0 & R_6 \end{bmatrix}. \tag{4.39}$$

4.3.4 State space extraction algorithm

Finally the structural equations, Eqs. (4.21) and (4.22), are combined with the elemental equations, Eqs. (4.34) - (4.36) to form a state space representation. The state space representation is written in terms of the state vectors $\mathbf{e}_{C,tr}$ and $\mathbf{f}_{L,co}$, and the source variables $\mathbf{e}_S$ and $\mathbf{f}_S$. The resulting state space representation can then be written as [10]

$$\begin{aligned}\begin{bmatrix}\mathbf{C} & \mathbf{0}\\ \mathbf{0} & \mathbf{L}\end{bmatrix}\frac{d}{dt}\begin{bmatrix}\mathbf{e}_{C,tr}\\ \mathbf{f}_{L,co}\end{bmatrix} &= \begin{bmatrix}\mathbf{A}_{11} & \mathbf{A}_{12}\\ \mathbf{A}_{21} & \mathbf{A}_{22}\end{bmatrix}\begin{bmatrix}\mathbf{e}_{C,tr}\\ \mathbf{f}_{L,co}\end{bmatrix}\\ + \begin{bmatrix}\mathbf{B}_{11} & \mathbf{B}_{12}\\ \mathbf{B}_{21} & \mathbf{B}_{22}\end{bmatrix}\begin{bmatrix}\mathbf{e}_S\\ \mathbf{f}_S\end{bmatrix} &+ \begin{bmatrix}\mathbf{D}_{11} & \mathbf{0}\\ \mathbf{0} & \mathbf{D}_{22}\end{bmatrix}\frac{d}{dt}\begin{bmatrix}\mathbf{e}_S\\ \mathbf{f}_S\end{bmatrix},\end{aligned} \tag{4.40}$$

where

$$\begin{aligned}\mathbf{C} &= \mathbf{C}_{tr} \;+\; \mathbf{H}_{CC}\,\mathbf{C}_{co}\,\mathbf{H}'_{CC},\\ \mathbf{L} &= \mathbf{L}_{co} \;+\; \mathbf{H}'_{LL}\,\mathbf{L}_{tr}\,\mathbf{H}_{LL}.\end{aligned}$$

The following equations represent the extraction part of the algorithm:

$$\begin{aligned}\mathbf{A}_{11} &= -\mathbf{H}_{CR}(\mathbf{R}_{co} \;+\; \mathbf{H}'_{RR}\,\mathbf{R}_{tr}\,\mathbf{H}_{RR})^{-1}\,\mathbf{H}'_{CR}\\ \mathbf{A}_{12} &= -\mathbf{H}_{CL} \;+\; \mathbf{H}_{CR}(\mathbf{R}_{co} \;+\; \mathbf{H}'_{RR}\,\mathbf{R}_{tr}\,\mathbf{H}_{RR})^{-1}\,\mathbf{H}'_{RR}\,\mathbf{R}_{tr}\,\mathbf{H}_{RL}\\ \mathbf{A}_{21} &= \mathbf{H}'_{CL} \;-\; \mathbf{H}'_{CR}(\mathbf{R}_{co} \;+\; \mathbf{H}'_{RR}\,\mathbf{R}_{tr}\,\mathbf{H}_{RR})^{-1}\,\mathbf{H}_{RR}\,\mathbf{R}_{tr}\,\mathbf{H}'_{RL}\\ &= -\mathbf{A}'_{12}\\ \mathbf{A}_{22} &= -\mathbf{H}'_{RL}(\mathbf{R}_{tr}^{-1} \;+\; \mathbf{H}_{RR}\,\mathbf{R}_{co}^{-1}\,\mathbf{H}'_{RR})^{-1}\,\mathbf{H}_{RL}\end{aligned}$$

$$\begin{aligned}\mathbf{B}_{11} &= -\mathbf{H}_{CR}(\mathbf{R}_{co} \;+\; \mathbf{H}'_{RR}\,\mathbf{R}_{tr}\,\mathbf{H}_{RR})^{-1}\,\mathbf{H}'_{SR}\\ \mathbf{B}_{12} &= -\mathbf{H}_{CS} \;+\; \mathbf{H}_{CR}(\mathbf{R}_{co} \;+\; \mathbf{H}'_{RR}\,\mathbf{R}_{tr}\,\mathbf{H}_{RR})^{-1}\,\mathbf{H}'_{RR}\,\mathbf{R}_{tr}\,\mathbf{H}_{RS}\\ \mathbf{B}_{21} &= \mathbf{H}'_{SL} \;-\; \mathbf{H}'_{RL}(\mathbf{R}_{tr}^{-1} \;+\; \mathbf{H}_{RR}\,\mathbf{R}_{co}^{-1}\,\mathbf{H}'_{RR})^{-1}\,\mathbf{H}_{RR}\,\mathbf{R}_{co}^{-1}\,\mathbf{H}_{SR}^{T}\\ \mathbf{B}_{22} &= -\mathbf{H}'_{RL}(\mathbf{R}_{tr}^{-1} \;+\; \mathbf{H}_{RR}\,\mathbf{R}_{co}^{-1}\,\mathbf{H}'_{RR})^{-1}\,\mathbf{H}_{RS}\end{aligned}$$

$$\begin{aligned}\mathbf{D}_{11} &= -\mathbf{H}_{CC}\,\mathbf{C}_{co}\,\mathbf{H}'_{SC}\\ \mathbf{D}_{22} &= -\mathbf{H}'_{LL}\,\mathbf{L}_{tr}\,\mathbf{H}_{LS}\end{aligned}$$

The state and input vectors for the electrical network in Fig. 4.3 are chosen as

$$\mathbf{e}_{C,tr} = \begin{bmatrix} v_{C_1} \\ v_{C_2} \end{bmatrix},\ \mathbf{e}_S = \begin{bmatrix} v_{S_1} \\ v_{S_2} \end{bmatrix}, \tag{4.41}$$

where v_{C_1} and v_{C_2} are the voltages over the capacitors, and v_{S_1} and v_{S_2} are the voltage sources. The state space extraction algorithm extracts the state space model in symbolic form given as follows:

$$\begin{bmatrix} \frac{dv_{C_1}}{dt} \\ \frac{dv_{C_2}}{dt} \end{bmatrix} = \begin{bmatrix} A_{11} & A_{12} \\ A_{21} & A_{22} \end{bmatrix}\begin{bmatrix} v_{C_1} \\ v_{C_2} \end{bmatrix} + \begin{bmatrix} B_{11} & B_{12} \\ B_{21} & B_{22} \end{bmatrix}\begin{bmatrix} v_{S_1} \\ v_{s_2} \end{bmatrix}, \tag{4.42}$$

where the elements of the matrices **A** and **B** are given in symbolic form in Appendix B. The symbolic values can then be substituted by numerical values given previously ($C_1, C_2 = 1\ \mu\text{F}; R_1, \ldots, R_7 = 1\ \text{k}\Omega$). The state space representation of the electrical network is given by

$$\begin{bmatrix} \frac{dv_{C_1}}{dt} \\ \frac{dv_{C_2}}{dt} \end{bmatrix} = \begin{bmatrix} -2625 & 1500 \\ 1500 & -2000 \end{bmatrix} \begin{bmatrix} v_{C_1} \\ v_{C_2} \end{bmatrix} + \begin{bmatrix} 1000 & 125 \\ 0 & 500 \end{bmatrix} \begin{bmatrix} v_{S_1} \\ v_{s_2} \end{bmatrix} \tag{4.43}$$

which is identical to the state space representation derived by hand in Chapter 3.

4.4 Conclusion

In this chapter the unifying concept of energy was used to develop a state space model extraction methodology. It was shown that energy handling systems can be abstracted into generalised variables and elements. The process of representing system elements in an energy network was demonstrated using electrical circuit examples.

A method for translating the network representation into an algebraic representation was discussed. The structural information of a network can be represented by means of an incidence matrix. In *Flownex®*, networks are algebraically presented by node and element connectivity matrices. The relationship between these matrices and the incidence matrix were pointed out. This relationship indicated that the state space extraction algorithm can easily be adapted for a *Flownex®* network.

Finally it was shown how to combine the structural equations, derived from the incidence matrix, with the elemental equations to form a state space representation. The algorithm was discussed using the electrical circuit of Chapter 3. A symbolic state space model of the circuit was generated by the extraction algorithm. Numerical values were substituted and the model was compared with the model in Chapter 3. The models showed to be identical.

This demonstrates that the state space extraction algorithm is cable of deriving state space models of systems represented by network representations. In the following chapter state space models of thermohydraulic systems will be derived using this algorithm.

CHAPTER 5

APPLICATIONS OF STATE SPACE MODEL EXTRACTION

5.1 Introduction

This chapter starts with a description of a network approach for discretising a thermohydraulic system. From this follows the development of generalised elements that can be used to develop reduced order state space models suitable for control applications. The fundamental equations and the discretisation of conservation equations are discussed. The generalised components will be used to construct network representations of thermohydraulic systems. These networks will then be evaluated by the developed state space extraction algorithm to extract state space models. State space models of three different thermohydraulic systems will be extracted namely a U-tube, a heat exchanger and finally a Brayton cycle-based power plant. These examples are used to validate the extracted state space models by comparing the solutions of the state space models with results obtained from *Flownex*®.

5.2 Thermohydraulic element characterisation

In Chapter 4 generalised system elements were derived that can be used to describe the key system phenomena namely energy generation, storage and dissipation. In this section these elements will be derived for thermohydraulic systems. Following a network approach, a thermohydraulic system can be represented by a network consisting of nodes connecting components as shown in Fig. 5.1. Each component can be broken up into energy networks of generalised variables representing the key dynamics of each physical domain present.

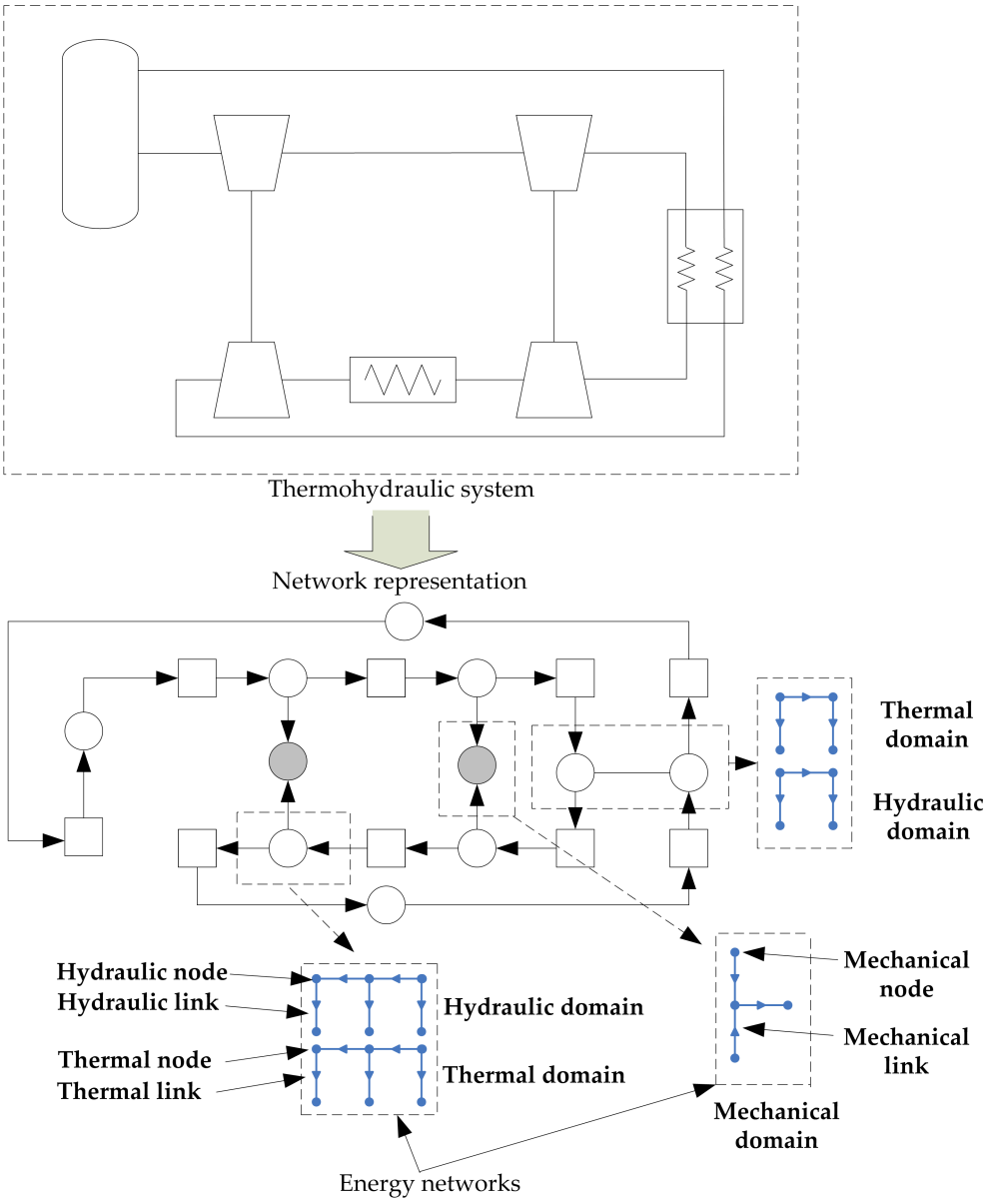

Figure 5.1: Network representation of thermohydraulic systems

5.2.1 Generalised hydraulic and thermal elements

The equations that govern fluid flow and heat transfer in networks are the continuity, momentum and energy equations. These equations can be described by first order partial differential equations. However by using finite volume discretisation, as shown in Fig. 5.2, these equations can be transformed into first order ordinary differential equations. The aim of a discretisation method is usually to get a system of equations that can be solved using standard matrix solution techniques. This is however not the goal in this study. Here the discretisation is used to obtain simpler ordinary differential equations from which the appropriate generalised elements can be derived. The focus is on the derivation of reduced order models for control purposes.

The basic building block of a network approach is the Control Volume (CV), or node, which can represent a certain volume of fluid or solid [22]. Inside this control volume scalar values are assumed to be representative of the average conditions inside the control volume.

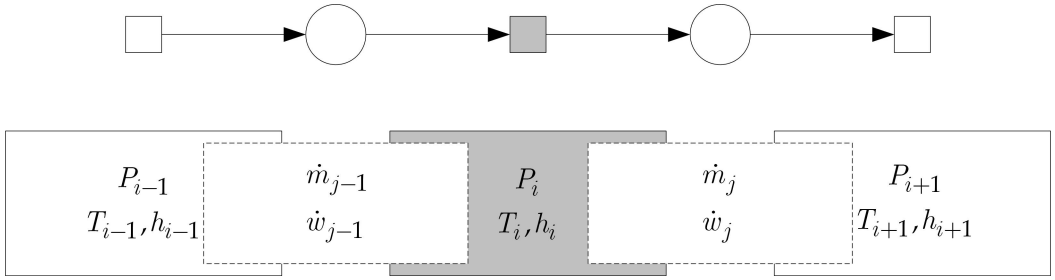

Figure 5.2: A pipe section discretised into control volumes

In each control volume average values of the velocity, density, pressure, temperature and enthalpy will be used. The fluid and energy flow inside the pipe is assumed to be one-dimensional. This means that only the flow velocity component normal to the cross-sectional area of the pipe is taken into account. Two kinds of control volumes can be defined as shown in Fig. 5.3. Conservation of mass and energy are applied over the node centred control volumes, and conservation of momentum is applied over the element centred control volumes.

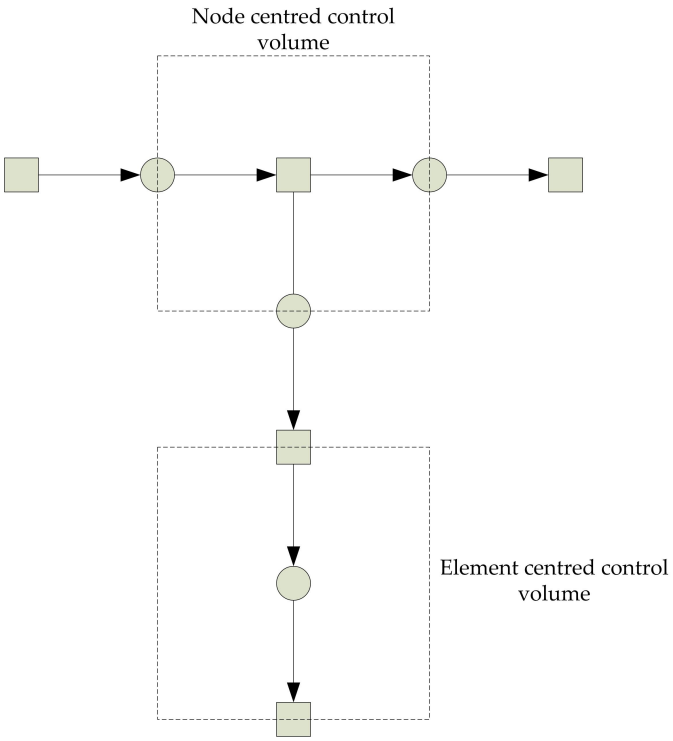

Figure 5.3: Two types of control volumes

Continuity equation

The continuity or conservation of mass equation states that the rate of change of the mass in the control volume is zero. The conservation of mass for a control volume is given as [67]:

$$\frac{\partial}{\partial t}\int_{\text{CV}} \rho \, dV + \int_{\text{CS}} \rho \mathbf{v} \cdot \hat{\mathbf{n}} \, dA = 0. \tag{5.1}$$

The first term of Eq. (5.1) gives the change of mass of the contents in the control volume, where ρ is the density and V is the volume. The second term gives the net rate of mass flow through the control surface (CS). The integrand of the second term contains the product of the normal component of velocity, $\mathbf{v} \cdot \hat{\mathbf{n}}$, with respect to the control surface. The product, $\rho \mathbf{v} \cdot \hat{\mathbf{n}}$, is the one-dimensional mass flow rate through the cross-sectional area of the control volume. Replacing the integration with summation, the mass conservation equation for the control volume can be written as:

$$\frac{dM_i}{dt} = \sum (Av\rho)_{j-1} - \sum (Av\rho)_j = \dot{m}_{j-1} - \dot{m}_j, \tag{5.2}$$

where M_i is the mass in the i-th control volume and $\dot{m}_{j-1}$ and $\dot{m}_j$ represents the mass flow entering and leaving the control volume respectively. The variables most often used in the hydraulic domain and which also form the state variables are the pressure, P, and mass flow rate, $\dot{m}$. It is therefore desirable to introduce the pressure variable into Eq. (5.2),

$$\frac{dM_i}{dP_i}\frac{dP_i}{dt} = \dot{m}_{j-1} - \dot{m}_j \tag{5.3}$$

and finally

$$\frac{dP_i}{dt} = \frac{1}{C_h}(\dot{m}_{j-1} - \dot{m}_j) \tag{5.4}$$

where

$$C_h = dM_i/dP_i = V_i(d\rho_i/dP_i) \tag{5.5}$$

is called the hydraulic capacitance element. It is an element that describes the compressibility of the fluid. The hydraulic capacitance may also be written in terms of the bulk modulus, B,

$$C_h = \rho_i V_i / B \tag{5.6}$$

Momentum equation

The next governing equation that will be considered is the momentum equation, also known as Newton's second law of motion. It states that the time rate of change of the momentum of the fluid in the control volume is equal to the sum of external forces acting on the fluid. The momentum equation is given as [67]:

$$\frac{\partial}{\partial t}\int_{\text{CV}} \mathbf{v}\rho \, dV = -\int_{\text{CS}} \mathbf{v}\rho \mathbf{v} \cdot \hat{\mathbf{n}} \, dA + \int_{\text{CS}} \bar{\tau} \, dA + \int_{\text{CV}} \bar{\beta}\rho dV \tag{5.7}$$

The term on the left of Eq. (5.7) is the time rate of change of the linear momentum of the contents in the control volume. The first term on the right gives the rate of linear momentum

flow through the control surface. The second term gives the total surface-force distribution acting on the control surface. Surface forces arise from direct contact between a body and the surrounding media. The third term gives the total body-force distribution acting on the fluid inside the control volume. Body forces are those forces acting on matter without the requirement of direct contact. Gravitational force on a body is the most common body-force distribution. After integrating and rewriting, Eq. (5.7) is written as:

$$\ell_j \frac{d\dot{m}_j}{dt} = P_i A_j - P_{i+1} A_j - A_j \, \kappa_j \, |\dot{m}_j| \dot{m}_j + A_j \, \rho_j \, g(z_i - z_{i+1}) \tag{5.8}$$

where ℓ_j is the length between the nodes i and $i+1$ and κ_j is a friction factor. The gravitational constant is given by g and $(z_i - z_{i+1})$ is the elevation difference between two nodes. Eq. (5.8) may then be written as:

$$\frac{d\dot{m}_j}{dt} = \frac{1}{L_h}(P_i - P_{i+1}) - \frac{R_h}{L_h}\dot{m}_j + \frac{1}{L_h} S_{eh}, \tag{5.9}$$

where

$$R_h = \kappa_j \, |\dot{m}_j| = \frac{f \, \ell_j / D_j + K}{2 \, A_j^2 \, \rho_j} |\dot{m}_j|, \tag{5.10}$$

$$L_h = \frac{\ell_j}{A_j} \tag{5.11}$$

and

$$S_{eh} = \rho_j g (z_i - z_{i+1}) = \rho_j g \Delta z_j. \tag{5.12}$$

R_h is a hydraulic resistance element and L_h is a hydraulic inductance element, where *f* is the Darcy-Weisbach friction factor, *K* is the secondary loss factor and D_j is the diameter.

Consider an example of a simple hydraulic network representation of a pipe section in Fig. 5.4.

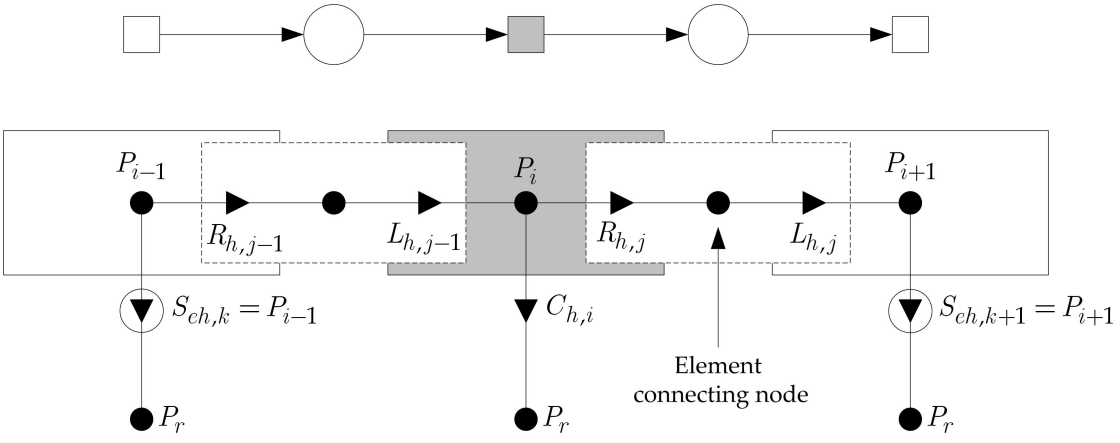

Figure 5.4: Hydraulic network of a pipe section

The pressure source elements at the end points represent boundary pressure variables. There are two types of source elements in the hydraulic domain, namely a pressure source S_{eh} and a mass flow source S_{fh}, where the e and f indicate the generalised variables (effort and flow) and h indicates the hydraulic domain. k is the source index. Sources may also represent elements such as a pump (flow source) or an elevation head (effort source). The hydraulic capacitance element models mass storage. The hydraulic resistance and inductance elements model the friction and momentum phenomena between the control volumes.

Table 5.1 summarises the generalised hydraulic elements.

Table 5.1: Summary of generalised hydraulic elements

Element description	R_h	L_h	C_h	S_{eh}	S_{fh}
Pressure source	-	-	-	P_i	-
Elevation head	-	-	-	$\rho_j g(z_i - z_{i+1})$	-
Mass flow source	-	-	-	-	$\dot{m}_j$
Hydraulic resistance	$\frac{f\,\ell_j/D_j+K}{2\,A_j^2\,\rho_j}\lvert\dot{m}_j\rvert$	-	-	-	-
Hydraulic inductance	-	$\frac{\ell_j}{A_j}$	-	-	-
Hydraulic capacitance	-	-	$V_i(d\rho_i/dP_i)$	-	-

Energy equation

The energy conservation equation, also known as the first law of thermodynamics states that the time rate of increase of the total energy stored in the control volume is equal to the net time rate of energy addition by heat transfer into the control volume plus the net time rate of energy addition by work transfer to the control volume. The energy equation for a fixed control volume is given by

$$\frac{\partial}{\partial t}\int_{\text{CV}} e\rho\, dV = -\int_{\text{CS}} e\rho\mathbf{v}\cdot\hat{\mathbf{n}}\, dA + \dot{Q} + \dot{W}, \tag{5.13}$$

where e is the total stored energy per unit mass. The heat transfer rate, $\dot{Q}$, represents all the ways in which energy is exchanged between the control volume contents and the surroundings because of temperature difference, and $\dot{W}$ represents the rate of work done on the control volume. In this case the energy due to work will be neglected. Eq. (5.13) can be written in terms of enthalpy values and the different heat transfer processes as follows

$$V_i\rho_i\frac{dh_i}{dt} = \sum(\dot{m}_{j-1}h_{i-1}) - \sum(\dot{m}_j h_i) + \dot{Q}_{\text{cond}} + \dot{Q}_{\text{conv}} + \dot{Q}_{\text{rad}} + \dot{Q}_{\text{gen}}, \tag{5.14}$$

where $\dot{Q}_{\text{cond}}$, $\dot{Q}_{\text{conv}}$ and $\dot{Q}_{\text{rad}}$ represent heat transfer by means of conduction, convection and radiation. $\dot{Q}_{\text{gen}}$ represents heat generation inside the control volume and $\sum(\dot{m}_{j-1}h_{i-1})$ and $\sum(\dot{m}_j h_i)$ represent the flow streams in and out of the control volume, each representing a loss or gain of enthalpy for the control volume. When an ideal gas is considered Eq. (5.14) may be written in terms of temperature values, knowing that $h = c_pT$:

$$V_i\rho_i c_p\frac{dT_i}{dt} = \sum(\dot{m}_{j-1}c_pT_{i-1}) - \sum(\dot{m}_j c_pT_i) + \dot{Q}_{\text{cond}} + \dot{Q}_{\text{conv}} + \dot{Q}_{\text{rad}} + \dot{Q}_{\text{gen}}. \tag{5.15}$$

The state variable pair for the thermal domain is enthalpy h or temperature T and energy flow, $\dot{w}$. Energy flow can be defined as

$$\dot{w} = \dot{m}h = \dot{m}c_pT. \tag{5.16}$$

Energy flow is also equivalent to energy heat transfer rate $\dot{Q}$ and therefore $\dot{w} = \dot{Q}$. Eq. (5.15) may be written in terms of temperature and energy flow as follows

$$\frac{dT_i}{dt} = \frac{1}{C_t}\dot{w}_{j-1} - \frac{1}{R_tC_t}T_i + \frac{1}{C_t}(\dot{w}_{\text{cond}} + \dot{w}_{\text{conv}} + \dot{w}_{\text{rad}} + \dot{w}_{\text{gen}}), \tag{5.17}$$

where

$$C_t = V_i\rho_i c_p \tag{5.18}$$

and

$$R_t = 1/\dot{m}_j c_p \tag{5.19}$$

are the generalised thermal resistance and capacitance elements respectively.

Conduction is the mode of heat transfer where a temperature difference is present in a solid material or fluid when there is no bulk motion present. When heat transfer through conduction takes place, $\dot{w}_{\text{cond}} \neq 0$, and is given by

$$\dot{w}_{\text{cond}} = \frac{1}{R_{t,\text{cond}}}(T_{\text{cond}} - T_i) \tag{5.20}$$

and

$$R_{t,\text{cond}} = \ell/(k_cA), \tag{5.21}$$

where T_{cond} is the temperature of the adjacent control volume with which heat is exchanged by conduction. $R_{t,\text{cond}}$ represents the generalised thermal resistance due to conduction.

Convective heat transfer is caused by energy transferred by the bulk of a fluid in addition to diffusive heat transfer by molecular motion. When heat transfer through convection takes place, $\dot{w}_{\text{conv}} \neq 0$, and is given by

$$\dot{w}_{\text{conv}} = \frac{1}{R_{t,\text{conv}}}(T_{\text{conv}} - T_i) \tag{5.22}$$

and

$$R_{t,\text{conv}} = 1/(h_NA), \tag{5.23}$$

where T_{conv} is the temperature of the adjacent control volume with which heat is exchanged by convection. $R_{t,\text{conv}}$ in this case represents the generalised thermal resistance due to convection.

Radiation heat transfer is caused by energy transferred by means of magnetic waves. When energy is transferred by means of radiation, $\dot{w}_{\text{rad}} \neq 0$, and is given by

$$\dot{w}_{\text{rad}} = \varepsilon A\sigma(T_{i-1}^4 - T_i^4) = S_{ft} \tag{5.24}$$

where S_{ft} is a generalised thermal flow source.

Consider an example of a thermal network of a pipe section in Fig. 5.5. The generalised capacitance element, C_t, models thermal energy storage in the control volumes.

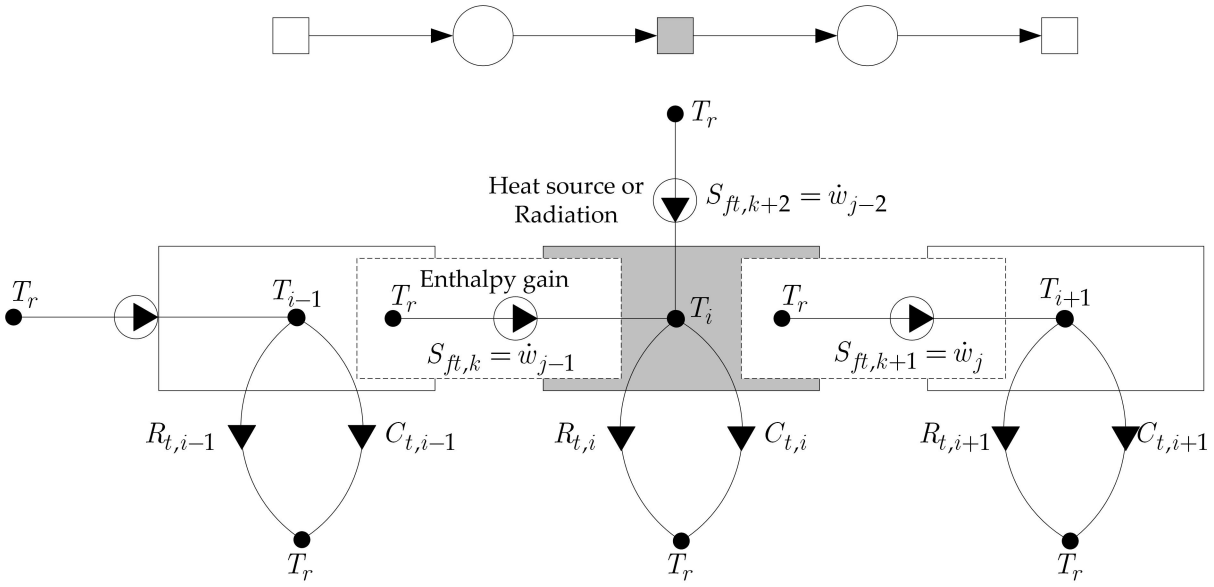

Figure 5.5: Thermal network of a pipe section

The resistance elements, R_t, can model enthalpy losses, conduction and convection. These elements are connected in parallel with the capacitance element giving rise to the equation forms of Eqs. (5.19), (5.21) and (5.23). Enthalpy gains, energy generation and radiation can be modelled with generalised thermal flow sources, S_{ft}. T_r is a reference temperature. Table 5.2 summarises the generalised thermal elements.

Table 5.2: Summary of generalised thermal elements

Element description	R_t	L_t	C_t	S_{et}	S_{ft}
Energy source	-	-	-	-	$\dot{w}_j$
Enthalpy gain	-	-	-	-	$\dot{w}_j$
Radiation	-	-	-	-	$\varepsilon A\sigma(T_i^4 - T_{i+1}^4)$
Enthalpy loss	$1/\dot{m}_j c_p$	-	-	-	-
Conduction	$\ell/(k_c A)$	-	-	-	-
Convection	$1/(h_N A)$	-	-	-	-
Thermal capacitance	-	-	$V_i \rho_i c_p$	-	-

5.2.2 Turbomachines and shafts in terms of generalised elements

The dynamics of compressors and turbines are modelled empirically by using their performance characteristic maps [10, 68, 69, 70]. Fig. 5.6 and Fig. 5.7 are typical examples of the pressure ratio and efficiency maps used for modelling compressors and turbines. This means that compressor and turbine models can be seen as mappings of input variables to output variables. From [69, 70, 71] it follows that the compressor and turbine models are dependent on the following variables:

- N = Speed of the machine shaft (in rev/s)
- $\dot{m}$ = Mass flow rate (in kg/s)
- P_{01} = Total inlet pressure (in bar)
- P_{02} = Total outlet pressure (in bar)
- T_{01} = Total inlet temperature (in K)
- T_{02} = Total outlet temperature (in K)

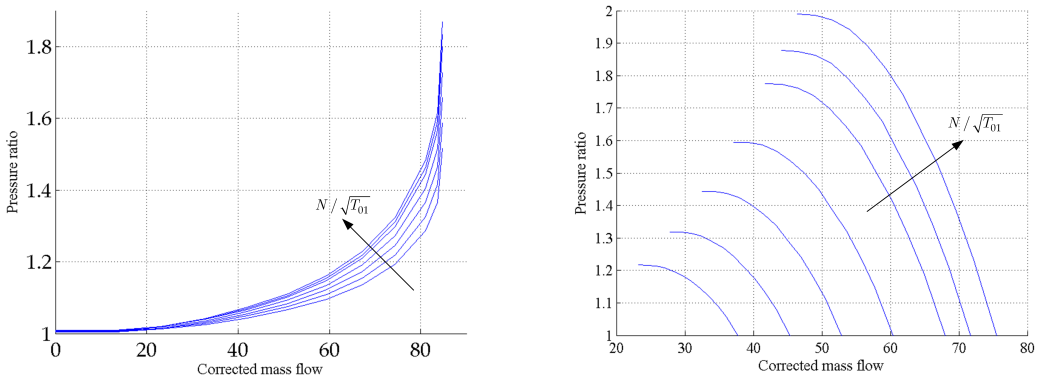

(a) (b)

Figure 5.6: Pressure ratio curve maps: (a) Turbine (b) Compressor [12]

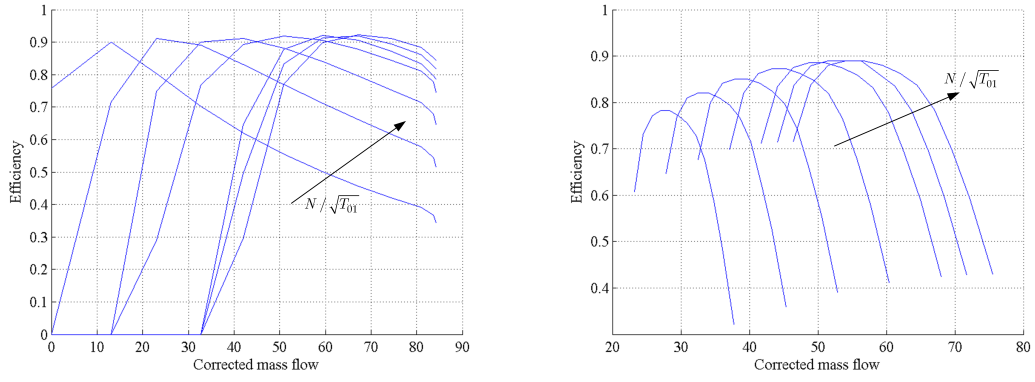

(a) (b)

Figure 5.7: Efficiency curve maps: (a) Turbine (b) Compressor [12]

The number of variables can be reduced by making use of dimensional analysis [67, 70]. The reduction leads to four non-dimensional parameters namely the pressure ratio P_r, isentropic efficiency η, non-dimensional mass flow Q' and non-dimensional speed N'. The mapping between these variables for a turbomachine is given as

$$\Omega(P_r, \eta, Q', N') = 0. \tag{5.25}$$

For the compressor the pressure ratio is defined as

$$P_{rc} = \frac{P_{02}}{P_{01}}, \tag{5.26}$$

and for the turbine the pressure ratio is defined as

$$P_{rt} = \frac{P_{01}}{P_{02}}. \tag{5.27}$$

Using isentropic flow relations, the isentropic efficiency for a compressor is defined as

$$\eta_c = \frac{P_{rc}^{(\frac{\gamma-1}{\gamma})} - 1}{T_{02}/T_{01} - 1}, \tag{5.28}$$

and the isentropic efficiency for the turbine is defined as

$$\eta_t = \frac{T_{02}/T_{01} - 1}{P_{rt}^{-(\frac{\gamma-1}{\gamma})} - 1}, \tag{5.29}$$

where γ is the specific heat ratio. It is defined in terms of the specific heat at constant pressure and constant volume as follows:

$$\gamma = \frac{c_p}{c_v}. \tag{5.30}$$

The non-dimensional mass flow and non-dimensional speed for both machines are defined as

$$Q' = \frac{\dot{m}\sqrt{T_{01}}}{P_{01}} \tag{5.31}$$

and

$$N' = \frac{N}{\sqrt{T_{01}}} \tag{5.32}$$

respectively. It should be noted that although the last two parameters carry the name non-dimensional, they are not dimensionless.

According to references [12, 70], a number of basic assumptions need to be made regarding models (linear or non-linear) of turbomachines:

1. One-dimensional flow is assumed at the turbomachine inlet and outlet.
2. There is no significant volume inside, or at the inlet and outlet of the machine. This means that mass and energy storage inside the machine is not allowed.
3. Adiabatic conditions are assumed. There is no energy exchange between the machine and its environment except via the fluid flowing through the machine and the shaft.
4. The performance maps of the machines are steady state maps. It is assumed that these maps can be used for transient conditions as well [69, 70].
5. The shaft dynamics are not part of the turbine and compressor models. The shaft dynamics are modelled separately.

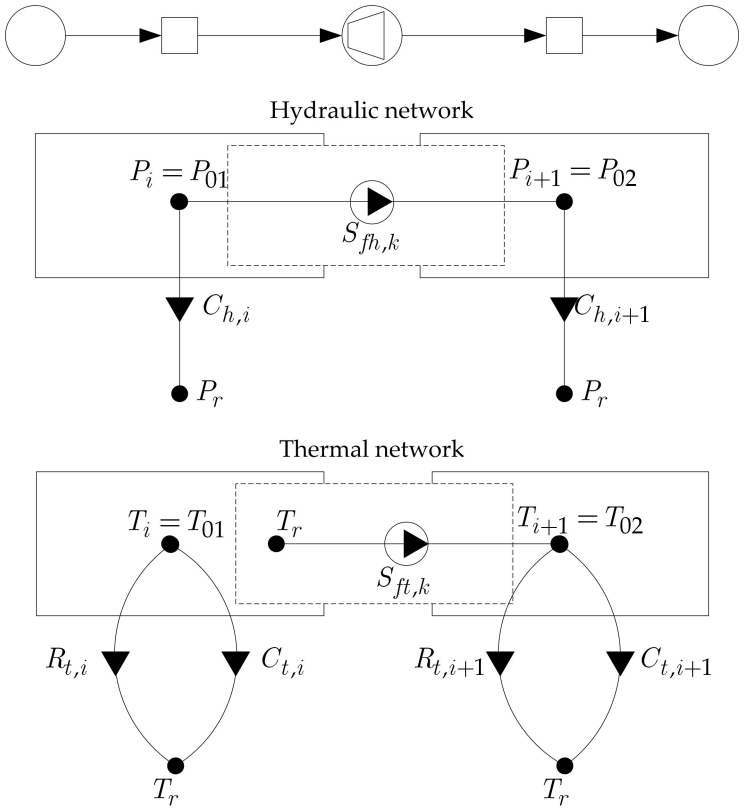

Figure 5.8: Generalised element modelling of turbomachines

With regards to assumption 2 a turbomachine cannot be modelled using generalised inductive or capacitive elements since it does not store any energy. It is therefore appropriate to model these machines as generalised sources. Fig. 5.8 shows the hydraulic and thermal generalised element representations of a turbomachine.

In the hydraulic domain the turbomachine is modelled as a flow source given by

$$S_{fh} = Q'(\sqrt{T_{01}}/P_{01})^{-1}. \tag{5.33}$$

The turbomachine is modelled as flow source in the thermal domain as well, but the source terms differ for compressors and turbines. For a turbine the flow source is given by

$$S_{ft} = T_{01} - \eta_t T_{01}(1 - P_{rt}^{-(\frac{\gamma-1}{\gamma})}), \tag{5.34}$$

and for a compressor it is given by

$$S_{ft} = T_{01} - 1/\eta_c T_{01}(1 - P_{rc}^{(\frac{\gamma-1}{\gamma})}). \tag{5.35}$$

The shafts in a thermalhydraulic system are the energy storage elements in the mechanical domain. The turbine and compressor models will be used to calculate the compressor and turbine power transfers on the shaft. The calculated powers are used in the calculation of the shaft speeds using Newton's second law of motion which states that the time rate of

change of the momentum of a shaft is equal to the sum of external forces acting on the shaft. Angular momentum is defined as inertia J times angular velocity ω and therefore the angular momentum equation for the shaft is given as

$$\frac{\partial}{\partial t}(J\omega) = \sum \tau_{\text{net}}, \tag{5.36}$$

where τ_{net} is the net accelerating torque on the shaft. For a shaft with external torques acting on it at each end as in the case of a compressor-turbine combination shown in Fig. 5.9, Eq. (5.36) may be written as

$$\frac{\partial \omega}{\partial t} = \frac{(\tau_t - \tau_c)}{(J_{\text{shaft}} + J_t + J_c)}, \tag{5.37}$$

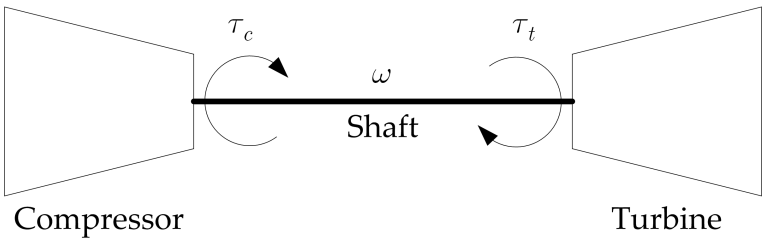

Figure 5.9: Compressor-turbine combination

where τ_c and τ_t are the torques acting on the shaft due to the compressor and turbine respectively. The power of the rotating shaft is related to the torque acting on the shaft by

$$\dot{W} = \tau\omega, \tag{5.38}$$

and Eq. (5.37) can be rewritten as

$$\frac{\partial \omega}{\partial t} = \frac{\eta_m \dot{W}_t - \eta_m \dot{W}_c}{\omega(J_{\text{shaft}} + J_t + J_c)}, \tag{5.39}$$

where η_m is the mechanical efficiency of the shaft. The mechanical efficiency takes into account the friction losses in both the turbine and compressor. The power of each machine can be calculated using

$$\dot{W} = \dot{m} C_p (T_{01} - T_{02}). \tag{5.40}$$

Considering Fig. 5.10, Eq. (5.39) can be written in terms of generalised elements as follows:

$$\frac{\partial \omega_i}{\partial t} = \frac{1}{C_{m,i}}(S_{fm,k} - S_{fm,k+1}), \tag{5.41}$$

where the turbine power is represented as a mechanical flow source

$$S_{fm,k} = \eta_m \dot{W}_t / \omega_i, \tag{5.42}$$

the compressor power is represented as a mechanical flow source

$$S_{fm,k+1} = \eta_m \dot{W}_c / \omega_i, \tag{5.43}$$

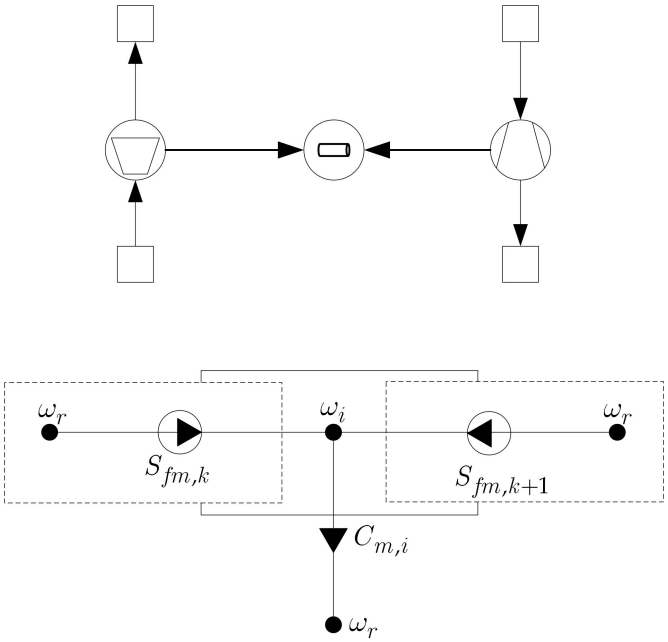

Figure 5.10: Mechanical network representation of a shaft

and the mechanical capacitance is given by

$$C_{m,i} = J_{\text{shaft}} + J_t + J_c. \tag{5.44}$$

It is interesting to notice that machines such as pumps, turbines and compressors are part of both thermodynamic and mechanical domains. Table 5.3 summarises the generalised components for rotating masses in terms of the different domains.

Table 5.3: Summary of generalised elements of rotating masses

Element description	R	L	C	S_e	S_f
Hydraulic source (Turb. or Comp.)	-	-	-	-	$Q'(\sqrt{T_{01}}/P_{01})^{-1}$
Thermal source (Turb.)	-	-	-	-	$T_{01} - \eta_t T_{01}(1 - P_{rt}^{-(\frac{\gamma-1}{\gamma})})$
Thermal source (Comp.)	-	-	-	-	$T_{01} - 1/\eta_c T_{01}(1 - P_{rc}^{(\frac{\gamma-1}{\gamma})})$
Mechanical flow source (Turb)	-	-	-	-	$\eta_m \dot{W}_t/\omega_i$
Mechanical flow source (Comp)	-	-	-	-	$\eta_m \dot{W}_c/\omega_i$
Mechanical capacitance	-	-	$J_{\text{shaft}} + J_t + J_c$	-	-

5.3 Thermohydraulic applications

5.3.1 State space model extraction of a U-tube

An interesting and commonly studied situation in thermohydraulic systems, is fluid motion without any external forcing condition (such as a pump). Such a situation is known as free or natural convection. This situation occurs due to a density gradient in the fluid caused by temperature differences. The net effect of the density gradient is a buoyancy force which induces convection currents. There are many thermohydraulic applications that utilise natural convection. One ingenious application is a Reactor Cavity Cooling System (RCCS). The basic concept of a RCCS system can be represented by a U-tube. The state space models of the different domains of a U-tube will be extracted automatically using the algorithm discussed in Chapter 4. The state space models will be solved in a specific order using standard *Matlab*® differential equation solvers. The models will be validated by comparing the solution results with results obtained from *Flownex*®.

Physical system description

The RCCS is a network of pipes surrounding a nuclear Reactor Pressure Vessel (RPV) wall as shown in Fig. 5.11. During normal operation water is circulated through the pipe network by means of forced convection (pumps), but provision is made in case of a Loss of Flow Accident (LOFA). Such a scenario may be due to a catastrophic mechanical failure of the pumps or due to the loss of power. This scenario is also called the passive operation mode of the RCCS, during which water will still be able to circulate through the pipes due to natural convection [13, 46].

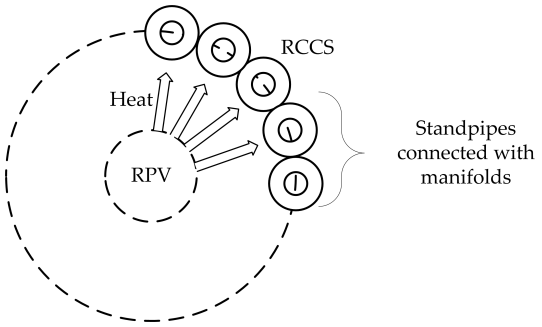

Figure 5.11: RCCS pipe network surrounding the RPV [13]

Two standpipes of the RCCS are shown in Fig. 5.12. Cold water enters the standpipe through an inlet manifold. The riser pipe is exposed to the heat radiated from the RPV which causes the water in the riser pipe to be less dense. The cold, more dense water in the downcomer pushes the water in the riser up into the outlet manifold. The water circulates due to natural convection. A standpipe may be viewed as a U-tube where one leg has a fixed temperature and the other leg is exposed to a heat source and both ends of the U-tube have the same pressure reference.

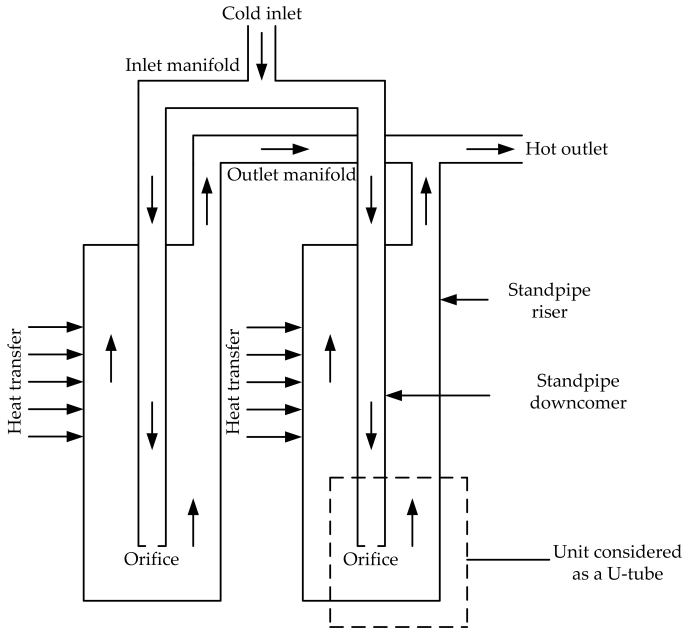

Figure 5.12: Two standpipes of the RCCS [13]

Consider a representation of a U-tube in Fig. 5.13. In the actual system the hot outlet is fed to heat exchangers and storage tanks. Taking this into account it will be assumed that the inlet and outlet of the U-tube are connected to an infinite heat sink. The inlet temperature can therefore be fixed at 15 °C. The RCCS system is open to the atmosphere and therefore the inlet and outlet pressure of the U-tube is fixed at 100 kPa. A constant heat transfer rate of 1 kW will be applied to the riser of the U-tube, simulating the heat radiated from the RPV wall. For illustrative purposes the U-tube will be discretised into four control volumes as shown in Fig. 5.13. Only a small part of the actual system is considered and hence the length and the diameter of the U-tube are chosen to be 0.6 m and 0.02 m respectively.

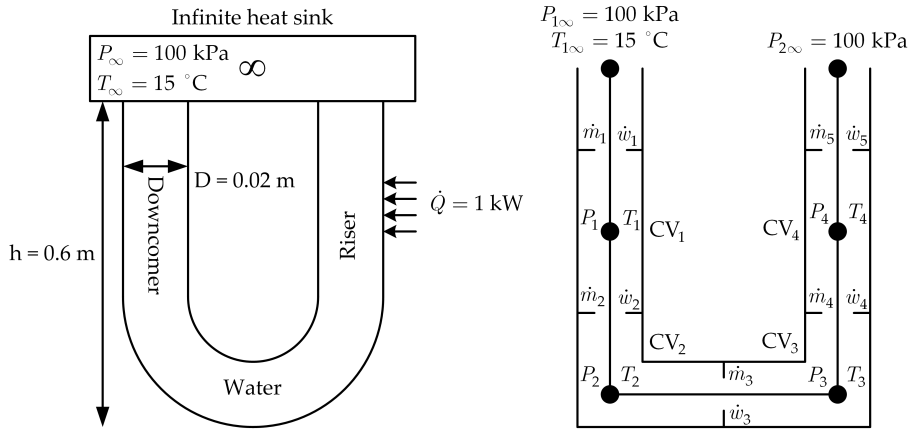

Figure 5.13: Representation of the U-tube and a conceptual view of the control volumes

The hydraulic and thermal behaviours of the U-tube will be represented by two state space models extracted from hydraulic and thermal networks respectively. These two state space

models are coupled by the mass flow rate through the U-tube. The hydraulic network of the U-tube is shown in Fig. 5.14. The atmospheric pressure at the input and output of the U-tube are modelled by hydraulic pressure sources ($S_{eh,1}, S_{eh,2}$). Natural convection is initiated when a body force acts on the fluid in which there are density gradients. This body force is due to gravitation [14]. This body force is modelled as a hydraulic effort source given by

$$S_{eh,k} = \rho_j g \Delta z_j \tag{5.45}$$

where

- k is the index of the sources modelling the body forces,
- ρ_j is the mean density between two nodes,
- g is the gravitational constant, and
- Δz_j is the height difference between two nodes.

In Fig. 5.14 it can be seen that the energy flow direction of the sources are in the opposite direction of the the other elements. This is to indicate that these sources are effort sources.

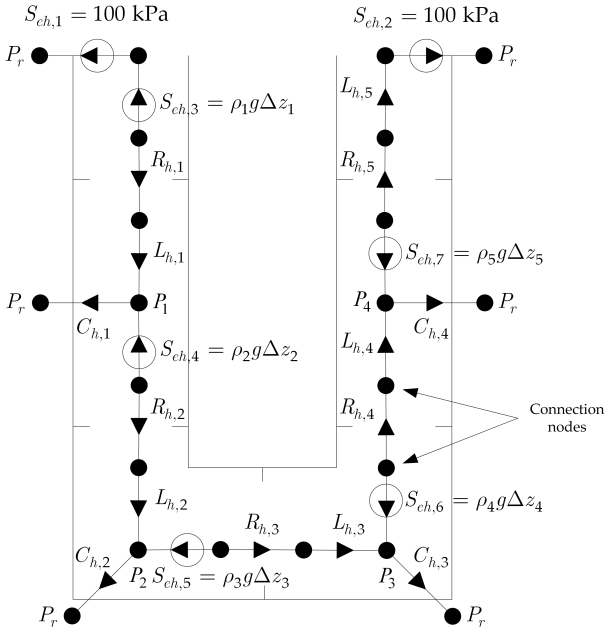

Figure 5.14: Hydraulic network of the U-tube

The hydraulic network is used to construct an incidence matrix (as described in Chapter 4) representing the structure of the hydraulic domain. Each hydraulic element has a specific elemental equation. All the elemental equations are also represented in matrix form. By applying the state space model extraction algorithm to the incidence and elemental matrices a symbolic hydraulic state space model is extracted (See appendix C). The hydraulic state space model is given by

$$\dot{\mathbf{X}}_h = \mathbf{A}_h(\mathbf{X}_h, t)\mathbf{X}_h + \mathbf{B}_h(t)\mathbf{U}_h \tag{5.46}$$

where

$$\mathbf{X}_h = \begin{bmatrix} P_1 & \dots & P_4 & \dot{m}_1 & \dots & \dot{m}_5 \end{bmatrix}' \tag{5.47}$$

$$\mathbf{U}_h = \begin{bmatrix} S_{eh,1} & \dots & S_{eh,7} \end{bmatrix}' \tag{5.48}$$

$$\mathbf{A}_h = \begin{bmatrix} 0 & 0 & \dots & 1/C_{h,1} & -1/C_{h,1} & 0 & \dots \\ 0 & 0 & \dots & 0 & 1/C_{h,2} & -1/C_{h,2} & \dots \\ 0 & 0 & \dots & 0 & 0 & 1/C_{h,3} & \dots \\ 0 & 0 & \dots & 0 & 0 & 0 & \dots \\ -1/L_{h,1} & 0 & \dots & -R_{h,1}/L_{h,1} & 0 & 0 & \dots \\ 1/L_{h,2} & -1/L_{h,2} & \dots & 0 & -R_{h,2}/L_{h,2} & 0 & \dots \\ 0 & 1/L_{h,3} & \dots & 0 & 0 & -R_{h,3}/L_{h,3} & \dots \\ 0 & 0 & \dots & 0 & 0 & 0 & \dots \\ 0 & 0 & \dots & 0 & 0 & 0 & \dots \end{bmatrix} \tag{5.49}$$

$$\mathbf{B}_h = \begin{bmatrix} 0 & 0 & 0 & 0 & \dots \\ 0 & 0 & 0 & 0 & \dots \\ 0 & 0 & 0 & 0 & \dots \\ 0 & 0 & 0 & 0 & \dots \\ 1/L_{h,1} & 0 & 1/L_{h,1} & 0 & \dots \\ 0 & 0 & 0 & 1/L_{h,2} & \dots \\ 0 & 0 & 0 & 0 & \dots \\ 0 & 0 & 0 & 0 & \dots \\ 0 & -1/L_{h,5} & 0 & 0 & \dots \end{bmatrix} \tag{5.50}$$

The state vector, $\mathbf{X}_h \in \mathbb{R}^{9\times 1}$, contains four internal pressures and five mass flow rates. The input vector, $\mathbf{U}_h \in \mathbb{R}^{7\times 1}$, contains the two effort sources representing the boundary pressures and five effort sources representing the body forces due to gravitation. The fragmented representations of $\mathbf{A}_h \in \mathbb{R}^{9\times 9}$ and $\mathbf{B}_h \in \mathbb{R}^{9\times 7}$ given in (5.49) and (5.50) contain resistive, capacitive and inductive elements that are time varying (due to densities that vary with time) and nonlinear (the resistive elements are dependent on the mass flow rate, Eq. (5.10)).

The thermal network of the U-tube is shown in Fig. 5.15. The energy flows between control volumes are represented by the energy flow sources $S_{ft,1}, \dots, S_{ft,4}$. These energy flow sources as well as the thermal resistances are functions of the mass flow rates that are calculated from the hydraulic state space model. The energy flow sources $S_{ft,5}, \dots, S_{ft,8}$ represent the external energy transfer.

By applying the state space model extraction algorithm a symbolic thermal state space model is extracted (See appendix C). The thermal state space model is given by

$$\dot{\mathbf{X}}_t = \mathbf{A}_t(t)\mathbf{X}_t + \mathbf{B}_t(t)\mathbf{U}_t \tag{5.51}$$

where

$$\mathbf{X}_t = \begin{bmatrix} T_1 & T_2 & T_3 & T4 \end{bmatrix}' \tag{5.52}$$

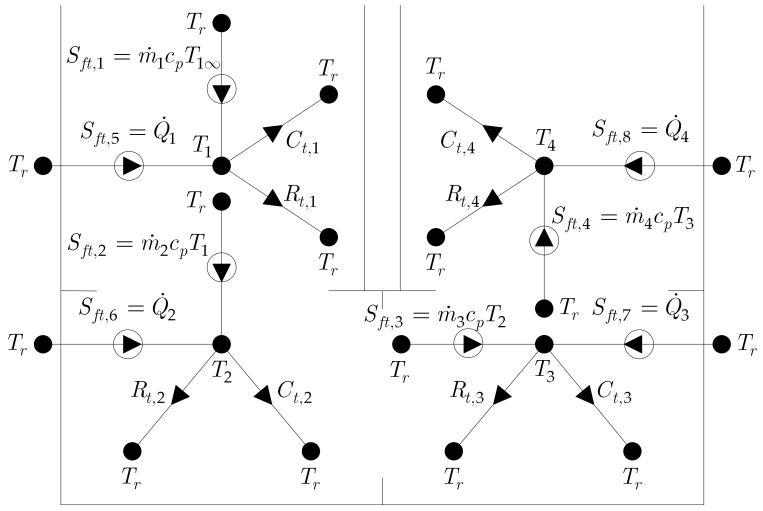

Figure 5.15: Thermal network of the U-tube

$$\mathbf{U}_t = \begin{bmatrix} S_{ft,1} & \dots & S_{ft,8} \end{bmatrix}' \tag{5.53}$$

$$\mathbf{A}_t = \begin{bmatrix} -1/C_{t,1}/R_{t,1} & 0 & 0 & 0 \\ 0 & -1/C_{t,2}/R_{t,2} & 0 & 0 \\ 0 & 0 & -1/C_{t,3}/R_{t,3} & 0 \\ 0 & 0 & 0 & -1/C_{t,4}/R_{t,4} \end{bmatrix} \tag{5.54}$$

$$\mathbf{B}_t = \begin{bmatrix} 1/C_{t,1} & 0 & \dots & 1/C_{t,1} & 0 & \dots \\ 0 & 1/C_{t,2} & \dots & 0 & 1/C_{t,2} & \dots \\ 0 & 0 & \dots & 0 & 0 & \dots \\ 0 & 0 & \dots & 0 & 0 & \dots \end{bmatrix} \tag{5.55}$$

The state vector, $\mathbf{X}_t \in \mathbb{R}^{4\times1}$, contains the four internal temperatures. The input vector, $\mathbf{U}_t \in \mathbb{R}^{8\times1}$, contains four energy flow sources representing the internal heat transfer and another four representing external heat transfer. The matrices $\mathbf{A}_t \in \mathbb{R}^{4\times4}$ and $\mathbf{B}_t \in \mathbb{R}^{4\times8}$ are time-varying due to the fact that the thermal resistance, $R_{t,i}$, depends on the mass flow rate and the thermal capacitances, $C_{t,i}$, on the density.

Fig. 5.16 shows the information flow between the different domains. The mass flow rate values are determined from the momentum equation. Mass flow rate and density are used to calculate the pressure values by means of the continuity equation. The density is calculated by means of correlations. The correlations are dependent on the enthalpy (or temperature) and pressure values. The enthalpy (or temperature) values are calculated using the energy equation. The energy equation is dependent on the mass flow rate. As illustrated in Fig. 5.16 the density connects the hydraulic and thermal domains.

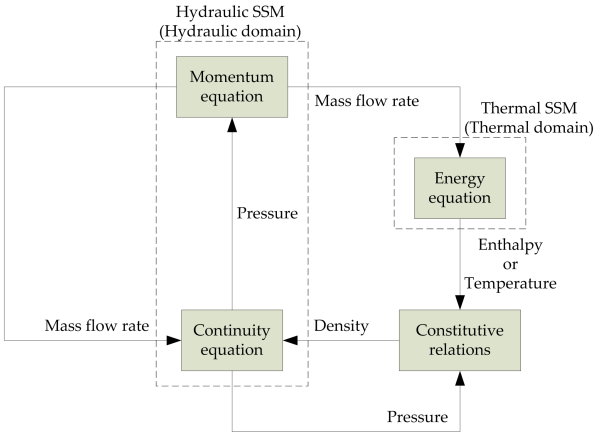

Figure 5.16: Information flow between domains

Model validation

Validation of the extracted state space models is crucial to ensure its suitability for control purposes. The approach followed from the physical system description up to a final model is portrayed in Fig. 5.17.

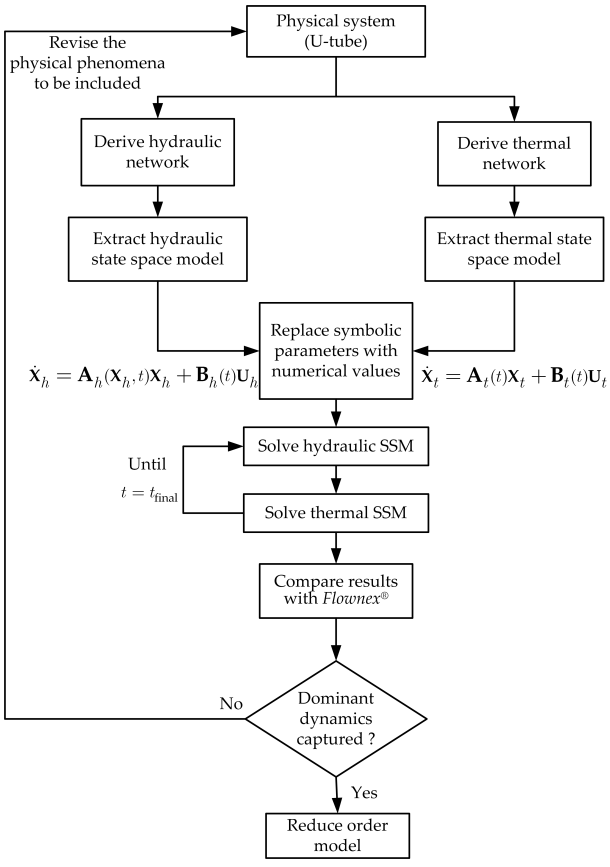

Figure 5.17: Methodology for reduced order model extraction and validation (U-tube)

Once the state space models for the different domains have been extracted in symbolic form, the symbolic parameters are substituted with numerical values. The state space models are solved in a specific order. The hydraulic state space model is solved first to calculate the mass flow rate used in the thermal state space model to calculate the temperatures. The solution is compared with results obtained from *Flownex*®. *Flownex*® is an advanced and extensively validated commercial thermohydraulic simulation package and is therefore used for validation of the state space models. The accuracy of the state space model is quantified by using the Integral of the Absolute magnitude of the Error (IAE) performance index. This particular index was used since it is widely used in modelling and computer simulation studies [66]. The Integral of Time multiplied by Absolute Error (ITAE) is used in control studies.

For natural convection to take place, density gradients have to exist. The density profiles of the downcomer and riser pipes are shown in Fig. 5.18 and were obtained from a *Flownex*® simulation. These density profiles are used when solving the state space model of the U-tube. It can be seen that the density of the water in the downcomer stays constant while the density of the water in the riser decreases as heat transfer takes place. The heat source was activated at time $t = 5$ s.

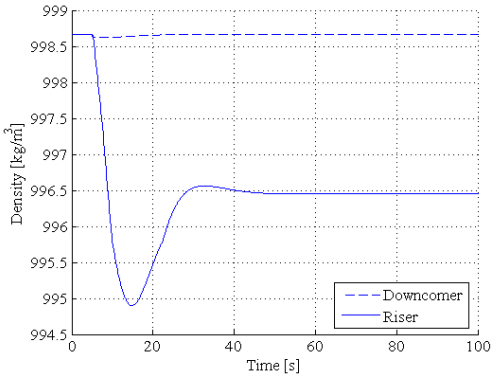

Figure 5.18: Downcomer and riser densities

Fig. 5.19 shows the temperature of the water in the riser pipe with respect to time. The temperature values calculated by solving the state space model compares well with the temperature values obtained from *Flownex*®.

Fig. 5.20 shows good correlation between the flow rate values obtained from the state space model and *Flownex*®. The calculated internal pressures are summarised in Table 5.4 and also show good correlation.

Table 5.4: Calculated internal pressures

Internal pressure	*Flownex*® (kPa)	State space model (kPa)
P_1	102.936	102.937
P_2	105.871	105.874
P_3	105.870	105.873
P_4	102.933	102.934

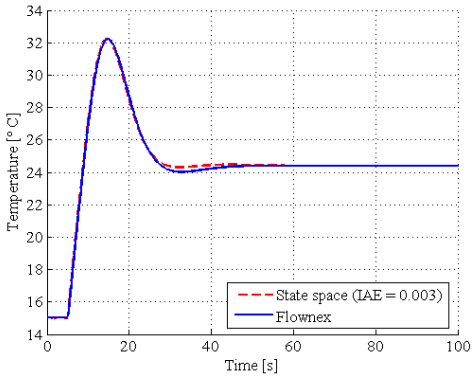

Figure 5.19: Temperature in the riser pipe

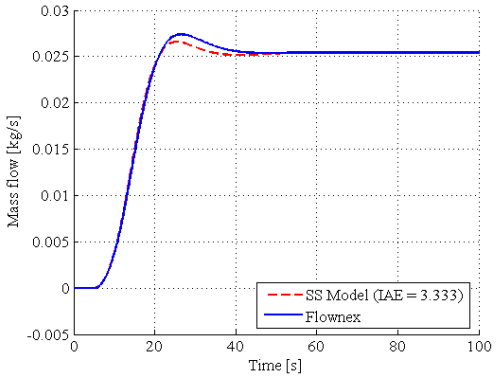

Figure 5.20: Mass flow rate due to natural convection

The smaller the value of the IAE performance index, the better the correlation between the state space model and *Flownex*®. The performance index also gives an indication if the state space model does portray the dominant dynamics of the actual system. The small difference between the state space model and *Flownex*® is due to the coarse lumping used in the state space extraction method.

5.3.2 State space model extraction of a heat exchanger

Heat exchanger applications can be found in many industries, for example in chemical processing, power plants and ventilation systems. A heat exchanger is a thermohydraulic device that exchanges heat between two fluids characterised by different temperatures. Heat exchangers can be classified according to their flow arrangement and type of construction. In this case a concentric tube construction is considered as shown in Fig. 5.21. In the parallel-flow arrangement the hot and cold fluids enter at the same end, and in the counterflow arrangement the fluids enter and leave at opposite ends [14].

A heat exchanger can be seen as a thermohydraulic network consisting of smaller heat

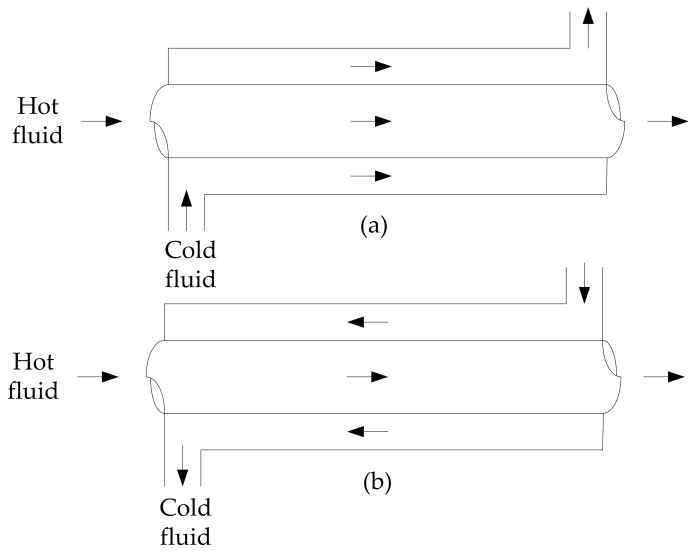

Figure 5.21: Concentric tube heat exchangers. (a) Parallel-flow. (b) Counterflow [14]

exchange units as shown in Fig. 5.22 [9, 47, 70]. It is assumed that the connections between the units do not cause any delay or dynamic effect. Each unit is represented by two control volumes or lumps (CV_p and CV_s) that are connected by a heat conducting wall. One side of the heat exchanger will be called the primary (hot) side and the other the secondary (cold) side. The properties of each lump is assumed to be uniform.

Let n be the number of lumps and $\dot{m}_p$ and $\dot{m}_s$, the mass flow rate of the primary and secondary side respectively. The energy balance equations, as an illustration, for two control volumes on each side are given as follows:

For the primary side

$$\begin{aligned}\frac{dT_{p(1)}}{dt} &= \frac{\dot{m}_p}{\rho_{p(1)}V_{p(1)}}(T_{p(i)} - T_{p(1)}) + \frac{AU}{c_{pp(1)}\rho_{p(1)}V_{p(1)}}(T_{s(2)} - T_{p(1)}) \\ \frac{dT_{p(o)}}{dt} &= \frac{dT_{p(2)}}{dt} = \frac{\dot{m}_p}{\rho_{p(2)}V_{p(2)}}(T_{p(1)} - T_{p(2)}) + \frac{AU}{c_{pp(2)}\rho_{p(2)}V_{p(2)}}(T_{s(1)} - T_{p(2)})\end{aligned} \tag{5.56}$$

and for the secondary side

$$\begin{aligned}\frac{dT_{s(1)}}{dt} &= \frac{\dot{m}_s}{\rho_{s(1)}\ V_{s(1)}}(T_{s(i)} - T_{s(1)}) + \frac{AU}{c_{ps(1)}\rho_{s(1)}V_{s(1)}}(T_{p(2)} - T_{s(1)}) \\ \frac{dT_{s(o)}}{dt} &= \frac{dT_{s(2)}}{dt} = \frac{\dot{m}_s}{\rho_{s(2)}V_{s(2)}}(T_{s(1)} - T_{s(2)}) + \frac{AU}{c_{ps(2)}\rho_{s(2)}V_{p(2)}}(T_{p(1)} - T_{s(2)}),\end{aligned} \tag{5.57}$$

where $T_{g(i)}$ and $T_{g(o)}$ are the temperature inputs and outputs respectively and $g \in [p, s]$. $V_{g(n)}$ and $c_{pg(n)}$ are the volumes and specific heats of the n-th lump. U is the heat transfer coefficient and A is the heat transfer area.

In order to extract a state space model automatically a network representation of the heat exchanger is needed. A general network representation of the heat exchanger structure is given in Fig. 5.23

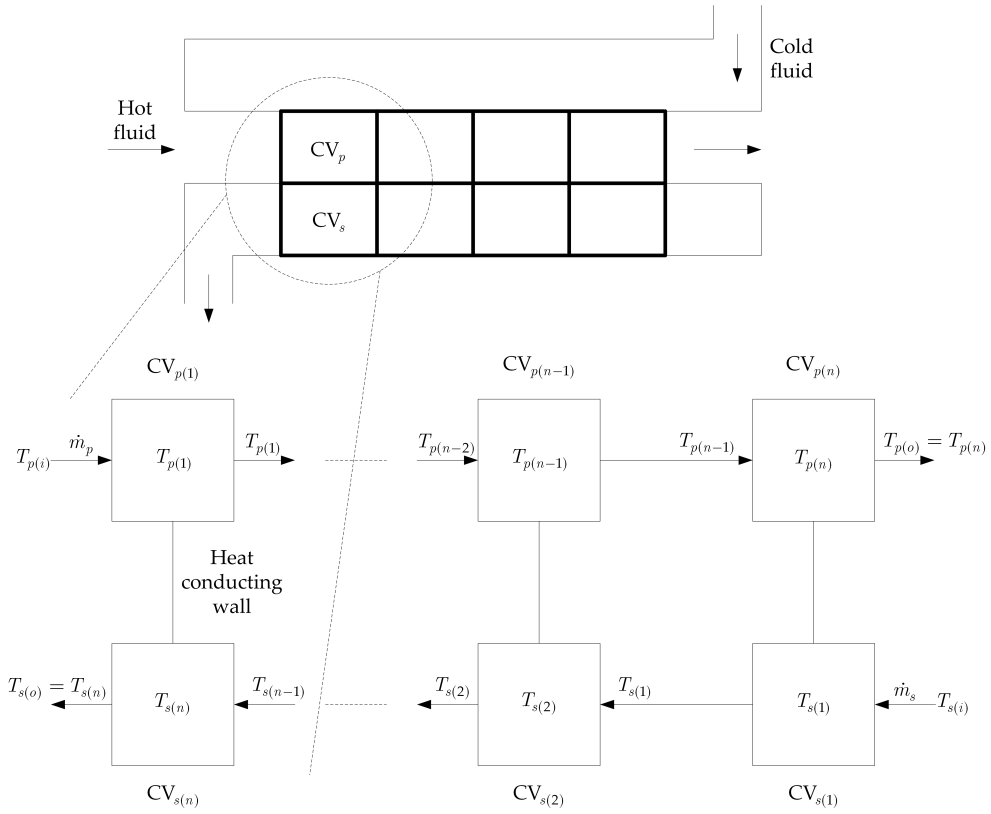

Figure 5.22: Structural representation of heat exchanger units

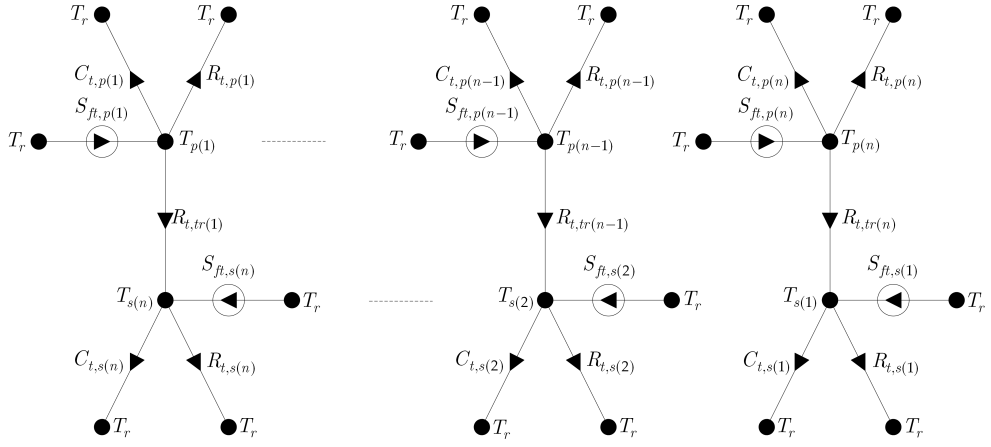

Figure 5.23: General network representation of a heat exchanger

The thermal capacitances and resistances are given by

$$C_{t,g(n)} = c_{pg(n)}\rho_{g(n)}V_{g(n)} \tag{5.58}$$

and

$$R_{t,g(n)} = 1/(\dot{m}_g c_{pg(n)}). \tag{5.59}$$

The thermal resistance due to the wall between the primary and secondary side is given by

$$R_{tr,g(n)} = \frac{c_{pg(n)}\rho_{g(n)}V_{g(n)}}{AU} \tag{5.60}$$

Considering the general network shown in Fig. 5.23 the extracted state space model for two control volumes on each side is given by

$$\begin{aligned}\begin{bmatrix} \dot{T}_{p(1)} \\ \dot{T}_{p(2)} \\ \dot{T}_{s(1)} \\ \dot{T}_{s(2)} \end{bmatrix} &= \begin{bmatrix} k_{p(1)} & 0 & 0 & a_{p(1)} \\ 0 & k_{p(2)} & a_{p(2)} & 0 \\ 0 & a_{s(1)} & k_{s(1)} & 0 \\ a_{s(2)} & 0 & 0 & k_{s(2)} \end{bmatrix} \begin{bmatrix} T_{p(1)} \\ T_{p(2)} \\ T_{s(1)} \\ T_{s(2)} \end{bmatrix} + \\ &\begin{bmatrix} b_{p(1)} & 0 & 0 & 0 \\ 0 & b_{p(2)} & 0 & 0 \\ 0 & 0 & b_{s(1)} & 0 \\ 0 & 0 & 0 & b_{s(2)} \end{bmatrix} \begin{bmatrix} S_{ft,p(1)} \\ S_{ft,p(2)} \\ S_{ft,s(1)} \\ S_{ft,s(2)} \end{bmatrix}\end{aligned} \tag{5.61}$$

where

$$k_{g(n)} = -\frac{1}{R_{t,g(n)}C_{t,g(n)}} - \frac{1}{R_{tr,g(n)}} \tag{5.62}$$

$$a_{g(n)} = \frac{1}{R_{tr,g(n)}} \tag{5.63}$$

$$b_{g(n)} = \frac{1}{C_{t,g(n)}} \tag{5.64}$$

$$S_{ft,g(n)} = \dot{m}_g c_{pg(n)} T_{g(n)} \tag{5.65}$$

and

$$\begin{aligned} S_{ft,p(1)} &= \dot{m}_p c_{pp(1)} T_{p(i)} \\ S_{ft,s(1)} &= \dot{m}_s c_{ps(1)} T_{s(i)} \end{aligned} \tag{5.66}$$

This form of the state space model can be used for simulation purposes. If this state space model is to be used for control some changes to the structure of the state space representation need to be made. The form of the state space model is based on assumptions and the choice of input-output variables. Three different forms are discussed namely: The Linear Time Invariant (LTI) form, Linear Time Varying (LTV) form and the Nonlinear (NL) form [9].

LTI state space model

The general matrix format of a state space model is given by

$$\dot{\mathbf{X}} = \mathbf{AX} + \mathbf{BU}, \tag{5.67}$$

where **X** is the state vector and **U** is the input vector. If an LTI state space model is required for control, the input vector, **U**, contains the input temperatures ($T_{p(i)}, T_{s(i)}$) and it is assumed that the mass flow rates are constant.

Considering the state space model in (5.61) and the assumption above, the **A** and **B** matrices are transformed as follows:

$$\mathbf{A} = \begin{bmatrix} -a_{p(1)} - k_{p(1)} & 0 & 0 & k_{p(1)} \\ a_{p(2)} & -a_{p(1)} - k_{p(1)} & k_{p(2)} & 0 \\ 0 & k_{s(1)} & -a_{s(1)} - k_{s(1)} & 0 \\ k_{s(2)} & 0 & a_{s(2)} & -a_{s(2)} - k_{s(2)} \end{bmatrix}, \tag{5.68}$$

$$\mathbf{B} = \begin{bmatrix} a_{p(1)} & 0 \\ 0 & 0 \\ 0 & a_{s(1)} \\ 0 & 0 \end{bmatrix}, \tag{5.69}$$

where

$$a_{g(n)} = \frac{1}{C_{t,g(n)} R_{t,g(n)}} = \frac{\dot{m}_g c_{pg(n)}}{V_{g(n)} \rho_{g(n)} c_{pg(n)}} = \frac{\dot{m}_g}{V_{g(n)} \rho_{g(n)}},\ g \in [p, s] \tag{5.70}$$

and

$$k_{g(n)} = \frac{1}{R_{tr,g(n)}} = \frac{AU}{c_{pg(n)} \rho_{g(n)} V_{g(n)}}\ g \in [p, s]. \tag{5.71}$$

LTV state space model

In many practical cases the mass flow rates through the heat exchanger change with time. A state space model allowing this, but still taking the input temperatures as inputs, is regarded as a time varying state space model. In this state space model the mass flow rates may also be called disturbances [48]. The form of the **A** and **B** matrices stay exactly the same as in the LTI case, except that (5.70) becomes time varying:

$$a_{g(n)}(t) = \frac{\dot{m}_g(t)}{V_{g(n)} \rho_{g(n)}},\ g \in [p, s]. \tag{5.72}$$

NL state space model

For a control scenario where the mass flow rates are considered as the manipulable (input) variables, the nature of the state space model becomes nonlinear [9]. In this case the input vector contains the mass flow rates $(\dot{m}_p, \dot{m}_s)$ and it is assumed that the inlet temperatures are constant. The **A** and **B** matrices of the NL state space model are given as follows:

$$\mathbf{A} = \begin{bmatrix} -k_{p(1)} & 0 & 0 & k_{p(1)} \\ 0 & -k_{p(2)} & k_{p(2)} & 0 \\ 0 & k_{s(1)} & -k_{s(1)} & 0 \\ k_{s(2)} & 0 & 0 & -k_{s(2)} \end{bmatrix} \tag{5.73}$$

$$\mathbf{B} = \begin{bmatrix} \frac{T_{p(i)}}{a_{p(1)}} - \frac{T_{p(1)}}{a_{p(1)}} & 0 \\ \frac{T_{p(1)}}{a_{p(2)}} - \frac{T_{p(2)}}{a_{p(2)}} & 0 \\ 0 & \frac{T_{s(i)}}{a_{s(1)}} - \frac{T_{s(1)}}{a_{s(1)}} \\ 0 & \frac{T_{s(1)}}{a_{s(2)}} - \frac{T_{s(2)}}{a_{s(2)}} \end{bmatrix}, \tag{5.74}$$

where

$$k_{g(n)} = \frac{1}{R_{tr,g(n)}} = \frac{AU}{c_{pg(n)}\rho_{g(n)}V_{g(n)}},\ g \in [p,s], \tag{5.75}$$

$$a_{g(n)} = \frac{1}{C_{t,g(n)}} = \frac{1}{V_{g(n)}\rho_{g(n)}},\ g \in [p,s]. \tag{5.76}$$

It is clear that the **B** matrix is a function of the state vector $\mathbf{X} = [T_{p(1)}\ T_{p(2)}\ T_{s(1)}\ T_{s(2)}]'$; from there the nonlinearity. The matrix form of this nonlinear state space model can be given by

$$\dot{\mathbf{X}} = \mathbf{A}\mathbf{X} + \mathbf{B}(\mathbf{X})\mathbf{U}. \tag{5.77}$$

Model validation

The majority of model-based controllers utilise LTI state space models in their control schemes. It is therefore decided to extract a LTI state space model of the heat exchanger and compare its solution with *Flownex*®.

The state space extraction of a four increment heat exchanger results in an eighth order state space model where

$$\mathbf{X} = \begin{bmatrix} T_{p(1)} & T_{p(2)} & T_{p(3)} & T_{p(4)} & T_{s(1)} & T_{s(2)} & T_{s(3)} & T_{s(4)} \end{bmatrix}', \tag{5.78}$$

with $T_{p(o)} = T_{p(4)}$ and $T_{s(o)} = T_{s(4)}$,

$$\mathbf{U} = \begin{bmatrix} T_{p(i)} \\ T_{s(i)} \end{bmatrix}, \tag{5.79}$$

$$\mathbf{A} = \begin{bmatrix} k_p(1) & 0 & 0 & 0 & 0 & 0 & 0 & d_{p(1)} \\ a_{p(2)} & k_{p(2)} & 0 & 0 & 0 & 0 & d_{p(2)} & 0 \\ 0 & a_{p(3)} & k_{p(3)} & 0 & 0 & d_{p(3)} & 0 & 0 \\ 0 & 0 & a_{p(4)} & k_{p(4)} & d_{p(4)} & 0 & 0 & 0 \\ 0 & 0 & 0 & d_{s(1)} & k_{s(1)} & 0 & 0 & 0 \\ 0 & 0 & d_{s(2)} & 0 & a_{s(2)} & k_{s(2)} & 0 & 0 \\ 0 & d_{s(3)} & 0 & 0 & 0 & a_{s(3)} & k_{s(3)} & 0 \\ d_{s(4)} & 0 & 0 & 0 & 0 & 0 & a_{s(4)} & k_{s(4)} \end{bmatrix}, \tag{5.80}$$

$$\mathbf{B} = \begin{bmatrix} a_{p(1)} & 0 \\ 0 & 0 \\ 0 & 0 \\ 0 & 0 \\ 0 & a_{s(1)} \\ 0 & 0 \\ 0 & 0 \\ 0 & 0 \end{bmatrix}, \tag{5.81}$$

$$a_{g(n)} = \frac{1}{R_{t,g(n)}C_{t,g(n)}} = \frac{\dot{m}_g}{V_{g(n)}\rho_{g(n)}},\ g \in [p,s], \tag{5.82}$$

$$d_{g(n)} = \frac{1}{R_{tr,g(n)}} = \frac{AU}{c_{pg(n)}\rho_{g(n)}V_{g(n)}},\ g \in [p,s], \tag{5.83}$$

$$k_g(n) = -a_{g(n)} - d_{g(n)},\ g \in [p,s]. \tag{5.84}$$

The solution results of the state space model will be compared with a *Flownex*® simulation of a heat exchanger component shown in Fig. 5.24

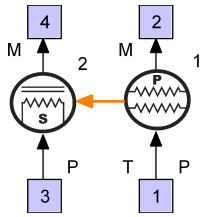

Figure 5.24: Heat exchanger component in *Flownex*®

A *Flownex*® link is used to incorporate the *Flownex*® results into the *Simulink*® environment. This facilitates the comparison of results between the extracted state space model and the *Flownex*® component as shown in Fig. 5.25.

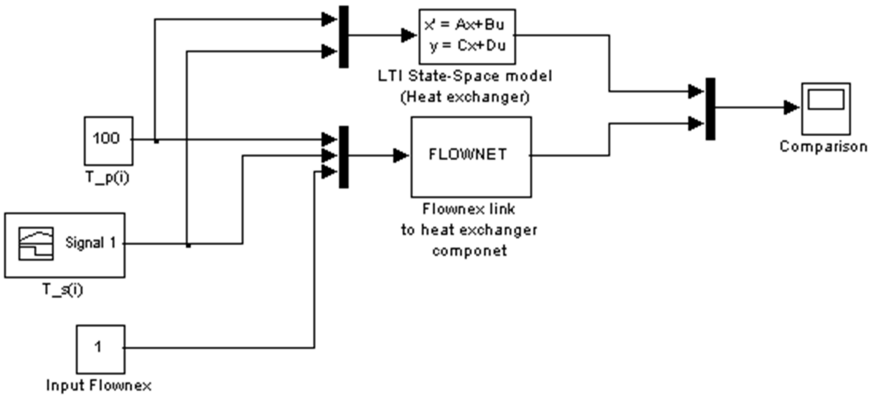

Figure 5.25: Result comparison in Simulink® environment

The temperature inputs applied to the state space model and the *Flownex*® component are given in Fig. 5.26 and a comparison between the primary and secondary output temperatures are shown in Figures 5.27 (a) and 5.27 (b) respectively.

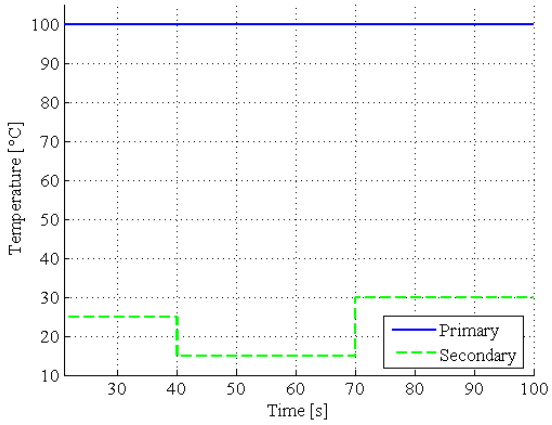

Figure 5.26: Primary and secondary temperature inputs

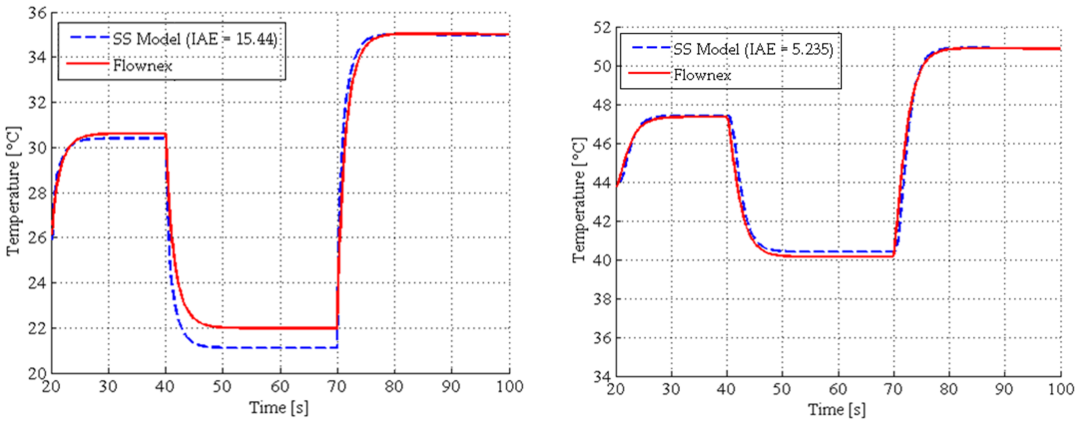

(a) (b)

Figure 5.27: (a) Primary output temperature (b) Secondary output temperature

The linear time-invariant state space model of the heat exchanger compares well with the *Flownex*® model. There is a larger model error for the primary output power though. The accuracy of the state space model can be increased by increasing the number of increments which in turn increases the order of the state space model.

5.3.3 State space model extraction of a PBMR PCU

The thermohydraulic system to be considered in this section is a three-shaft PBMR PCU shown in Fig. 5.28. This unit is a power station that can generate approximately 110 MW of electrical power [72]. The modularity of the system allows for units to be combined to form a larger

power plant that can generate more power. The PBMR is a graphite-moderated, helium-cooled reactor that uses the Brayton direct gas cycle to convert heat generated in the core by nuclear fission. The heat is transferred to the coolant gas (helium), and converted into electrical energy by means of a gas turbo-generator [72, 73].

The power output of the system can be controlled by either adding or removing helium from the system. A helium inventory control system (HICS) constitutes helium storage tanks and bypass valves which allow three different power control modes:

- Helium injection
- Helium extraction
- Helium bypass

Helium can be injected at the low pressure side and extracted at the high pressure side of the system. Helium injection and extraction, increases and decreases the power output respectively. The power output can also be increased or decreased by either closing or opening the gas bypass control valve.

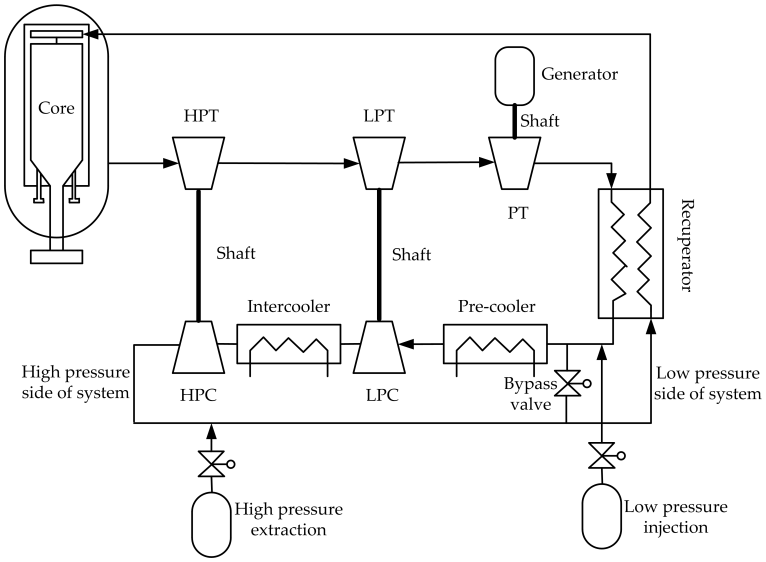

Figure 5.28: Thermohydraulic system: PBMR PCU

In the following sections a network approach will be used to represent the PCU. The network representations will be given for each domain of the system.

Conceptual model of the system

For the purpose of modelling the PBMR PCU, a few assumptions are in order. A complex neutronics model can be constructed for the reactor that is quite accurate, but for the purpose

of this study it is modelled as a heat source [12, 26]. Active control on the pre- and inter-coolers is assumed and therefore their outlet temperatures are considered constant as shown in Fig. 5.28.

The HICS is modelled by means of two constant mass flow sources. Active control on the valves in the control system is assumed to ensure constant mass flow from the tanks as well as through the bypass valve. A schematic diagram of the conceptual model is given in Fig. 5.29. Helium can be injected into the system by activating the mass flow source, S_1, at the low pressure side of the system. Helium can be extracted from the system by activating the mass flow source, S_2, at the high pressure side of the system. Lastly helium can be bypassed from the high pressure side to the low pressure side by activating both sources simultaneously.

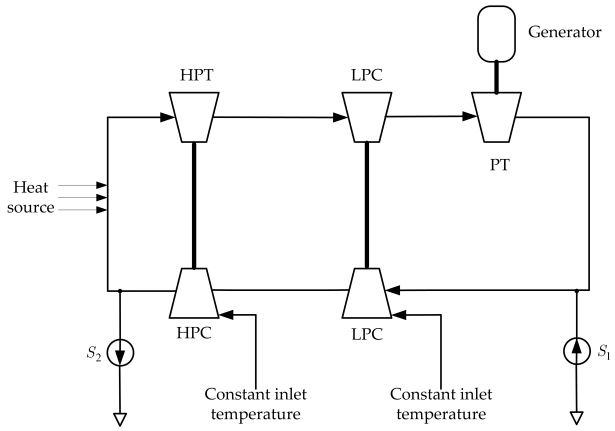

Figure 5.29: Conceptual model of the PCU

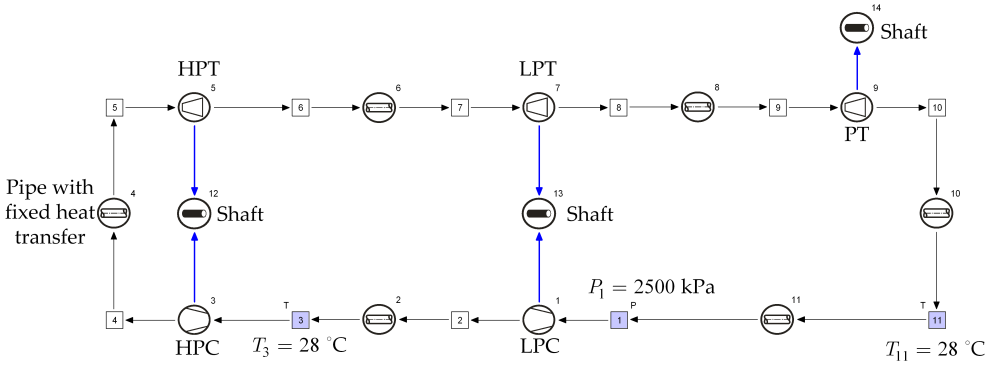

Figure 5.30: *Flownex*® network of the PCU

Hydraulic network and state space model

A *Flownex*® network of the PCU is constructed as shown in Fig. 5.30. The reactor is modelled as a heat source by specifying the heat transfer rate of a pipe element. The inlet temperatures of the compressors are fixed at 28 °C at the nodes of the network. *Flownex*® allows the user to specify the number of control volumes to be used. It was decided to discretise the system

into eleven control volumes. Therefore each node represents a control volume. The hydraulic graph representing the network is given in Fig. 5.31

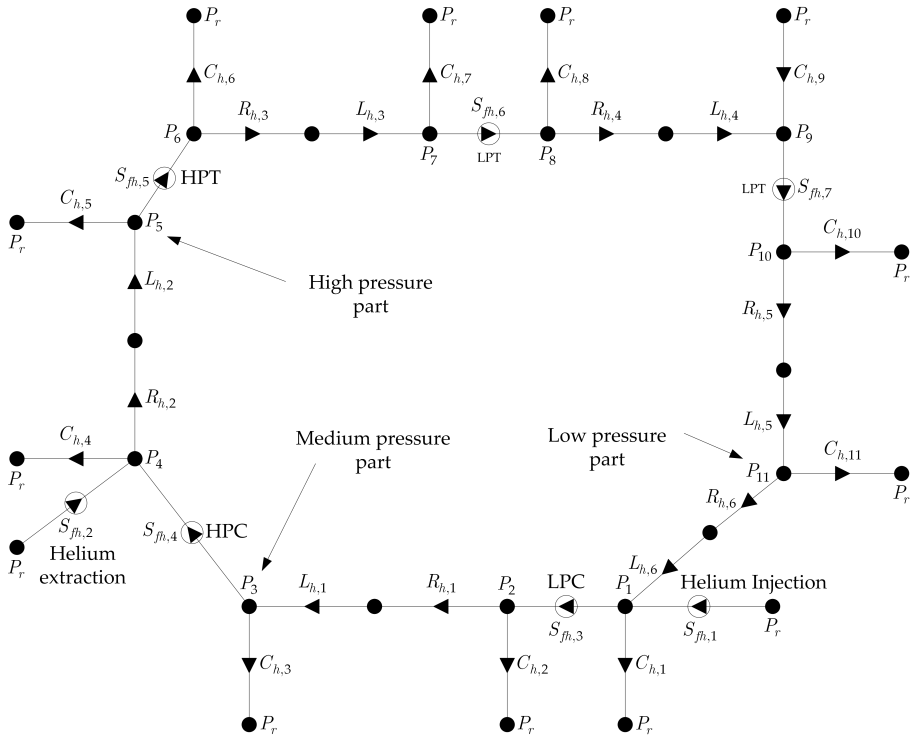

Figure 5.31: Hydraulic network of the PCU

Seven hydraulic flow sources are defined for the system. Flow sources, $S_{fh,1}$ and $S_{fh,2}$, model the HICS system. As mentioned two sources can be used to activate the different power control modes. The remaining flow sources $S_{fh,3}, \ldots, S_{fh,7}$ model the turbomachines. By applying the state space extraction algorithm the hydraulic state space model is extracted. The hydraulic state space is given by

$$\dot{\mathbf{X}}_h = \mathbf{A}_h(\mathbf{X}_h, t)\mathbf{X}_h + \mathbf{B}_h(t)\mathbf{U}_h \tag{5.85}$$

where

$$\mathbf{X}_h = \begin{bmatrix} P_1 & \ldots & P_1 & \dot{m}_1 & \ldots & \dot{m}_6 \end{bmatrix}', \ \mathbf{X}_h \in \mathbb{R}^{17\times 1} \tag{5.86}$$

$$\mathbf{U}_h = \begin{bmatrix} S_{fh,1} & \ldots & S_{fh,7} \end{bmatrix}', \ \mathbf{U}_h \in \mathbb{R}^{7\times 1} \tag{5.87}$$

$$\mathbf{A}_h = \begin{bmatrix} 0 & 0 & 0 & \dots & 0 & 0 & \dots & 1/C_{h,1} \\ 0 & 0 & 0 & \dots & -1/C_{h,2} & 0 & \dots & 0 \\ 0 & 0 & 0 & \dots & 1/C_{h,3} & 0 & \dots & 0 \\ 0 & 0 & 0 & \dots & 0 & -1/C_{h,4} & \dots & 0 \\ \vdots & \vdots & \vdots & \dots & \vdots & \vdots & \dots & \vdots \\ 0 & 1/L_{h,1} & -1/L_{h,1} & \dots & -R_{h,1}/L_{h,1} & 0 & \dots & 0 \\ 0 & 0 & 0 & \dots & 0 & -R_{h,2}/L_{h,2} & \dots & 0 \\ 0 & 0 & 0 & \dots & 0 & 0 & \dots & 0 \\ \vdots & \vdots & \vdots & \vdots & \vdots & \vdots & \vdots & \vdots \\ 0 & 0 & 0 & \dots & 0 & 0 & \dots & -R_{h,6}/L_{h,6} \end{bmatrix} \tag{5.88}$$

$$\mathbf{B}_h = \begin{bmatrix} 1/C_{h,1} & 0 & -1/C_{h,1} & 0 & \dots \\ 0 & 0 & 1/C_{h,2} & 0 & \dots \\ 0 & 0 & 0 & -1/C_{h,3} & \dots \\ 0 & 1/C_{h,4} & 0 & 1/C_{h,4} & \dots \\ 0 & 0 & 0 & 0 & \dots \\ \vdots & \vdots & \vdots & \vdots & \vdots \\ 0 & 0 & 0 & 0 & \dots \end{bmatrix} \tag{5.89}$$

with $\mathbf{A}_h \in \mathbb{R}^{17\times 7}$ and $\mathbf{B}_h \in \mathbb{R}^{17\times 7}$.

Thermal network and state space model

The thermal network of the PCU is shown in Fig. 5.32. Six temperatures (state variables) are of interest; the five outlet temperatures of the turbomachines, $T_1, T_2, T_4, \dots, T_6$, and the reactor outlet temperature, T_3. The thermal flow source $S_{ft,1}$ models the heat transfer of the reactor and the thermal flow sources $S_{ft,2}, \dots, S_{ft,7}$ model the heat transfer of the turbomachines.

The thermal graph is used to extract the symbolic thermal state space model of the PCU given by

$$\dot{\mathbf{X}}_t = \mathbf{A}_t(t)\mathbf{X}_t + \mathbf{B}_t(t)\mathbf{U}_t \tag{5.90}$$

where

$$\mathbf{X}_t = \begin{bmatrix} T_1 & \dots & T_6 \end{bmatrix}', \ \mathbf{X}_t \in \mathbb{R}^{6\times 1} \tag{5.91}$$

$$\mathbf{U}_t = \begin{bmatrix} S_{ft,1} & \dots & S_{ft,7} \end{bmatrix}', \ \mathbf{U}_t \in \mathbb{R}^{7\times 1} \tag{5.92}$$

$$\mathbf{A}_t = \begin{bmatrix} -1/C_{t,1}/R_{t,1} & 0 & 0 & \dots & 0 \\ 0 & -1/C_{t,2}/R_{t,2} & 0 & \dots & 0 \\ \vdots & \vdots & \vdots & \vdots & \vdots \\ 0 & 0 & 0 & 0 & -1/C_{t,6}/R_{t,6} \end{bmatrix} \tag{5.93}$$

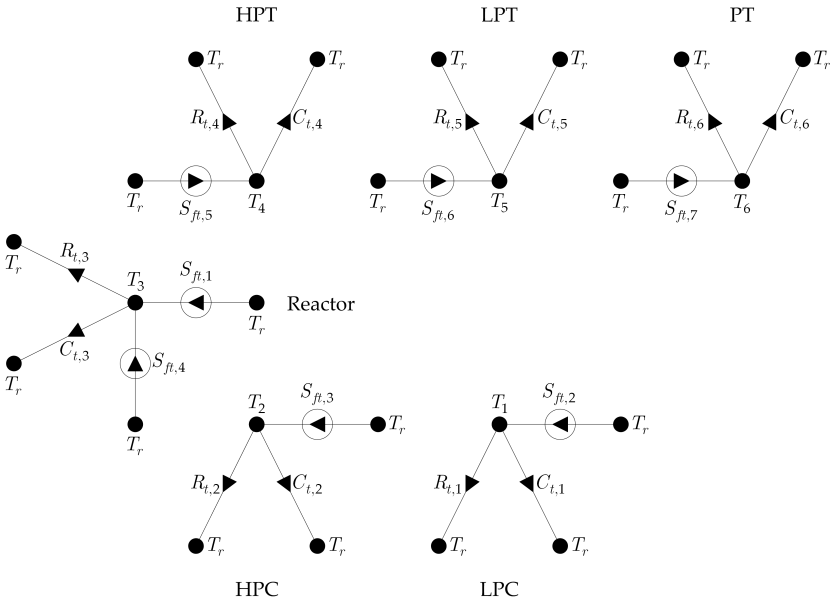

Figure 5.32: Thermal network of the PCU

$$\mathbf{B}_t = \begin{bmatrix} 0 & 1/C_{t,1} & 0 & \dots & 0 \\ 0 & 0 & 1/C_{t,2} & \dots & 0 \\ 1/C_{t,3} & 0 & 0 & \dots & 0 \\ 0 & 0 & 0 & \dots & 0 \\ \vdots & \vdots & \vdots & \vdots & \vdots \\ 0 & 0 & 0 & 0 & 1/C_{t,6} \end{bmatrix} \tag{5.94}$$

with $\mathbf{A}_t \in \mathbb{R}^{6\times 6}$ and $\mathbf{B}_t \in \mathbb{R}^{6\times 7}$.

Mechanical network and state space model

The mechanical network shown in Fig. 5.33 represents the two shafts that connect the respective compressors and turbines. The state variables of interest are the shaft speeds. The rotational speed of the power turbine is fixed and therefore not included as a state variable. The sources, $S_{fm,1}$ and $S_{fm,2}$, represent the high pressure compressor and high pressure turbine torques. $S_{fm,3}$ and $S_{fm,4}$ represent the low pressure compressor and low pressure turbine torques.

The mechanical state space model is given by

$$\dot{\mathbf{X}}_m = \mathbf{A}_m\mathbf{X}_m + \mathbf{B}_m\mathbf{U}_m \tag{5.95}$$

where

$$\mathbf{X}_m = \begin{bmatrix} \omega_1 & \omega_2 \end{bmatrix}' \tag{5.96}$$

$$\mathbf{U}_m = \begin{bmatrix} S_{fm,1} & S_{fm,1} & S_{fm,1} & S_{fm,1} \end{bmatrix}' \tag{5.97}$$

$$\mathbf{A}_m = \begin{bmatrix} 0 & 0 \\ 0 & 0 \end{bmatrix} \tag{5.98}$$

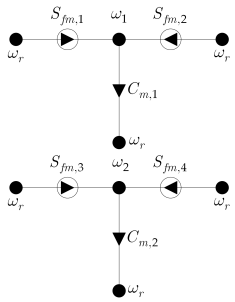

Figure 5.33: Mechanical network of the PCU

$$\mathbf{B}_m = \begin{bmatrix} -1/C_{m,1} & -1/C_{m,1} & 0 & 0 \\ 0 & 0 & -1/C_{m,2} & -1/C_{m,2} \end{bmatrix} \tag{5.99}$$

The mechanical A-matrix in (5.98) contains zeros, since the mechanical damping is accounted for in the mechanical efficiencies of the shafts used in the torque calculations.

Model validation

Fig. 5.34 illustrates the solution and validation process. The state space models derived for each domain are interdependent. They have to be solved in a specific order. The thermal solution is dependent on the hydraulic solution. The mechanical solution is dependent on both the hydraulic and thermal solution. This means that the hydraulic state space model is solved first, then the thermal and finally the mechanical state space. The ordered solution process is iterated until time $t = t_{\text{final}}$ is reached.

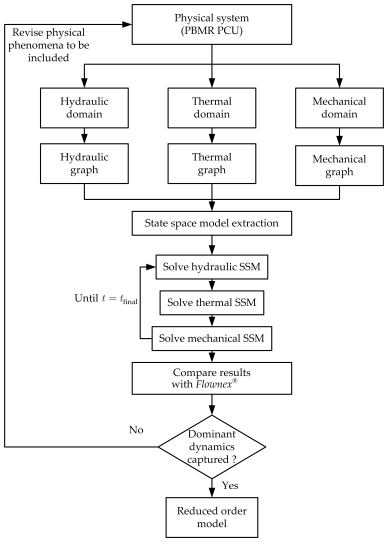

Figure 5.34: Methodology for reduced order model extraction and validation (PBMR PCU)

The state space models are consecutively solved for the three different modes:

- **Helium injection**: For helium injection the flow source, $S_{fh,1}$, is assigned a value of 1 kg/s. The flow source, $S_{fh,2}$, is kept at zero.
- **Helium extraction**: For helium extraction the flow source, $S_{fh,2}$, is assigned a value of -1 kg/s and the flow source, $S_{fh,1}$, is kept at zero.
- **Helium bypass**: For helium bypass, $S_{fh,1}$ is assigned a value of 1 kg/s and $S_{fh,2}$ is assigned a value of -1 kg/s.

The solution results and comparison with *Flownex*® are given in the following sections under the same headings in the list above. Each source input stated above begins at time, $t = 20$ s, and ends at time, $t = 40$ s. For each of these scenarios state variables were compared with results obtained from *Flownex*® and the steady state values are subtracted from each state variable. The results therefore represent the change in the state variables.

Figures 5.35, 5.40 and 5.45 show the state variables $\dot{m}_1$ and $\dot{m}_3$ which represent the mass flow rates through the low pressure compressor (LPC) and high pressure turbine (HPT). Figures 5.36, 5.41 and 5.46 show the state variables P_{11}, P_3 and P_5 which are the pressures at the low pressure (LP), medium pressure (MP) and high pressure (HP) parts in the system as indicated in Fig. 5.31.

Figures 5.37, 5.42 and 5.47 show the first three temperature state variables T_1, T_2 and T_3 which are the temperature outputs of the low pressure compressor (T2LPC), high pressure compressor (T2HPC) and the reactor (TReactor) respectively. Figures 5.38, 5.43 and 5.48 show the last three temperature state variables T_4, T_5 and T_6 which are the temperature outputs of the low pressure turbine (T2LPT), high pressure turbine (T2HPT) and the power turbine (T2PT) respectively.

Figures 5.39, 5.44 and 5.49 show the state variables ω_1 and ω_2 representing the speeds of the high pressure shaft (HP) and low pressure shaft (LP) respectively.

5.3.4 Helium injection

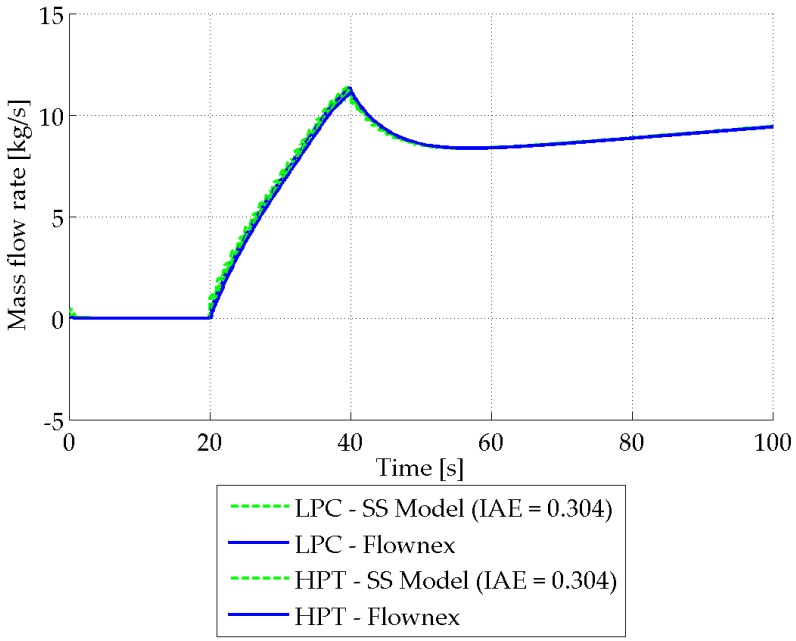

Figure 5.35: Helium injection: Mass flow rate comparison

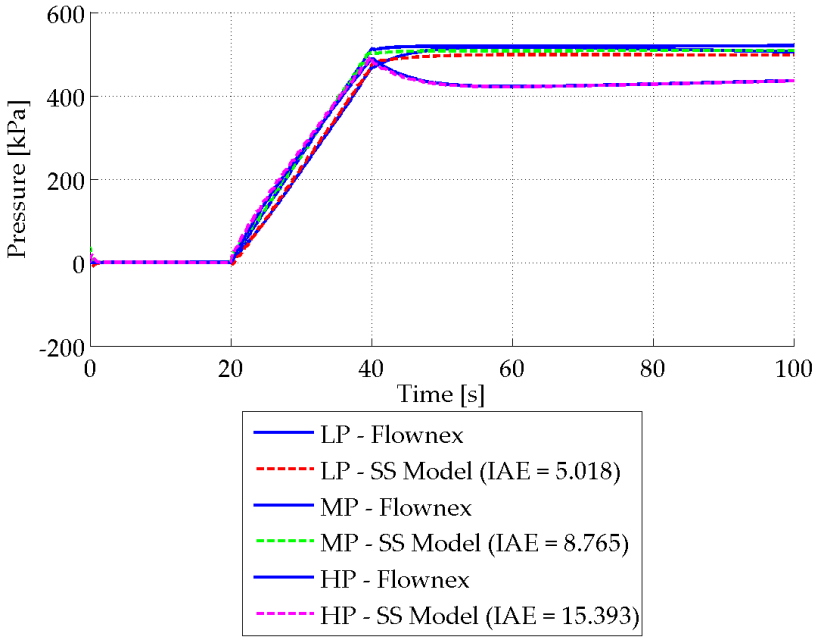

Figure 5.36: Helium injection: Pressure comparison

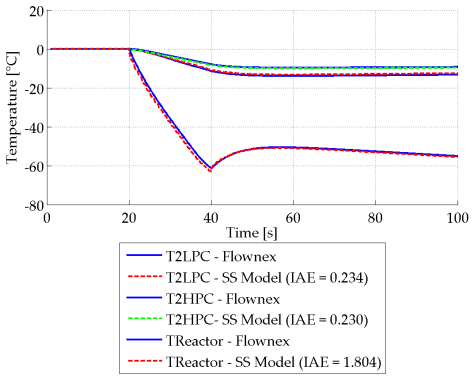

Figure 5.37: Helium injection: Temperature comparison (compressors and reactor)

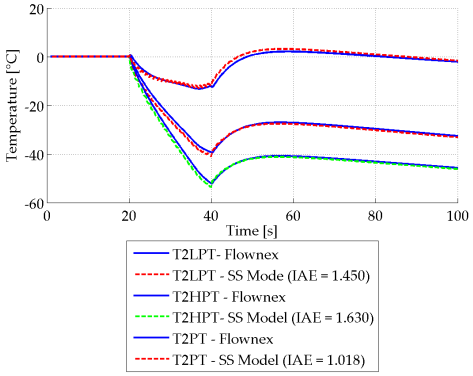

Figure 5.38: Helium injection: Temperature comparison (turbines)

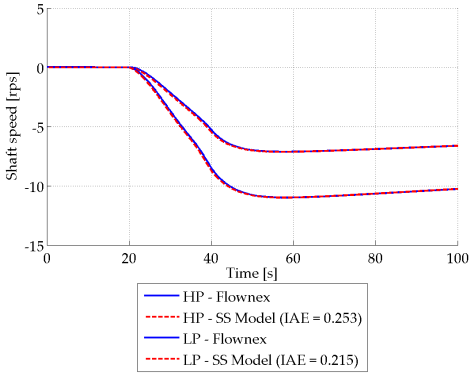

Figure 5.39: Helium injection: Shaft speed

5.3.5 Helium extraction

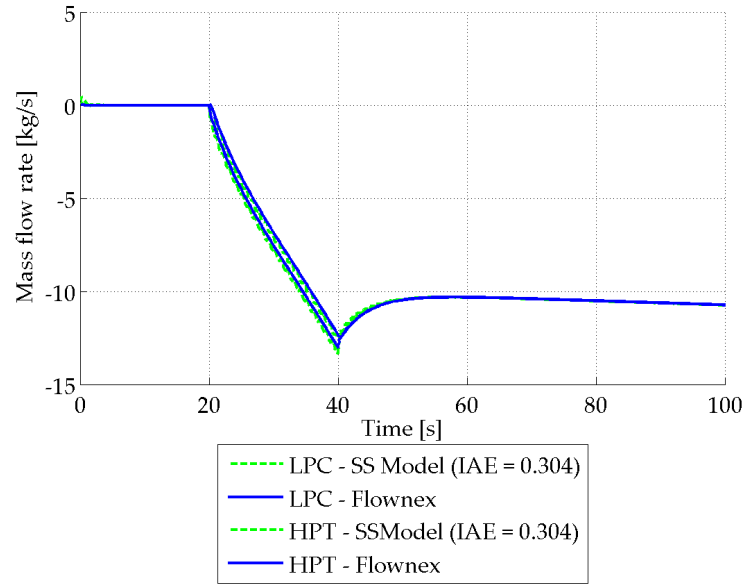

Figure 5.40: Helium extraction: Mass flow rate comparison

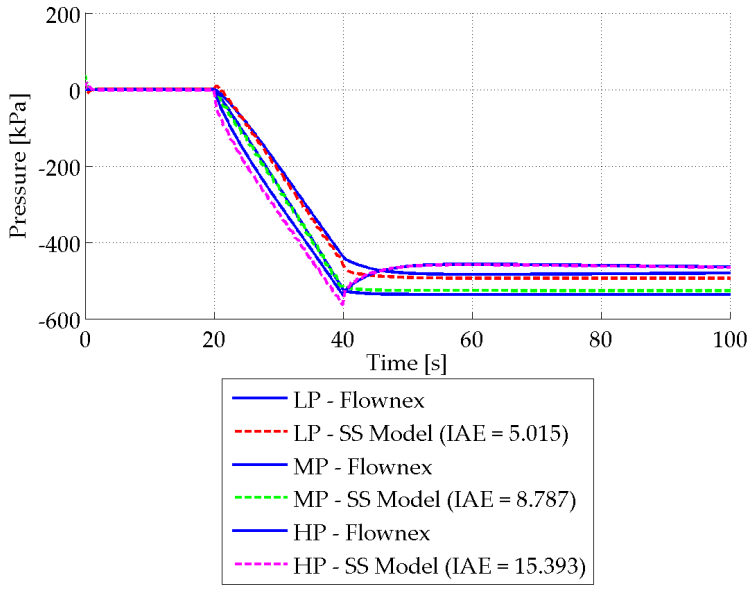

Figure 5.41: Helium extraction: Pressure comparison

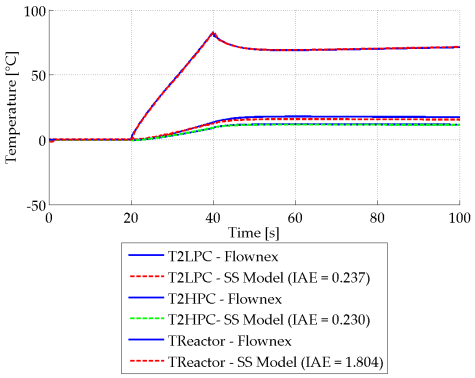

Figure 5.42: Helium extraction: Temperature comparison (compressors and reactor)

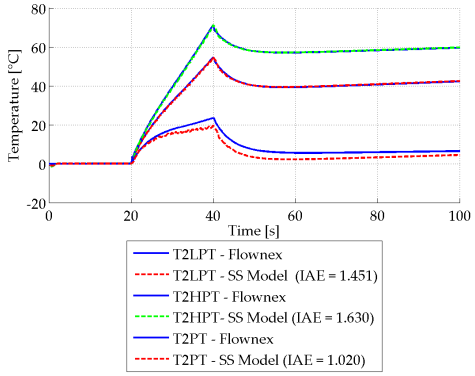

Figure 5.43: Helium extraction: Temperature comparison (turbines)

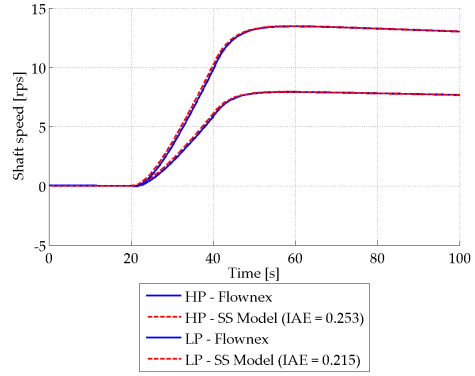

Figure 5.44: Helium extraction: Shaft speed

5.3.6 Helium bypass

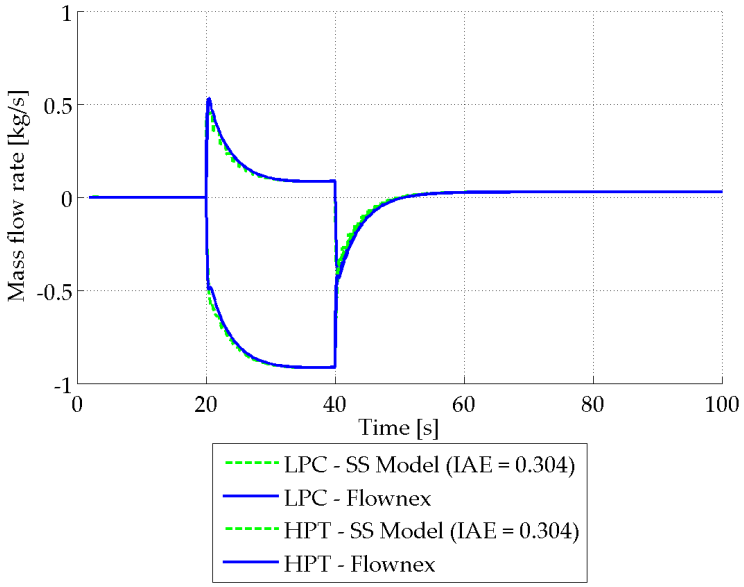

Figure 5.45: Helium bypass: Mass flow rate comparison

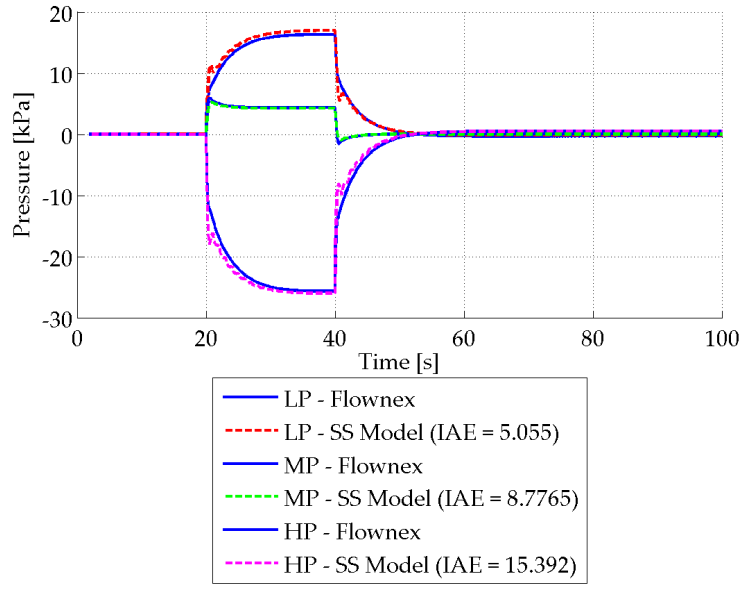

Figure 5.46: Helium bypass: Pressure comparison

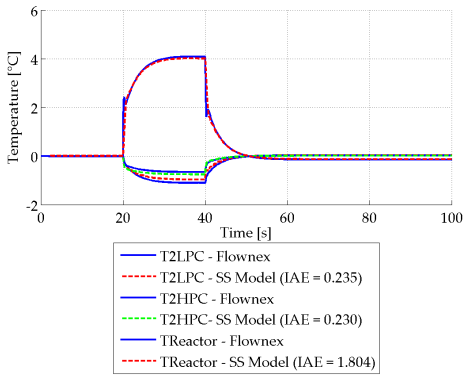

Figure 5.47: Helium bypass: Temperature comparison (compressors and reactor)

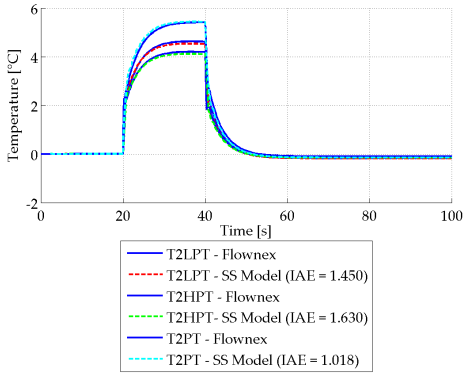

Figure 5.48: Helium bypass: Temperature comparison (turbines)

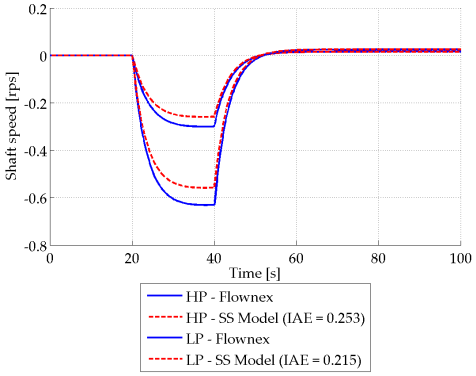

Figure 5.49: Helium bypass: Shaft speed

The solutions of the state space model for the three scenarios compares well with the *Flownex*® results. The 25^{th} order state space model is nonlinear and time-invariant. This allows the user to implement the state space model in a nonlinear MIMO control strategy. The controller will be able to control the system over a wide range of operating points. However since it

is a nonlinear model, linear control analysis can't be applied to the model. It is therefore not possible to determine the dominant system dynamics from this model. A reduced order, linear state space model will be more useful in this case.

5.4 Conclusion

In this chapter generalised thermohydraulic elements were derived from the governing equations. These elements model the key dynamics in a thermohydraulic system namely energy storage, dissipation and generation. These elements were used to develop multi-domain network representations of thermohydraulic systems. The network representations describe the key dynamics of the systems they represent. The developed state space extraction algorithm takes the networks as input and derives the desired state space models in symbolic form. The symbolic values are then substituted with numeric values and the state equations can then be solved using standard differential equation solvers. The results were compared with *Flownex*® simulations. The results show good correlation.

It can therefore be concluded that the state space extraction approach can be successfully used to derive state space models of thermohydraulic networks. These models can be used in advanced control strategies. However insight with regards to the dominant system dynamics can more readily be obtained from linear state space models. In the following chapter a reduced order linear state space model of the PBMR PCU will be extracted that can be used in model-based control strategies, but also to determine the dominant system dynamics.

CHAPTER 6

MODEL-BASED CONTROL

6.1 Introduction

This chapter describes the automatic and symbolic extraction of a linear state space model of the PBMR power conversion unit. This state space model will be imbedded in an optimal control scheme to control the power output of the system. A number of optimal model-based control schemes using state space models do exist of which Linear Quadratic Control (LQR), Linear Quadratic Gaussian (LQG) and Model Predictive Control (MPC) are the most popular. These controllers use state space models to determine optimal control laws. These controllers can handle MIMO systems that may be time-invariant or -varying. Model predictive control is similar to the other strategies in the sense that the control strategy is expressed as a problem of minimising a cost function, however what distinguishes MPC from the other is that the cost function can be subjected to constraints. Another feature of MPC is the ability to predict future effects of control actions at the present time. The implemented MPC controller will be compared with optimised PID and Fuzzy PID control systems.

6.2 Brief plant description

A typical three-shaft Brayton cycle based power conversion unit of the original PBMR design is considered. A simplified schematic diagram of the power conversion unit is given in Fig. 6.1. This unit can produce approximately 110 MW of electric power. At full power conditions, helium enters the reactor at a temperature of approximately 500 °C and at a pressure of 70 bar. The helium moves downward between hot fuel sphere. It then picks up heat from the fuel spheres, which have been heated by nuclear reaction. The helium leaves the reactor at a very high temperature of approximately 900 °C [73].

Next, the helium gas moves through the High-pressure Turbine (HPT) and drives the High-

pressure Compressor (HPC). Then the helium moves through the Low-pressure Turbine (LPT), which drives the Low-pressure Compressor (LPC).

From the LPT the helium moves through the Power Turbine (PT), which drives the generator. At this stage the helium is still at a very high temperature. It passes through the recuperator where the heat is transferred from the high temperature helium from the PT to the low temperature helium returning to the reactor.

The helium is cooled down by the means of a pre-cooler. This increases the density of the helium and improves the efficiency of the compressors. The LPC compresses the helium. From the LPC the helium is cooled down further when it passes through the intercooler. The helium is compressed further by the HPC and then passes through the recuperator that heats the helium up again. The helium then returns to the reactor.

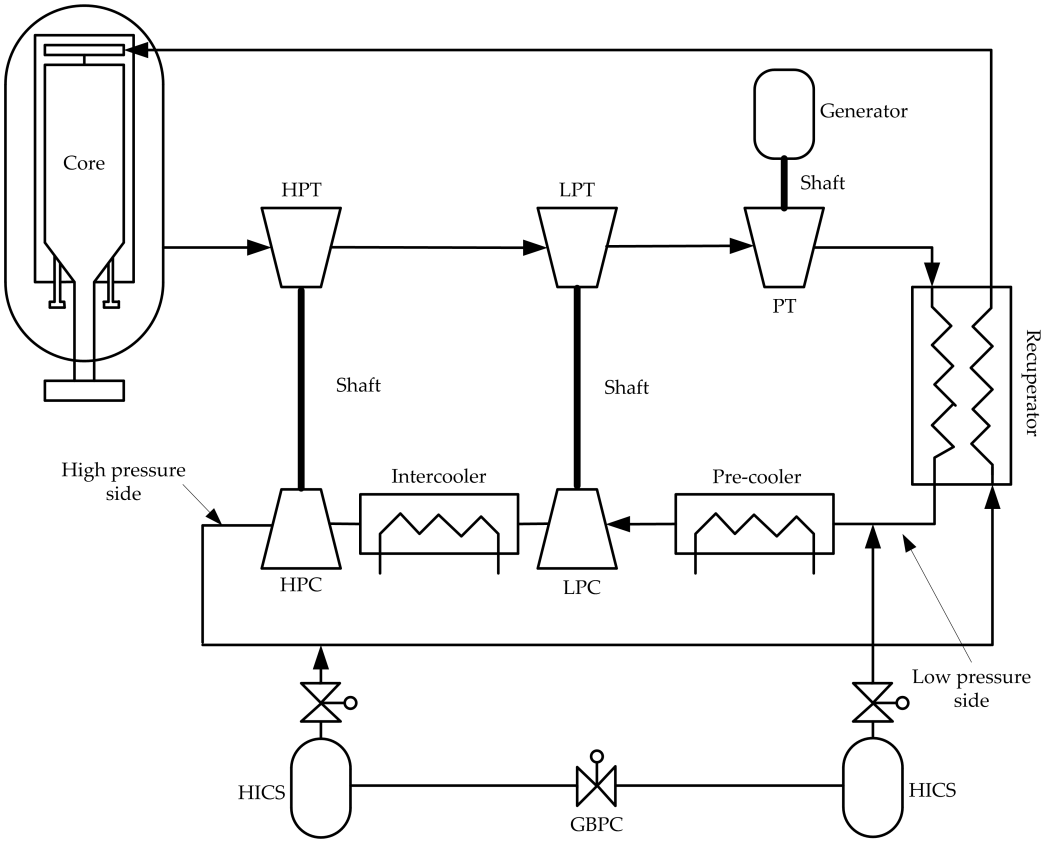

Figure 6.1: Simplified schematic drawing of the PBMR power conversion unit

6.3 Power output control

The power output of the system can be controlled by either adding or removing helium in the circuit. The power control is achieved by a series of helium storage tanks ranging from low to high pressure that maintain the required gas pressure in the circuit. Adjustable stator blades on

the turbomachinery and bypass flow are used to achieve short-term control [72]. The Helium Inventory Control System (HICS) and the Gas Cycle Bypass Control Valve (GBPC) are shown in Fig. 6.1. These two mechanisms are used to adjust the helium inventory of the cycle.

Helium is normally injected into the cycle at the low pressure side and extracted at the high pressure side. A limited amount of helium can also be injected at the high pressure side by means of a booster tank. Opening the GBPC has the effect of extracting a certain amount of helium at the high pressure side and injecting the same amount at the low pressure side.

6.4 Linear state space model of the PCU

Pritchard [12] developed a linear state space model from first principles that captured most of the dynamic behaviour of the power conversion unit for small perturbations in the control valves of the HICS. In order to compare the results of the derived linear model with predictions given by *Flownet*, (a research version of *Flownex*®, previously referred to as *Flownet 5*) he constructed a simplified model of the PCU in Flownet. The network diagram of the simplified model is given in Fig. 6.2.

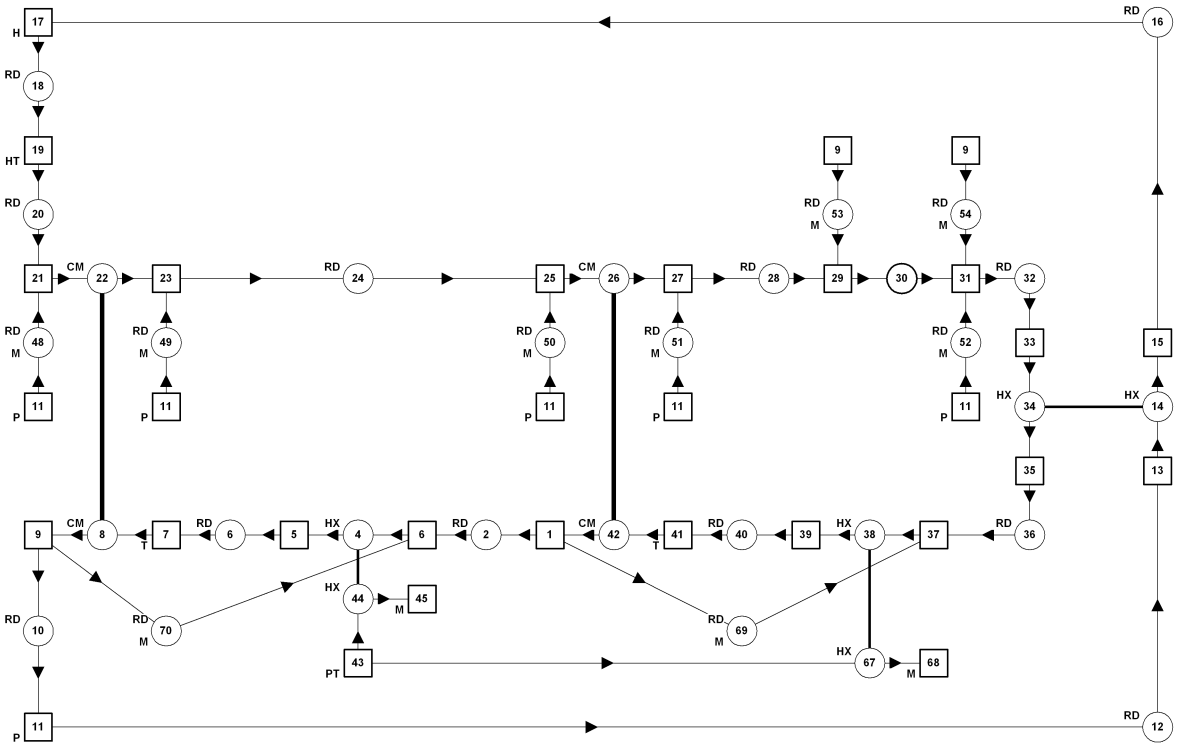

Figure 6.2: Simplified Flownet model of the PBMR PCU used for model validation [12]

The following simplifying settings were made by Pritchard:

- The reactor is modelled as a constant temperature node (node 19).

- The inlet temperatures of the LPC and HPC are fixed at 28 °C.
- Flow resistances are neglected by setting the flow areas in the pipe elements to 10 m^2.
- Leak flows were included to ensure that the turbomachines operate at similar operating points on the machine maps as compared to the detailed *Flownex*® model of the PBMR.

With all these assumptions, a simplified state space model of the PCU was constructed according to Fig. 6.3.

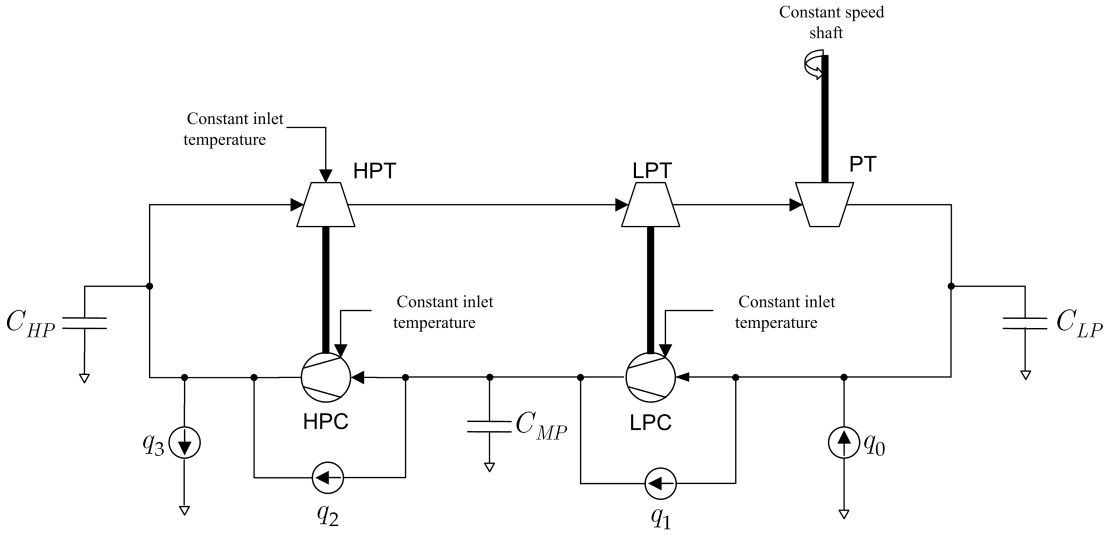

Figure 6.3: Schematic diagram of the conceptual model of the PCU [12]

The figure shows the significant volumes in the system indicated as capacitances (C_{HP}, C_{MP} and C_{LP}). The subscripts indicate the high, medium and low pressure regions in the system. The bypass valves over the compressors and the HICS tanks are modelled by constant mass flow sources ($q_0, \ldots, q_3$). The state variables of the system are the pressures at the indicated regions and the shaft speeds of the two turbine-compressor combinations. This resulted in a fifth order state space model given by

$$\dot{\mathbf{X}}(t) = \mathbf{A}\mathbf{X}(t) + \mathbf{B}\mathbf{U}(t), \tag{6.1}$$

where

$$\mathbf{X}(t) = \begin{bmatrix} P_{LP} & P_{MP} & P_{HP} & N_{HP} & N_{LP} \end{bmatrix}', \tag{6.2}$$

$$\mathbf{U}(t) = \begin{bmatrix} q_0 & q_1 & q_2 & q_3 \end{bmatrix}'. \tag{6.3}$$

The comparisons between the linear state space model of Pritchard and the Flownet model are shown in Fig. 6.4 and Fig. 6.5. The steady state values are subtracted from the results to isolate the perturbations from the steady state.

Fig. 6.4 compares the perturbations in pressure at the different pressure regions indicated in Fig. 6.3 for a scenario where helium is injected via flow source q_0 for a period $t = 4.5$ s up to

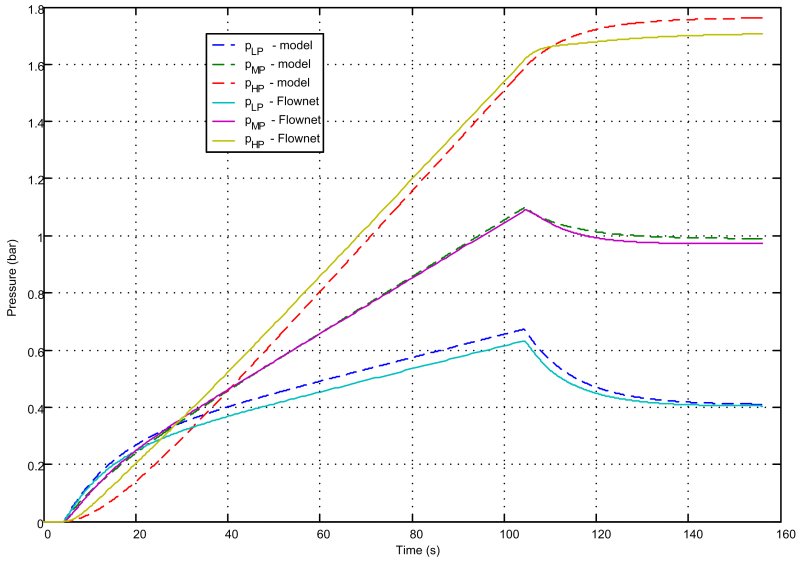

Figure 6.4: Perturbations in pressures predicted by the linear model and Flownet [12]

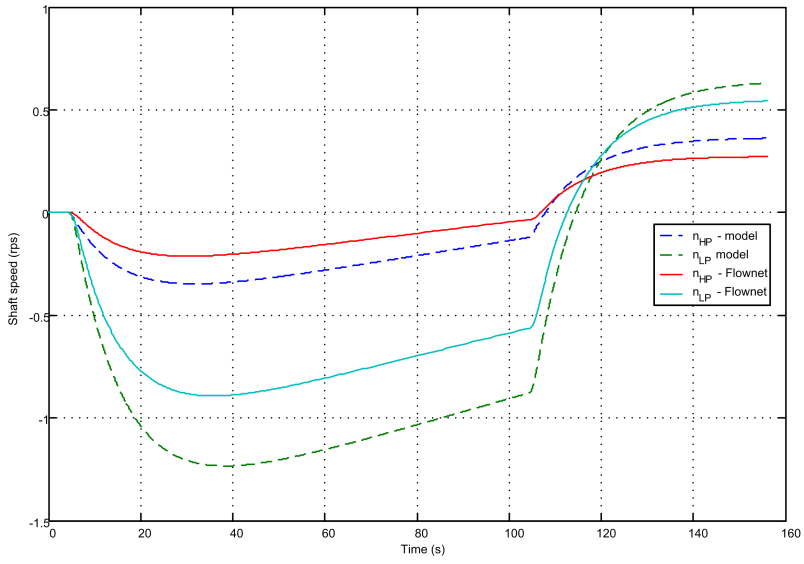

Figure 6.5: Perturbations in shaft speed predicted by the linear model and Flownet [12]

$t = 104.5$ s. Fig. 6.5 compares the perturbations in shaft speed for the low and high pressure turbine-compressor combinations also for the same flow source input and time period. From these results it can be seen that the linear state space model correlates well with the *Flownet* model.

Rubin [15] developed an extended linear *Simulink*® model based on the work done by

Pritchard. The *Simulink*® model includes dynamics such as leak flows, thermal effects and also the volumes between the turbines are taken into account as shown in Fig. 6.6.

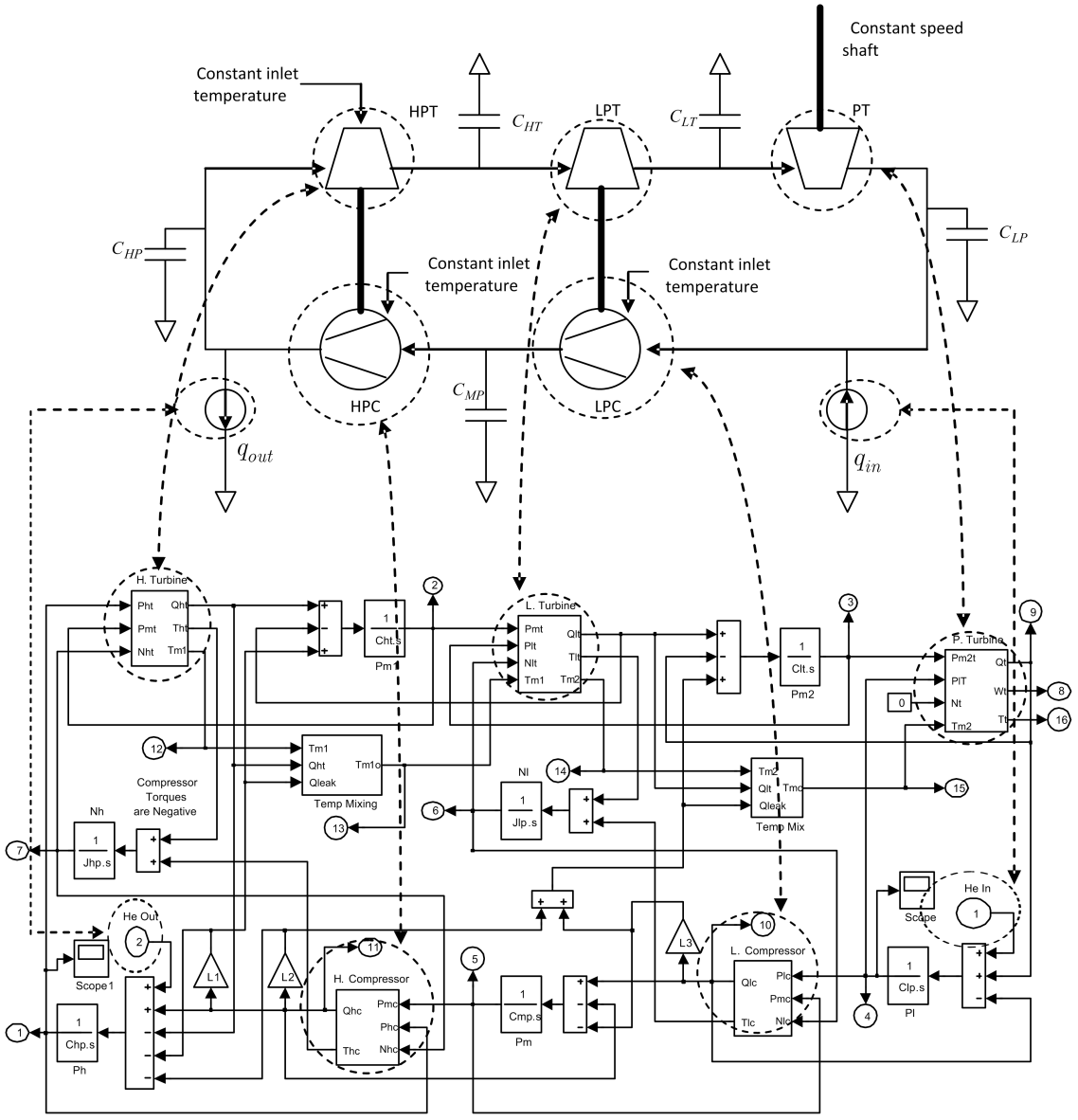

Figure 6.6: Linear *Simulink*® model of the PCU [15]

Fig. 6.7 compares the change in output power of the power turbine predicted by the *Simulink*® model and *Flownet* about an operating point, in response to a step change in helium injection. The figure also shows that the effect of helium injection is to first reduce the power and taking well over a minute before there is a net increase in power. This effect is called the non-minimum phase effect. This just shows how valuable a simplified model can be in terms of understanding the dominant dynamics of the system. It is also crucial for control system design.

Uren [16] implemented optimal PID and Fuzzy PID control strategies on the linear *Simulink*® model developed by Rubin. These controllers manipulated the helium inventory to the gas

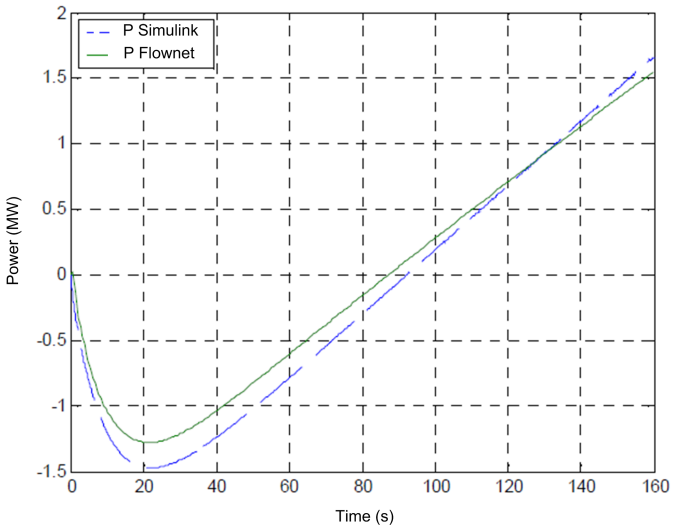

Figure 6.7: Comparison between *Simulink*® and Flownet models [15]

cycle in order to control the power output. The parameters of the controllers were optimised using a Genetic Algorithm (GA). By comparing their performance the Fuzzy PID control strategy showed to be superior. In this chapter the performance of a model-based MPC controller (which is an optimal control technique) will be compared with the optimised PID and Fuzzy controllers.

In Chapter 5 a nonlinear and time variant state space model of the PBMR PCU was extracted using the developed state space model extraction algorithm. This model also included the thermal state variables. For MPC a low order, linear time invariant state space model is required. It was therefore decided to extract a state space model from the hydraulic and mechanical network representations of the system as shown in Fig. 6.8. The flow sources that model the turbomachines were linearised around operating points. The HICS and bypass valve are modelled using two mass flow sources, where:

- $S_{fh,in}$ is activated with a positive value for helium injection,
- $S_{fh,out}$ is activated with a negative value for helium extraction,
- $S_{fh,in}$ and $S_{fh,out}$ are activated with positive and negative values respectively for helium bypass,
- $S_{fh,out}$ is activated with a positive value for helium boosting.

It was also decided to neglect the flow resistances and thermal effects as in the case of Pritchard's state space model. From the network representations the symbolic state space

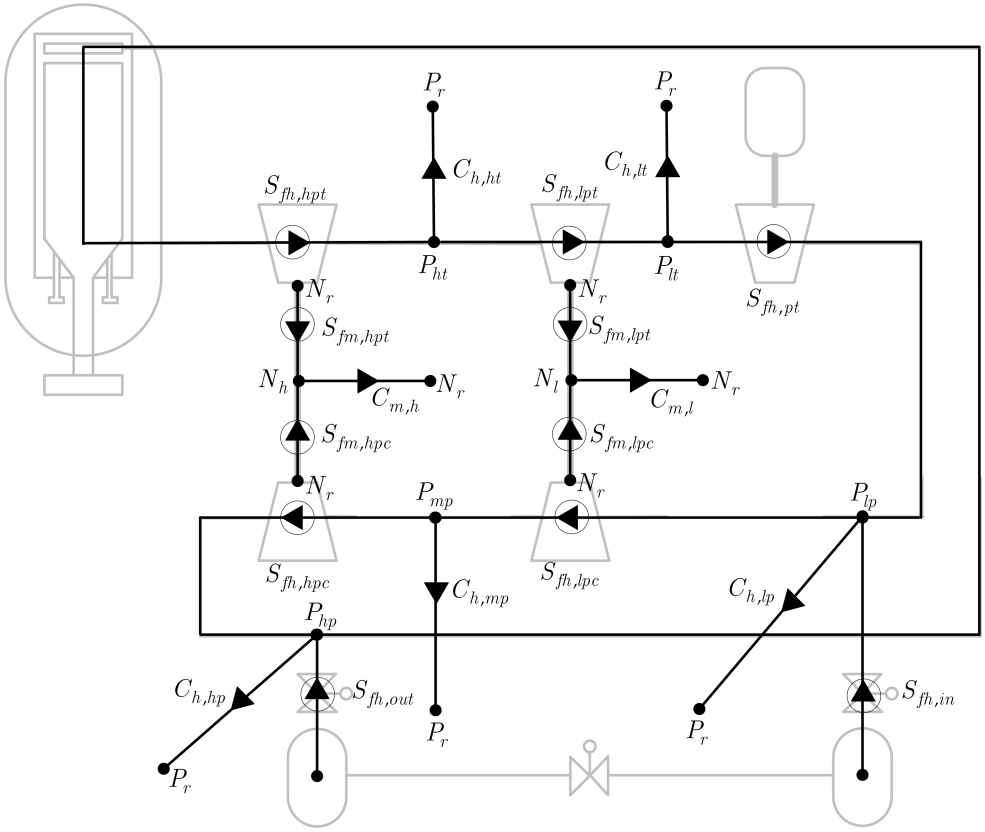

Figure 6.8: Hydraulic and mechanical network representation of the PCU

model was extracted and the result in Eq. (6.4) obtained.

$$\begin{bmatrix} \dot{P}_{hp} \\ \dot{P}_{ht} \\ \dot{P}_{lt} \\ \dot{P}_{lp} \\ \dot{P}_{mp} \\ \dot{N}_l \\ \dot{N}_h \end{bmatrix} = \begin{bmatrix} A_{11} & A_{12} & A_{13} & A_{14} & A_{15} & A_{16} & A_{17} \\ A_{21} & A_{22} & A_{23} & A_{24} & A_{25} & A_{26} & A_{27} \\ A_{31} & A_{32} & A_{33} & A_{34} & A_{35} & A_{36} & A_{37} \\ A_{41} & A_{42} & A_{43} & A_{44} & A_{45} & A_{46} & A_{47} \\ A_{51} & A_{52} & A_{53} & A_{54} & A_{55} & A_{56} & A_{57} \\ A_{61} & A_{62} & A_{63} & A_{64} & A_{65} & A_{66} & A_{67} \\ A_{71} & A_{72} & A_{73} & A_{74} & A_{75} & A_{76} & A_{77} \end{bmatrix} \begin{bmatrix} P_{hp} \\ P_{ht} \\ P_{lt} \\ P_{lp} \\ P_{mp} \\ N_l \\ N_h \end{bmatrix} + \begin{bmatrix} B_{11} & B_{12} \\ B_{21} & B_{22} \\ B_{31} & B_{32} \\ B_{41} & B_{42} \\ B_{51} & B_{52} \\ B_{61} & B_{62} \\ B_{71} & B_{72} \end{bmatrix} \begin{bmatrix} S_{fh,out} \\ S_{fh,in} \end{bmatrix} \tag{6.4}$$

In the following sections the symbolic linearised elements of the **A** and **B** matrices will be obtained by deriving linearised equations for the flow sources of the hydraulic and mechanical domains.

6.4.1 Hydraulic flow sources

The generalised flow source for compressors can be determined using the pressure ratio equation and the pressure ratio map. The pressure ratio of a compressor is given by

$$P_{rc} = \frac{P_{02}}{P_{01}}. \tag{6.5}$$

The linearised approximation of Eq. (6.5) is given by

$$\tilde{P}_{rc} = \frac{\partial P_{rc}}{\partial P_{01}}\tilde{P}_{01} + \frac{\partial P_{rc}}{\partial P_{02}}\tilde{P}_{02}, \tag{6.6}$$

where the tilde over a variable indicates the perturbation of the variable. Looking at the compressor pressure ratio map (Fig. 5.6), it can be seen that the pressure ratio is a function of the non-dimensional mass flow rate and non-dimensional speed. Therefore

$$\tilde{P}_{rc} = \frac{\partial P_{rc}}{\partial Q'}\tilde{Q}' + \frac{\partial P_{rc}}{\partial N'}\tilde{N}', \tag{6.7}$$

where

$$\tilde{Q}' = \frac{\partial Q'}{\partial \dot{m}}\tilde{\dot{m}} + \frac{\partial Q'}{\partial P_{01}}\tilde{P}_{01} + \frac{\partial Q'}{\partial T_{01}}\tilde{T}_{01}, \tag{6.8}$$

$$\tilde{N}' = \frac{\partial N'}{\partial N}\tilde{N} + \frac{\partial N'}{\partial T_{01}}\tilde{T}_{01}, \tag{6.9}$$

are linear approximations of the non-dimensional mass flow rate, $Q' = \dot{m}\sqrt{T_{01}}/P_{01}$, and non-dimensional speed, $N' = N/\sqrt{T_{01}}$.

Eq. (6.7) may be expanded to yield

$$\tilde{P}_{rc} = \frac{\partial P_{rc}}{\partial Q'}\left(\frac{\partial Q'}{\partial \dot{m}}\tilde{\dot{m}} + \frac{\partial Q'}{\partial P_{01}}\tilde{P}_{01} + \frac{\partial Q'}{\partial T_{01}}\tilde{T}_{01}\right) + \frac{\partial P_{rc}}{\partial N'}\left(\frac{\partial N'}{\partial N}\tilde{N} + \frac{\partial N'}{\partial T_{01}}\tilde{T}_{01}\right). \tag{6.10}$$

Substituting Eq. (6.6) into Eq. (6.10) gives

$$\begin{aligned}\left(\frac{\partial P_{rc}}{\partial Q'}\frac{\partial Q'}{\partial \dot{m}}\right)\tilde{\dot{m}} =& \left(\frac{\partial P_{rc}}{\partial P_{01}} - \frac{\partial P_{rc}}{\partial Q'}\frac{\partial Q'}{\partial P_{01}}\right)\tilde{P}_{01} + \left(\frac{\partial P_{rc}}{\partial P_{02}}\right)\tilde{P}_{02} - \\ & \left(\frac{\partial P_{rc}}{\partial N'}\frac{\partial N'}{\partial N}\right)\tilde{N} - \left(\frac{\partial P_{rc}}{\partial Q'}\frac{\partial Q'}{\partial T_{01}} + \frac{\partial P_{rc}}{\partial N'}\frac{\partial N'}{\partial T_{01}}\right)\tilde{T}_{01}.\end{aligned} \tag{6.11}$$

The inlet temperature term in Eq. (6.11) is neglected since the state space model does not contain any thermal states. The linearised flow source representing a compressor may then be given by

$$S_{fh,c} = \tilde{\dot{m}} = \frac{1}{\beta_{Q'}^{P_{rc}}}\left(\xi_{P_{01}}^{P_{rc}} \cdot \tilde{P}_{01} + \xi_{P_{02}}^{P_{rc}} \cdot \tilde{P}_{02} - \xi_{N'}^{P_{rc}} \cdot \tilde{N}\right), \tag{6.12}$$

where

$$\beta_{Q'}^{P_{rc}} = \left(\frac{\partial P_{rc}}{\partial Q'}\frac{\partial Q'}{\partial \dot{m}}\right), \tag{6.13}$$

$$\xi_{P_{01}}^{P_{rc}} = \left(\frac{\partial P_{rc}}{\partial P_{01}} - \frac{\partial P_{rc}}{\partial Q'}\frac{\partial Q'}{\partial P_{01}}\right), \tag{6.14}$$

$$\xi_{P_{02}}^{P_{rc}} = \left(\frac{\partial P_{rc}}{\partial P_{02}}\right), \tag{6.15}$$

$$\xi_{N'}^{P_{rc}} = \left(\frac{\partial P_{rc}}{\partial N'}\frac{\partial N'}{\partial N}\right). \tag{6.16}$$

In a similar way the linearised flow source representing a turbine may be given by

$$S_{fh,t} = \tilde{\dot{m}} = \frac{1}{\beta_{Q'}^{P_{rt}}}\left(\xi_{P_{01}}^{P_{rt}} \cdot \tilde{P}_{01} + \xi_{P_{02}}^{P_{rt}} \cdot \tilde{P}_{02} - \xi_{N'}^{P_{rt}} \cdot \tilde{N}\right). \tag{6.17}$$

The linearised equations for the compressor flow sources, $S_{fh,lpc}$ and $S_{fh,hpc}$, are as follows:

$$\begin{aligned} S_{fh,lpc} &= \frac{1}{\beta_{Q',lpc}^{P_{rc}}}\left(\xi_{P_{01},lpc}^{P_{rc}} \cdot P_{lp} + \xi_{P_{02},lpc}^{P_{rc}} \cdot P_{mp} - \xi_{N',lpc}^{P_{rc}} \cdot N_l\right) \\ &= K_{lpc,1} \cdot P_{lp} + K_{lpc,2} \cdot P_{mp} - K_{lpc,3} \cdot N_l, \end{aligned} \tag{6.18}$$

where

$$K_{lpc,1} = \frac{\xi_{P_{01},lpc}^{P_{rc}}}{\beta_{Q',lpc}^{P_{rc}}},\ K_{lpc,2} = \frac{\xi_{P_{02},lpc}^{P_{rc}}}{\beta_{Q',lpc}^{P_{rc}}},\ K_{lpc,3} = \frac{\xi_{N',lpc}^{P_{rc}}}{\beta_{Q',lpc}^{P_{rc}}}. \tag{6.19}$$

$$\begin{aligned} S_{fh,hpc} &= \frac{1}{\beta_{Q',hpc}^{P_{rc}}}\left(\xi_{P_{01},hpc}^{P_{rc}} \cdot P_{mp} + \xi_{P_{02},lpc}^{P_{rc}} \cdot P_{hp} - \xi_{N',hpc}^{P_{rc}} \cdot N_h\right) \\ &= K_{hpc,1} \cdot P_{mp} + K_{hpc,2} \cdot P_{hp} - K_{hpc,3} \cdot N_h, \end{aligned} \tag{6.20}$$

where

$$K_{hpc,1} = \frac{\xi_{P_{01},hpc}^{P_{rc}}}{\beta_{Q',hpc}^{P_{rc}}},\ K_{hpc,2} = \frac{\xi_{P_{02},hpc}^{P_{rc}}}{\beta_{Q',hpc}^{P_{rc}}},\ K_{hpc,3} = \frac{\xi_{N',hpc}^{P_{rc}}}{\beta_{Q',hpc}^{P_{rc}}}. \tag{6.21}$$

The linearised equations for the turbine flow sources, $S_{fh,lpt}$, $S_{fh,hpt}$ and $S_{fh,pt}$, are as follows:

$$\begin{aligned} S_{fh,lpt} &= \frac{1}{\beta_{Q',lpt}^{P_{rt}}}\left(\xi_{P_{01},lpt}^{P_{rt}} \cdot P_{ht} + \xi_{P_{02},lpt}^{P_{rt}} \cdot P_{lt} - \xi_{N',lpt}^{P_{rt}} \cdot N_l\right) \\ &= K_{lpt,1} \cdot P_{ht} + K_{lpt,2} \cdot P_{lt} - K_{lpt,3} \cdot N_l, \end{aligned} \tag{6.22}$$

where

$$K_{lpt,1} = \frac{\xi_{P_{01},lpt}^{P_{rt}}}{\beta_{Q',lpt}^{P_{rt}}},\ K_{lpt,2} = \frac{\xi_{P_{02},lpt}^{P_{rt}}}{\beta_{Q',lpt}^{P_{rt}}},\ K_{lpt,3} = \frac{\xi_{N',lpt}^{P_{rt}}}{\beta_{Q',lpt}^{P_{rt}}}. \tag{6.23}$$

$$\begin{aligned} S_{fh,hpt} &= \frac{1}{\beta_{Q',hpt}^{P_{rt}}}\left(\xi_{P_{01},hpt}^{P_{rt}} \cdot P_{hp} + \xi_{P_{02},hpt}^{P_{rt}} \cdot P_{ht} - \xi_{N',hpt}^{P_{rt}} \cdot N_h\right) \\ &= K_{hpt,1} \cdot P_{hp} + K_{hpt,2} \cdot P_{ht} - K_{hpt,3} \cdot N_h, \end{aligned} \tag{6.24}$$

where

$$K_{hpt,1} = \frac{\xi^{P_{rt}}_{P_{01},hpt}}{\beta^{P_{rt}}_{Q',hpt}},\ K_{hpt,2} = \frac{\xi^{P_{rt}}_{P_{02},hpt}}{\beta^{P_{rt}}_{Q',hpt}},\ K_{hpt,3} = \frac{\xi^{P_{rt}}_{N',hpt}}{\beta^{P_{rt}}_{Q',hpt}}. \tag{6.25}$$

$$\begin{aligned} S_{fh,pt} &= \frac{1}{\beta^{P_{rt}}_{Q',pt}}\left(\xi^{P_{rt}}_{P_{01},pt} \cdot P_{lt} + \xi^{P_{rt}}_{P_{02},pt} \cdot P_{lp}\right) \\ &= K_{pt,1} \cdot P_{lt} + K_{pt,2} \cdot P_{lp}, \end{aligned} \tag{6.26}$$

where

$$K_{pt,1} = \frac{\xi^{P_{rt}}_{P_{01},pt}}{\beta^{P_{rt}}_{Q',pt}},\ K_{pt,2} = \frac{\xi^{P_{rt}}_{P_{02},pt}}{\beta^{P_{rt}}_{Q',pt}}. \tag{6.27}$$

6.4.2 Mechanical flow sources

The flow sources in the mechanical domain represent the torques acting on the shafts of the system. In the PCU shafts in turbine-compressor combinations are considered. The torques on the shaft are therefore due to the turbine and compressor acting on the shaft. For a compressor the flow source is given by

$$S_{fm,c} = \tilde{\tau}_c = \frac{\partial \tau_c}{\partial W_c}\tilde{W}_c + \frac{\partial \tau_c}{\partial N}\tilde{N}, \tag{6.28}$$

which is a linear approximation of the torque equation, $\tau_c = \eta_m W_c / 2\pi N$. The linear approximation of the work, $W_c = \dot{m} C_p \Delta T$, done by the shaft on the compressor is

$$\tilde{W}_c = \frac{\partial W_c}{\partial \dot{m}}\tilde{\dot{m}} + \frac{\partial W_c}{\partial \Delta T}\Delta\tilde{T}. \tag{6.29}$$

Discarding the temperature term, Eq. (6.29) may be written as

$$\tilde{\tau}_c = \left(\frac{\partial \tau_c}{\partial W_c}\frac{\partial W_c}{\partial \dot{m}}\right)\tilde{\dot{m}} + \frac{\partial \tau_c}{\partial N}\tilde{N}. \tag{6.30}$$

Substituting Eq. (6.12) into Eq.(6.30), the mechanical flow source representing a compressor may be given as

$$S_{fm,c} = \tilde{\tau}_c = K_{\tau_c,1} \cdot \tilde{P}_{01} + K_{\tau_c,2} \cdot \tilde{P}_{02} + K_{\tau_c,3} \cdot \tilde{N} \tag{6.31}$$

where

$$K_{\tau_c,1} = \left(\frac{\xi^{P_{rc}}_{P_{01}}}{\beta^{P_{rc}}_{Q'}}\frac{\partial \tau_c}{\partial W_c}\frac{\partial W_c}{\partial \dot{m}}\right), \tag{6.32}$$

$$K_{\tau_c,2} = \left(\frac{\xi^{P_{rc}}_{P_{02}}}{\beta^{P_{rc}}_{Q'}}\frac{\partial \tau_c}{\partial W_c}\frac{\partial W_c}{\partial \dot{m}}\right), \tag{6.33}$$

$$K_{\tau_c,3} = \left(-\frac{\xi^{P_{rc}}_{N'}}{\beta^{P_{rc}}_{Q'}}\frac{\partial \tau_c}{\partial W_c}\frac{\partial W_c}{\partial \dot{m}} + \frac{\partial \tau_c}{\partial N}\right). \tag{6.34}$$

In the same way the mechanical flow source representing a turbine can be written as

$$S_{fm,t} = \tilde{\tau}_t = K_{\tau_t,1} \cdot \tilde{P}_{01} + K_{\tau_t,2} \cdot \tilde{P}_{02} + K_{\tau_t,3} \cdot \tilde{N}. \tag{6.35}$$

The linearised mechanical flow sources representing the compressors, $S_{fm,lpc}$ and $S_{fm,hpc}$, are as follows:

$$S_{fm,lpc} = K_{\tau_{lpc},1} \cdot P_{lp} + K_{\tau_{lpc},2} \cdot P_{mp} + K_{\tau_{lpc},3} \cdot N_l, \tag{6.36}$$

$$S_{fm,hpc} = K_{\tau_{hpc},1} \cdot P_{mp} + K_{\tau_{hpc},2} \cdot P_{hp} + K_{\tau_{hpc},3} \cdot N_h. \tag{6.37}$$

The mechanical flow sources representing the turbines, $S_{fm,lpt}$ and $S_{fm,hpt}$, are as follows:

$$S_{fm,lpt} = K_{\tau_{lpt},1} \cdot P_{ht} + K_{\tau_{lpt},2} \cdot P_{lt} + K_{\tau_{lpt},3} \cdot N_l, \tag{6.38}$$

$$S_{fm,hpt} = K_{\tau_{hpt},1} \cdot P_{hp} + K_{\tau_{hpt},2} \cdot P_{ht} + K_{\tau_{hpt},3} \cdot N_h. \tag{6.39}$$

6.4.3 Symbolic matrix elements

The elements of the **A** and **B** matrices of Eq. (6.4) can be symbolically derived by substituting the equations of the generalised flow sources in the following extracted state equations:

$$\dot{P}_{hp} = \frac{1}{C_{h,hp}}(S_{fh,hpc} - S_{fh,hpt} + S_{fh,out}), \tag{6.40}$$

$$\dot{P}_{ht} = \frac{1}{C_{h,ht}}(S_{fh,hpt} - S_{fh,lpt}), \tag{6.41}$$

$$\dot{P}_{lt} = \frac{1}{C_{h,lt}}(S_{fh,lpt} - S_{fh,pt}), \tag{6.42}$$

$$\dot{P}_{lp} = \frac{1}{C_{h,lp}}(S_{fh,pt} - S_{fh,lpc} + S_{fh,in}), \tag{6.43}$$

$$\dot{P}_{mp} = \frac{1}{C_{h,mp}}(S_{fh,lpc} - S_{fh,hpc}), \tag{6.44}$$

$$\dot{N}_l = \frac{1}{C_{m,l}}(S_{fm,lpt} + S_{fm,lpc}), \tag{6.45}$$

$$\dot{N}_h = \frac{1}{C_{m,h}}(S_{fm,hpt} + S_{fm,hpc}). \tag{6.46}$$

Then

- From Eq. (6.40): $A_{11} = \frac{K_{hpc,2} - K_{hpt,1}}{C_{h,hp}}$, $A_{12} = -\frac{K_{hpc,2}}{C_{h,hp}}$, $A_{15} = \frac{K_{hpc,1}}{C_{h,hp}}$, $A_{17} = \frac{-K_{hpc,3} + K_{hpt,3}}{C_{h,hp}}$, and $B_{11} = \frac{1}{C_{h,hp}}$.
- From Eq. (6.41): $A_{21} = \frac{K_{hpt,1}}{C_{h,ht}}$, $A_{22} = \frac{K_{hpt,2} - K_{lpt,1}}{C_{h,ht}}$, $A_{23} = -\frac{K_{lpt,2}}{C_{h,ht}}$, $A_{26} = \frac{K_{lpt,3}}{C_{h,ht}}$, $A_{27} = -\frac{K_{hpt,3}}{C_{h,ht}}$.
- From Eq. (6.42): $A_{32} = \frac{K_{lpt,1}}{C_{h,lt}}$, $A_{33} = \frac{K_{lpt,2} - K_{pt,1}}{C_{h,lt}}$, $A_{34} = -\frac{K_{pt,2}}{C_{h,lt}}$, $A_{36} = -\frac{K_{lpt,3}}{C_{h,lt}}$.
- From Eq. (6.43): $A_{43} = \frac{K_{pt,1}}{C_{h,lp}}$, $A_{44} = \frac{K_{pt,2} - K_{lpc,1}}{C_{h,lp}}$, $A_{45} = -\frac{K_{lpc,2}}{C_{h,lp}}$, $A_{46} = \frac{K_{lpc,3}}{C_{h,lp}}$, and $B_{42} = \frac{1}{C_{h,lp}}$.

- From Eq. (6.44): $A_{51} = -\frac{K_{hpc,2}}{C_{h,mp}}$, $A_{54} = \frac{K_{lpc,1}}{C_{h,mp}}$, $A_{55} = \frac{K_{lpc,2}-K_{hpc,1}}{C_{h,mp}}$, $A_{56} = \frac{K_{lpc,3}}{C_{h,mp}}$, $A_{57} = \frac{K_{hpc,3}}{C_{h,mp}}$.
- From Eq. (6.45): $A_{62} = \frac{K_{\tau_{lpt},1}}{C_{m,l}}$, $A_{63} = \frac{K_{\tau_{lpt},2}}{C_{m,l}}$, $A_{64} = \frac{K_{\tau_{lpc},1}}{C_{m,l}}$, $A_{65} = \frac{K_{\tau_{lpc},2}}{C_{m,l}}$, $A_{66} = \frac{K_{\tau_{lpt},3}+K_{\tau_{lpc},3}}{C_{m,l}}$.
- From Eq. (6.46): $A_{71} = \frac{K_{\tau_{hpt},1}+K_{\tau_{hpc},3}}{C_{m,h}}$, $A_{72} = \frac{K_{\tau_{hpt},2}}{C_{m,h}}$, $A_{75} = \frac{K_{\tau_{hpc},1}}{C_{m,h}}$, $A_{77} = \frac{K_{\tau_{hpt},3}+K_{\tau_{hpc},3}}{C_{m,h}}$.

The remainder of the matrix elements are zeros.

6.5 Extracted linear state space model validation

The extracted state space model will be compared with the linear *Simulink*® model developed by Rubin [15]. Operating point values obtained from the *Flownet* simulation model and used in the development of the *Simulink*® model, are also used to derive some of the numeric coefficients of the extracted state space model. These operating points are given in Table 6.1.

Table 6.1: Operating points of the turbomachines

	HPT	LPT	PT	HPC	LPC
Inlet Pressure [bar]	66.6297	54.6362	40.1385	43.353	22.6753
Outlet Pressure [bar]	54.8958	40.4244	23.2309	71.1325	44.9211
Inlet Temperature [K]	1167.8709	1077.6134	951.0655	294.0547	294.5871
Outlet Temperature [K]	1081.2458	958.1085	773.8077	364.6934	397.3649
Shaft speed [rps]	100.0288	117.1042	50	100.0288	117.1042
Mass flow [kg/s]	145.9751	148.9716	153.1759	152.2948	157.472
Efficiency	0.87584	0.90909	0.8902	0.8902	0.88956
Power output [MW]	57.8144	86.041	137.4871	-57.2363	-85.1805

The numerical state space model is given as

$$\dot{\mathbf{X}}(t) = \mathbf{A}\mathbf{X}(t) + \mathbf{B}\mathbf{U}(t) \tag{6.47}$$

$$\mathbf{Y}(t) = \mathbf{C}\mathbf{X}(t) + \mathbf{D}\mathbf{U}(t), \tag{6.48}$$

where

$$\mathbf{X}(t) = \begin{bmatrix} P_{hp}(t) & P_{ht}(t) & P_{lt}(t) & P_{lp}(t) & P_{mp}(t) & N_l(t) & N_h(t) \end{bmatrix}',$$

$$\mathbf{U}(t) = \begin{bmatrix} S_{fh,out} & S_{fh,in} \end{bmatrix}',$$

$$\mathbf{Y}(t) = \begin{bmatrix} \dot{m}_{lc} & \dot{m}_{hc} & \dot{m}_{ht} & \dot{m}_{lt} & \dot{m}_t & W_t \end{bmatrix}',$$

and

$$\mathbf{A} = \begin{bmatrix} -0.1113 & 0.0688 & 0 & 0 & 0.0869 & 0 & 0.0424 \\ 12.22 & -20.18 & 6.998 & 0 & 0 & -0.4724 & -0.1151 \\ 0 & 10.56 & -18.38 & 6.787 & 0 & 0.4724 & 0 \\ 0 & 0 & 0.2414 & -0.5977 & 0.0832 & -0.1117 & 0 \\ 0.1023 & 0 & 0 & 0.6577 & -0.4938 & 0.1619 & -0.1786 \\ 0 & 4.159 & -4.557 & 0.0844 & -1.099 & -0.7397 & 0 \\ 3.143 & -4.008 & 0 & 0 & 0.1898 & 0 & -0.73 \end{bmatrix},$$

$$\mathbf{B} = \begin{bmatrix} 0.0143 & 0 \\ 0 & 0 \\ 0 & 0 \\ 0 & 0.0424 \\ 0 & 0 \\ 0 & 0 \\ 0 & 0 \end{bmatrix},$$

$$\mathbf{C} = \begin{bmatrix} 0 & 0 & 0 & 10.69 & -1.960 & 2.632 & 0 \\ -1.663 & 0 & 0 & 0 & 6.067 & 0 & 2.903 \\ 6.110 & -4.809 & 0 & 0 & 0 & 0 & -0.0575 \\ 0 & 5.278 & -3.499 & 0 & 0 & 0.2362 & 0 \\ 0 & 0 & 5.690 & -3.394 & 0 & 0 & 0 \\ 0 & 0 & 10330000 & -12500000 & 0 & 0 & 0 \end{bmatrix},$$

$$\mathbf{D} = \begin{bmatrix} 0 & 0 \\ 0 & 0 \\ 0 & 0 \\ 0 & 0 \\ 0 & 0 \\ 0 & 0 \end{bmatrix}.$$

In order to test the validity of the extracted state space model, four different dynamic simulations will be performed and compared with the validated *Simulink*® model of Rubin [15]. These are

- Helium injection: Inject mass at a rate of 1 kg/s by setting $S_{fh,in} = 1$.
- Helium extraction: Extract mass at a rate of 1 kg/s by setting $S_{fh,out} = -1$.
- Helium bypass: Bypass helium at a rate of 1 kg/s by setting $S_{fh,in} = 1$ and $S_{fh,out} = -1$.
- Helium boosting: Boost at a rate of 1 kg/s by setting $S_{fh,out} = 1$.

It should be noted that the perturbations where isolated from the steady state values in the following results. For all the tests, the step input begins at $t = 10$ s and ends at time $t = 100$ s.

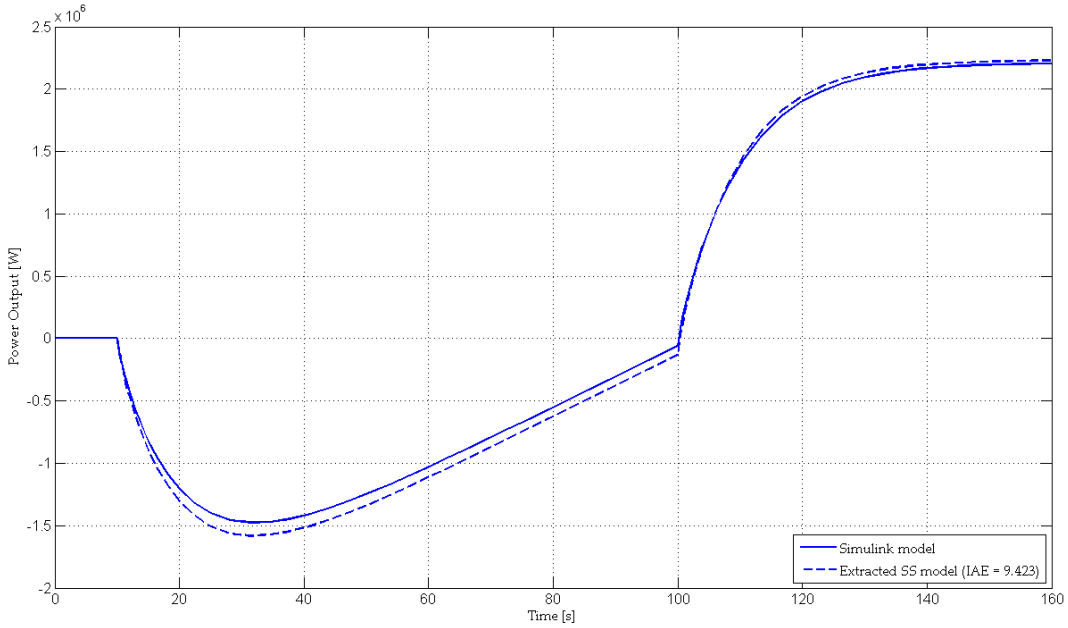

Figure 6.9: Helium injection: A comparison between perturbations in power output

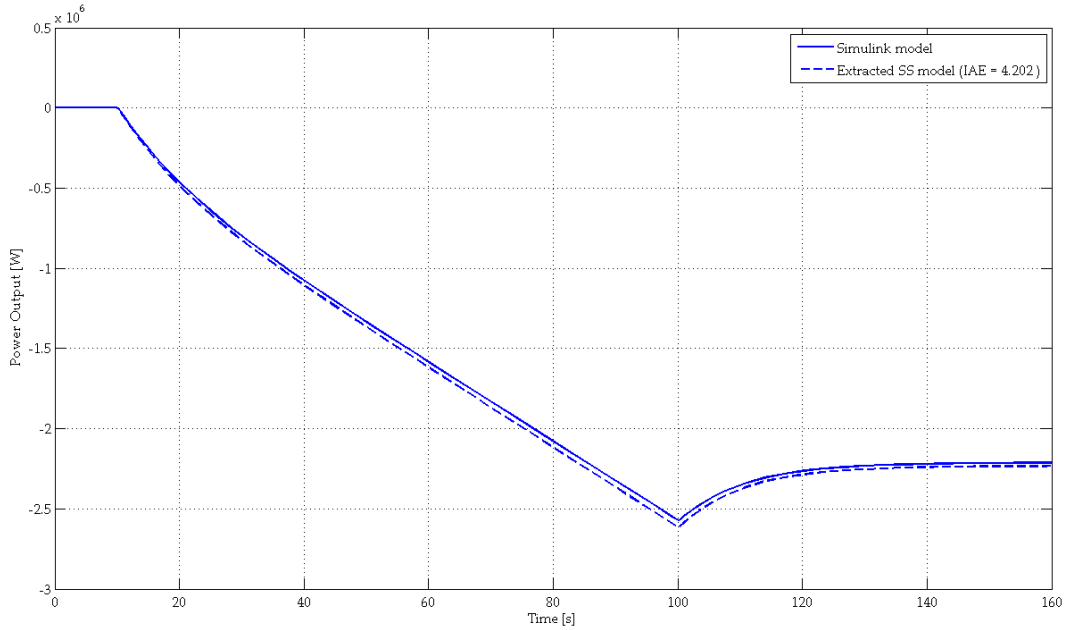

Figure 6.10: Helium extraction: A comparison between perturbations in power output

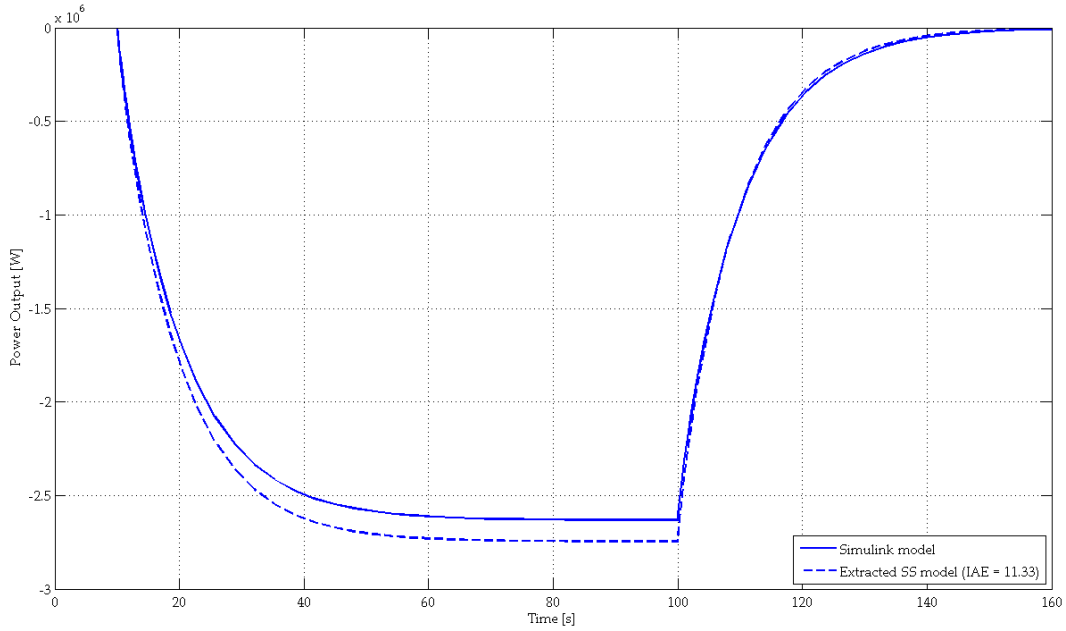

Figure 6.11: Helium bypass: A comparison between perturbations in power output

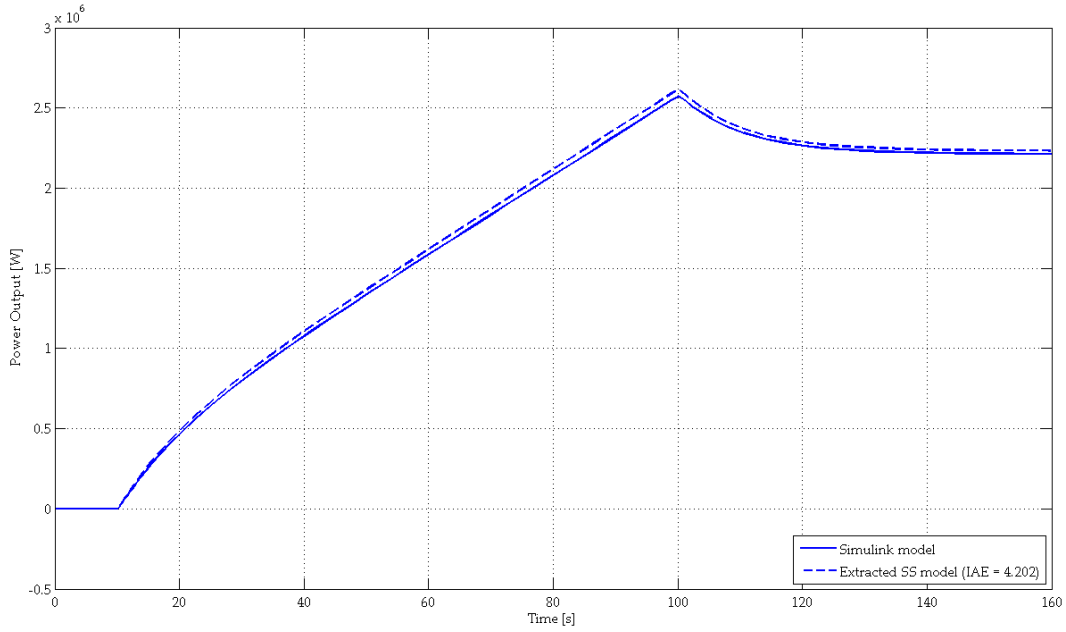

Figure 6.12: Helium boost: A comparison between perturbations in power output

The results presented in Figs. 6.9 - 6.12 and the low values of the IAE index show that the extracted state space model compares well with the *Simulink*® model. The extracted linear state space model therefore portrays the dominant system dynamics of the PBMR PCU. This state space model can now be used for control system design purposes.

6.6 Model based control

The extracted state space model can be used to realise a model-predictive controller for optimal control of the power output of the PBMR PCU. The state space model is used to predict the behaviour of the power output with respect to changes to the helium inventory. A model-predictive controller uses the state space model and current plant measurements to predict future moves of the inputs that will produce the desired plant outputs. The controller has a feedback mechanism that compensates for prediction errors due to un-modelled dynamics or disturbances.

The state space model is used in an online, iterative, finite horizon optimisation algorithm. At time $t = t_k$ where k is the current sample, the current state is sampled and a cost minimising control strategy (law) is computed for a short time window in the future $[t_k, \ldots, t_{k+p}]$. The size of the prediction window is represented by p. The prediction encompasses the exploration of the state trajectories and the solution of a cost function from the current time t_k up to time t_{k+p}. The best control action is then applied and the sequence repeats, calculating a new control and predicted state path. The model predictive state diagram is given in Fig. 6.13.

The cost function to be minimised has a quadratic form and relates closely to the cost function used by LQR control. It is given by [2]

$$J = \sum w_{x_i}(r_i - x_i)^2 + \sum w_{u_i}\Delta u_i^2, \tag{6.49}$$

where

- x_i is the i^{th} state variable - The pressures and shaft speeds are the states variables,
- r_i is the i^{th} set point or reference - The desired output power is the set point,
- u_i is the i^{th} input (manipulable) variable - The input variables are the injected and extracted mass flow rates,
- w_{x_i} is the weighting factor reflecting the relative importance of the i^{th} state variable,
- w_{u_i} is the weighting factor penalising large changes in the i^{th} input.

An advantage MPC has over other state space model based controllers is the fact that it can accommodate constraints. For example, the output of the controller may be limited between two boundaries or the rate of change of the input can be specified. Also the allowable output variable boundaries may be specified.

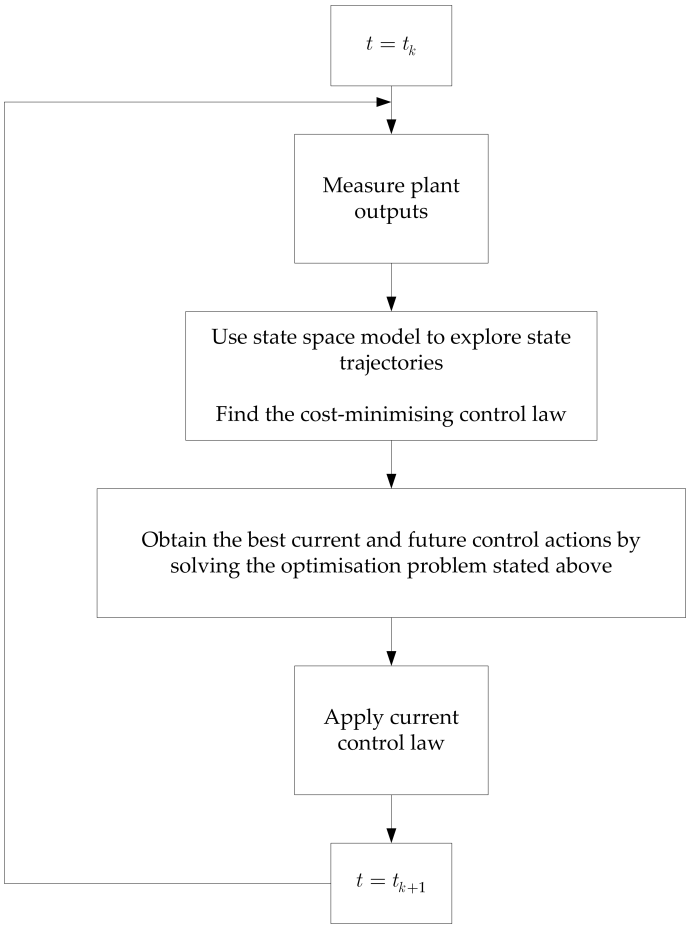

Figure 6.13: Model predictive control scheme

In this section the performance of the model-predictive controller will be compared with two other optimal control strategies developed by Uren [16]. He evaluated optimal PID and Fuzzy PID control strategies on the *Simulink*® model of the PBMR PCU developed by Rubin [15]. Fig. 6.14 shows the control configuration used.

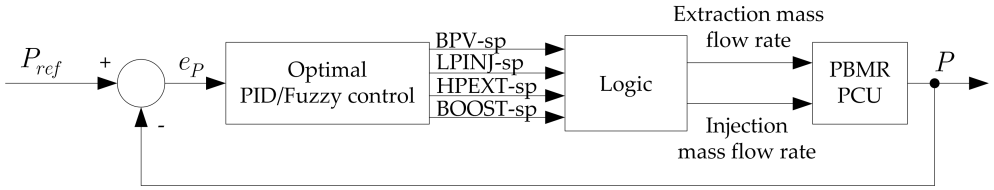

Figure 6.14: Conceptual diagram of the optimal PID and Fuzzy control strategies

P is the power output of the system and P_{ref} is the desired power reference value. The control system takes the power error (e_P) as input and generates set point values for the four helium manipulation actuators. These set point values are converted to signals that specify the desired amount of helium to be injected or extracted. These signals are the two inputs of the PBMR PCU *Simulink*® model.

The parameters of the PID controller were optimised using a Genetic Algorithm (GA) and the ITAE performance index was used as a cost function. Fig. 6.15 compares the power output of the system with a power reference signal. Fig. 6.16 shows the ITAE performance function values. The ITAE performance index is useful in control performance analysis, since it reduces the contribution of the large initial error to the value of the performance integral, as well as emphasises errors occurring later in the response [66]. Therefore the ITAE performance index is used in this case.

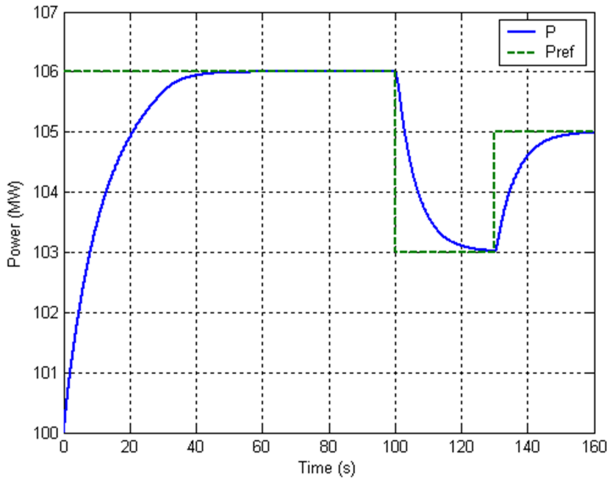

Figure 6.15: Optimal PID control [16]

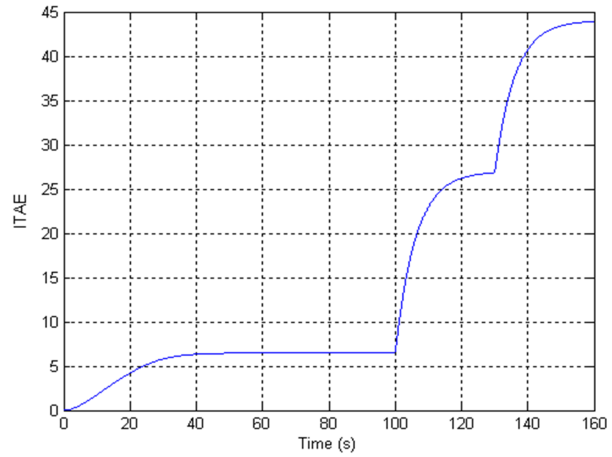

Figure 6.16: Performance of the optimal PID control strategy (ITAE = 43.9) [16]

The optimal PID control strategy shows good performance in terms of overshoot and settling time. However, the rise time for the first step from 100 MW to 106 MW is 40 s which means the response of the controller is not very swift.

A Fuzzy PID control system was also optimised using a GA and the ITAE performance index as cost function. Fig. 6.17 compares the power output of the system with a power reference signal. Fig. 6.18 shows the ITAE performance function values.

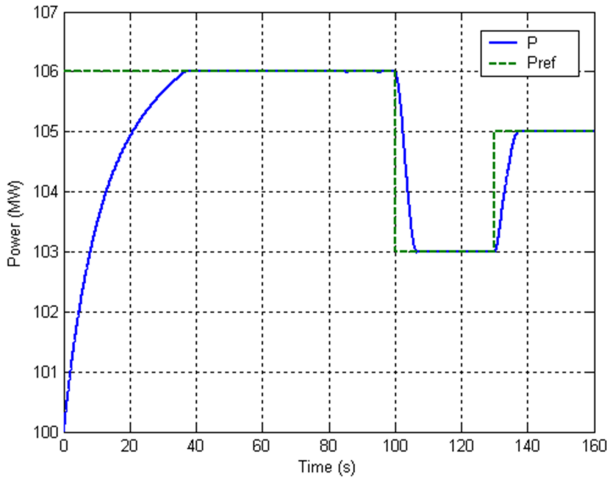

Figure 6.17: Optimal Fuzzy PID control [16]

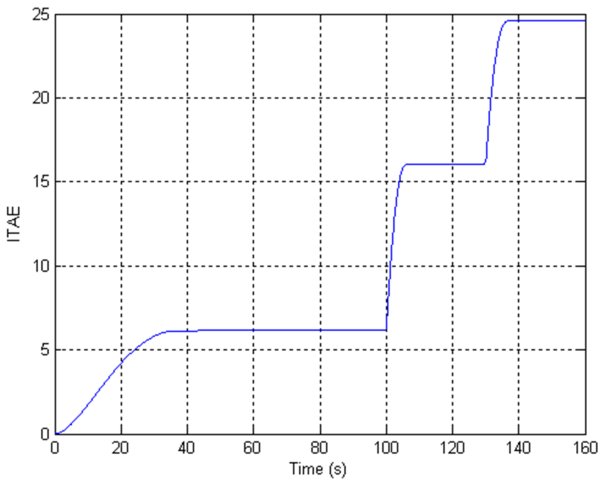

Figure 6.18: Performance of the optimal Fuzzy PID control strategy (ITAE = 24.62) [16]

The Fuzzy PID controller shows good performance in terms of tracking the power reference. It also shows a significant improvement in terms of the rise time of the system and therefore an improvement in swiftness.

Fig. 6.19 shows the model-predictive control system. The controller takes the power error (e_P) as input and generates the best possible values for the amount of helium to be injected or extracted.

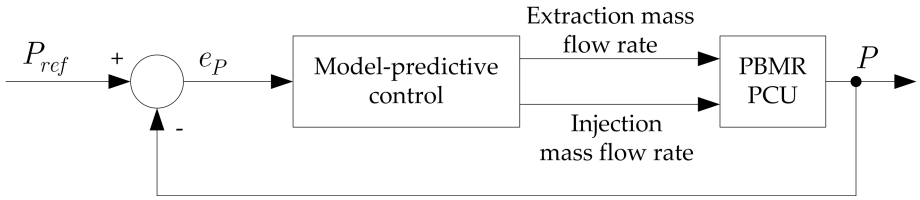

Figure 6.19: Conceptual diagram of the Model-predictive control strategy

Fig. 6.20 shows the comparison between the desired output power and the actual power output. Fig. 6.21 shows the ITAE performance function values.

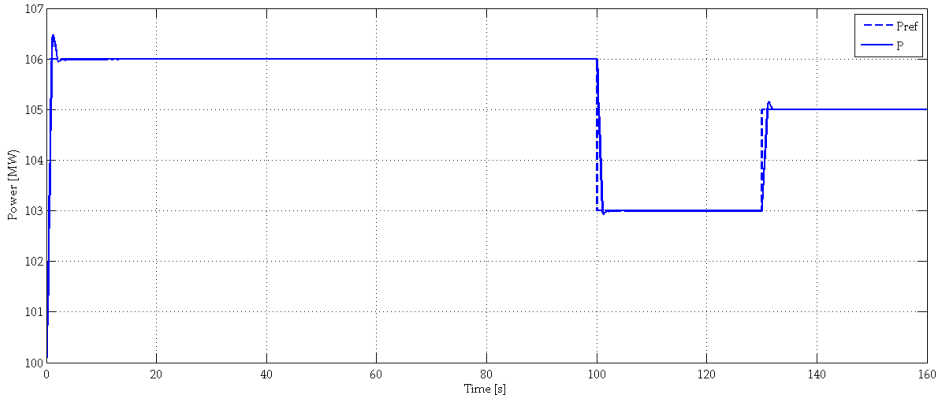

Figure 6.20: Model predictive control

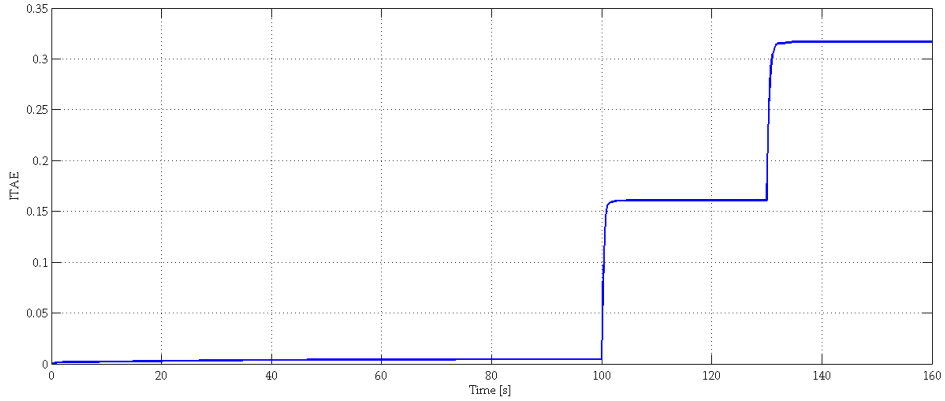

Figure 6.21: Performance of the model-predictive controller (ITAE = 0.3169)

The model-predictive controller proves to be superior compared to the optimal PID and Fuzzy PID controllers with a performance index value of 0.3169. The power output shows small overshoots, but impressive improvements in terms of tracking the power output and response times. Figs. 6.22 and 6.23 show the output signals of the model-predictive controller.

Constraints were placed on the outputs of the model-predictive controller. The amount of

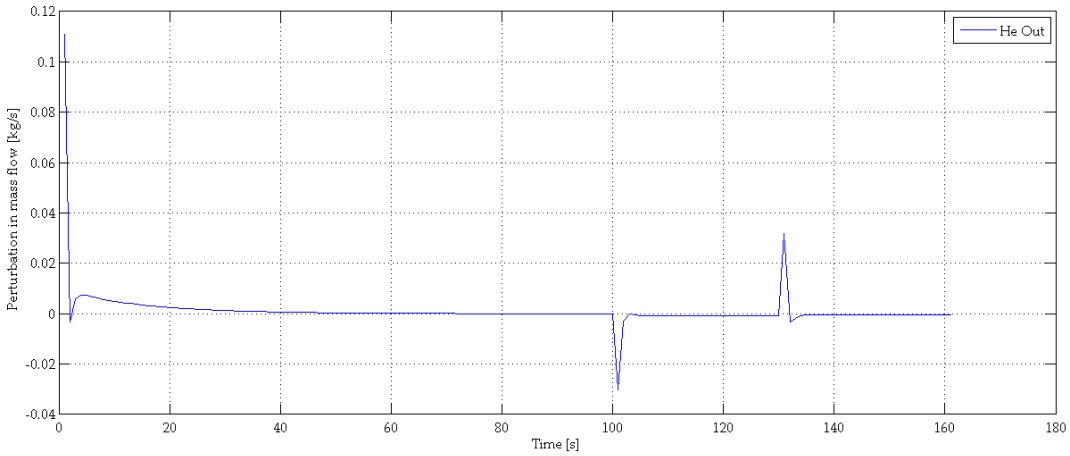

Figure 6.22: Perturbation in helium mass flow rate at high pressure side

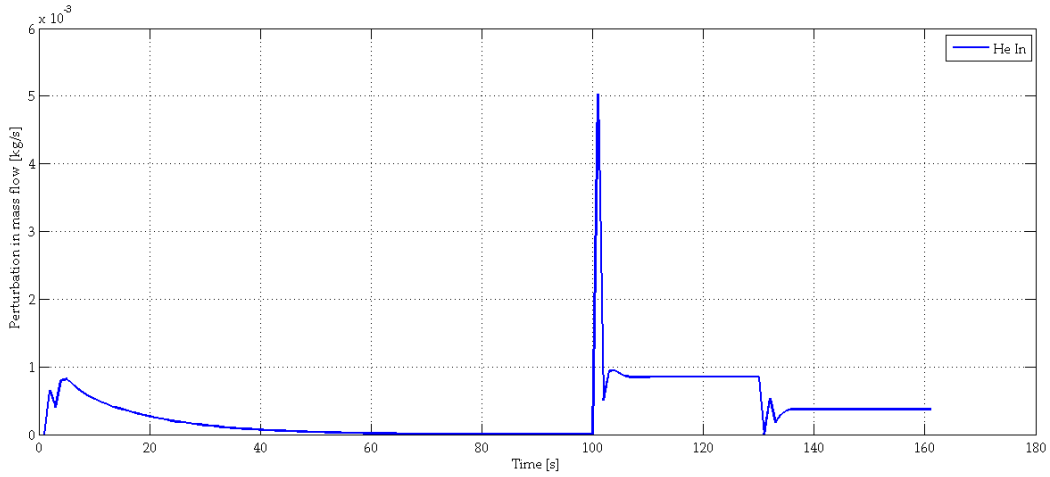

Figure 6.23: Perturbation in helium mass flow rate at the low pressure side

helium to be injected at the high pressure side is limited to 1 kg/s. The controller allows helium to be extracted at the high pressure side. The rate at which helium is injected or extracted is another constraint which the controller takes into account.

Helium cannot be extracted at the low pressure side. Fig. 6.23 shows that this constraint is taken into account by the controller by not allowing the helium mass flow rate to become negative at the low pressure side. The controller allows helium injection at the low pressure side.

6.7 Conclusion

The goal of this chapter was to demonstrate the advantages of using control schemes that embeds state space models in optimal control algorithms. In this chapter the state space extraction algorithm was used to extract a state space model of the PBMR PCU. The extracted state space model was linearised using linearised source elements in the different domains. The only energy storage elements in the system are the inertias making up the shafts (mechanical domain) of the turbine-compressor pairs and the volumes (hydraulic domain) in the system. All other energy storage elements (e.g. energy storage elements) are considered to have dynamics that are either much slower of much faster than that being considered. Therefore the state space model takes the pressures and shaft speeds as states of the system. The model was compared with a linear *Simulink*® model of the PBMR developed by Rubin [15] and showed good correlation.

The extracted state space model was embedded in a model-predictive controller. The performance of the controller was compared to two other optimal control schemes, an optimal PID controller and an optimal Fuzzy PID controller. The MPC controller showed superior performance compared to these control schemes. The controller also showed much faster reaction times compared to the other controllers.

CHAPTER 7

CONCLUSIONS

7.1 Introduction

In this chapter the state space model extraction method for thermohydraulic systems is discussed in terms of its valuable attributes, its uniqueness and its shortcomings. Recommendations are also made for future work in the area of state space model extraction techniques.

7.2 Overview

Thermohydraulic systems are characterised by the coupling of several phenomena of different natures. It is therefore a challenging task to derive models for these systems compared to purely electrical or mechanical systems. Today a number of well developed thermohydraulic simulation packages are available for the purpose of detailed analysis and design. These codes provide accurate results, but are too detailed to make simple predictions necessary for control and system engineering. It is also not always possible to derive the dominant system dynamics from these detailed simulations.

The model format preferred for control system design and analysis during preliminary system design is the state space format. Well developed system identification techniques exist for obtaining state space models from input-output data. However, these models are not transparent, which means that one cannot identify system parameters such as heat or mass transfer coefficients. An alternative approach, commonly used in practice, is to write down the model equations from first principles to form a reduced order state space model that can be coded in an environment such as *Matlab*® [12]. This kind of model is transparent, but takes effort and time to develop. A need is therefore recognised to develop a model extraction tool that automates the process of generating reduced order state space models of thermohydraulic

systems for control purposes.

The focus of this study is therefore to develop a state space model extraction algorithm that will reduce the time and effort of model development, but will deliver models of reduced order that has physical meaning (transparent). A research area, still relatively new, that is capable of addressing this challenge is called model extraction [10, 62, 63]. This research area focuses on the development of model extraction algorithms capable of automatically extracting dynamic system models from graphical representations of physical systems. A considerable amount of work has been done on state space model extraction of thermohydraulic systems represented by bond graphs [6, 33]. However, the majority of commercial thermohydraulic simulation codes follow a network approach for representing thermohydraulic systems. Considering the literature, not much attention has been given to the development of state space model extraction methods following a network approach.

The state space model extraction methodology is derived based on a unified approach to system modelling. This unifying approach considers systems as energy manipulators. The dynamic behaviour of a system can then be perceived as the result of energy exchange within the system. This allows multi-domain systems such as thermohydraulic systems to be considered in a common framework. A network approach is adopted where the energy interactions of the system elements are represented by a network representation of the system.

The state space extraction algorithm was applied to small scale thermohydraulic systems such as a U-tube and a heat exchanger, but also on a larger, more complex system such as the PBMR PCU. It was also shown that the algorithm can extract linear, nonlinear, time-varying and time-invariant state space models. The extracted state space models were validated by solving the state space models and comparing the solutions with *Flownex*® results. The state space models compared well with *Flownex*® results.

The usefulness of the state space model extraction algorithm in model-based control system design was illustrated by extracting a linear time-invariant state space model of the PBMR PCU. This model was embedded in an optimal model-based control scheme, Model-Predictive Control (MPC). The controller was compared with standard optimised control schemes such as PID and Fuzzy PID control. The MPC controller showed superior performance compared to the conventional control schemes.

7.3 Unique contribution

Researchers such as Filho and Conçalves [61], Wellstead [10] and Altun *et al.* [62, 63] worked on network approaches for state space model extraction. Their applications focussed on single domain systems such as pure electrical, mechanical, hydraulic and thermal systems. In this study an existing, network-based state space extraction method used for electrical system analysis is adapted to accommodate multi-domain systems and applied in a new way to extract state space models of more complex systems.

The developed method will be described by considering Fig. 7.1. A thermohydraulic network is partitioned into hydraulic, thermal and mechanical networks. These networks contain the structural and elemental information about the particular thermohydraulic network. This information is converted algebraically into the incidence and element matrices respectively. These matrices are used along with selections made in terms of the trees, co-trees as well as input and state variables to extract state space representations of the thermohydraulic system. The symbolic parameters are then substituted with the relevant numerical values. The state space model can then be solved and validated to make sure it captures the dominant system dynamics. Due to the interdependence of the physical domains in thermohydraulic systems, the state space models need to be solved in a specific order: hydraulic, thermal and then mechanical. The thermal domain couples to the hydraulic domain by means of parameters such as density and the mechanical domain depends on both hydraulic and thermal parameters such as mass flow and temperature.

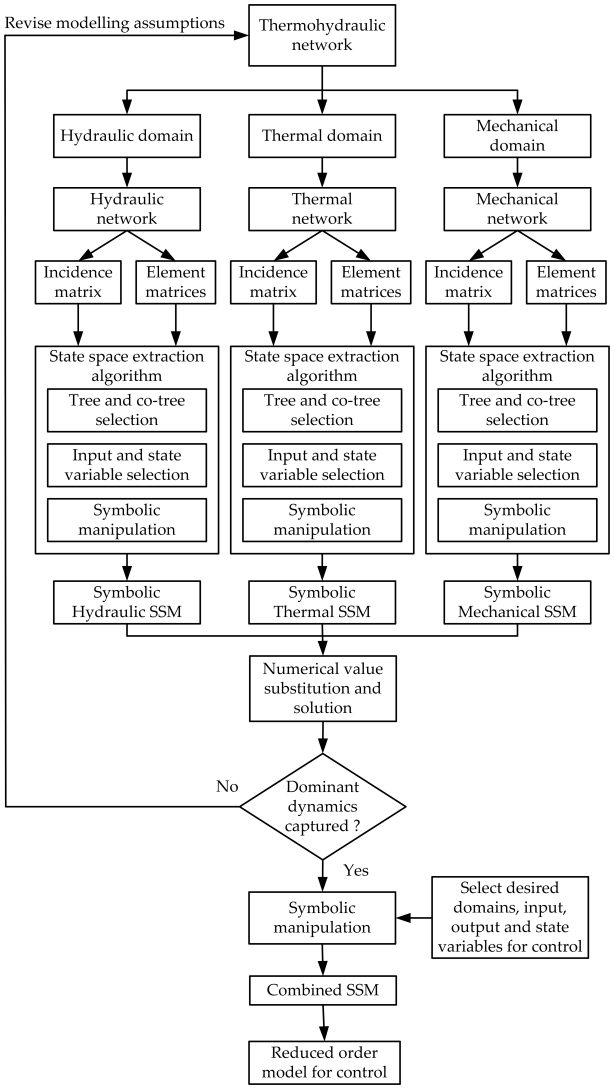

Figure 7.1: Unique contribution: Thermohydraulic state space model extraction method

Depending on the control application, the desired domains, input, output and state variables can be selected and the extracted state space models can be symbolically manipulated to form one combined state space model. This model can then be embedded in a model-based control scheme.

This method is unique since a whole new thermohydraulic state space model extraction methodology based on a network approach is developed. Previous research work on state space model extraction of multi-domain systems such as thermohydraulic systems focussed on bond graphs [6, 33, 56].

The developed state space model extraction method has some shortcomings. It considerers basic thermohydraulic phenomena, and needs to be expanded to incorporate more complex phenomena such as valve dynamics, chemical reactions and neutronics. The state space extraction method generates a state variable for each node variable and also for some link variables as discussed in Chapter 5. This may cause high order state space models to be extracted when systems are discretised into many control volumes. The explicit form of the state space models and large differences in time constants of thermal and hydraulic state space models (stiff systems), may result in increased computational intensiveness in model-based controllers.

7.4 Recommendations

To fully demonstrate the possibilities of the derived extraction algorithm it should be embedded in an existing thermohydraulic simulation code such as *Flownex*®. The extraction algorithm should also be extended to other physical domains (e.g. nuclear and chemical).

Pre- and post-processing routines need to be developed for the extraction algorithm. The pre-processing routines may include algorithms that first reduce the thermohydraulic system to the essential components. The post-processing routines may include symbolic manipulation algorithms.

The concept of using the state space extraction algorithm combined with a model-based control scheme in an integrated control design code, needs further investigation. Further work on model-predictive controllers for thermohydraulic system control also needs to be done in terms of stability analysis using techniques such as μ-analysis. The computational intensiveness of model-based controllers using extracted state space models also warrants further investigation.

7.5 Closure

The objective of deriving a method capable of extracting reduced order state space models of thermohydraulic systems was achieved. The method was evaluated on small- and large-scale thermohydraulic systems to demonstrate its capability to extract state space models portraying the dominant dynamics of a system. The usefulness of the method was illustrated by extracting

a state space model of a large and complex thermohydraulic system and embedding the model in a model-predictive control scheme.

BIBLIOGRAPHY

[1] E. Doebelin, *System dynamics modeling and response*. Bell & Howell Company, Columbu, Ohio, 1972.

[2] J. Maciejowski, *Predictive control with constraints*. Prentice Hall, 2002.

[3] K. Hangos and I. Cameron, *Process modelling and model analysis*. Academic Press Ltd, 2001.

[4] M. J. Willis and M. T. Tham, "Advanced Process Control," Departmenat of Chemical and Process Engineering, University of Newcastle upon Tyne, Tech. Rep., 1994. [Online]. Available: http://lorien.ncl.ac.uk/ming/advcontrl/apc.htm

[5] C. Brosilow and B. Joseph, *Techniques of Model-Based Control*. Prentice Hall PTR, Upper Saddle River, New Jersey, 2002.

[6] B. O. Bouamama, "Bond graph approach as analysis tool in thermofluid model library conception," *Journal of the Franklin Institute*, vol. 340, pp. 1–23, 2003.

[7] G. Greyvenstein and P. Rousseau, "Design of a physical model of the PBMR with the aid of Flownet," *Nuclear Engineering and Design*, vol. 222, pp. 203–213, 2002.

[8] D. Flynn, Ed., *Thermal Power Plant Simulation and Control*. The Institution of Electrical Engineers, 2003.

[9] K. Hangos, J. Bokor, and Szederkényi, *Analysis and control of nonlinear process systems*. Springer-Verlag, Londen, Ltd., 2004.

[10] P. E. Wellstead, *Introduction to Physical System Modelling*. Academic Press Ltd, 1979.

[11] G. Greyvenstein and D. Laurie, "A segregated CFD approach to pipe network analysis," *International journal for numerical methods in engineering*, vol. 37, pp. 3685–3705, 1994.

[12] J. Pritchard, "PBMR plant control development of a linear model of the brayton cycle," PBMR (Pty) Ltd, Tech. Rep., 2002.

[13] P. Oosthuizen, "Detail simulation of the RCCS using Flownet," M-tech Industrial (Pty) Ltd, Tech. Rep., 2006.

[14] F. Incropera, D. Dewitt, T. Bergman, and A. Lavine, *Fundamentals of heat and mass transfer*. John Wiley & Sons Inc, 2007.

[15] O. Rubin and J. Pritchard, "Dynamic modelling for control of a new generation nuclear power station," in *IFAC*, 2002.

[16] K. Uren, "Optimal Power Control of a Brayton Cycle Based Power Plant," Master's thesis, School of Electrical, Electronic and Computer Engineering at the NWU Potchefstroom campus, 2005.

[17] J. Shearer, A. Murphy, and H. Richardson, *Introduction to system dynamics*. Addison-Wesley, 1967.

[18] K. Takahashi, M. Rabins, and D. Auslander, *Control of dynamic systems*. Addison-Wesley Publishing, 1970.

[19] L. G. Birta and G. Arbez, *Modelling and Simulation*. Springer-Verlag, 2007.

[20] F. Cellier, *Continous System Modelling*. Springer-Verlag, 1991.

[21] L. Ljung and T. Glad, *Modelling of dynamics*. Prentice Hall, 1994.

[22] H. van Antwerpen, "Modelling a pebble bed High Temperature Gas-cooled Reactor using a system-CFD approach," Ph.D. dissertation, School of Mechanical Engineering at the NWU Potchefstroom campus, 2007.

[23] IAEA, "Convention on Nuclear Safety," Tech. Rep., 1997. [Online]. Available: http://www.iaea.org.at/worldatom/Documents/Infcircs/Others/inf449.html

[24] C. Phillips and H. Nagle, *Digital Control System Analysis and Design*, 3rd ed. Prentice Hall, 1995.

[25] K. Åström and B. Wittenmark, *Adaptive Control*, 2nd ed. Addison-Wesley, 1995.

[26] J. Kikstra, "Modelling, design and control of a cogenerating nuclear gas turbine plant," Ph.D. dissertation, Technische Universiteit Delft, 2001.

[27] F. Botha, "An explicit method for the analysis of transient compressible flow in pipe networks," Master's thesis, School of Mechanical Engineering at the NWU Potchefstroom campus, 2003.

[28] P. Eykhoff, *System identification: parameter and state estimation*. Londen: Wiley, 1974.

[29] C. Bishop, *Neural Networks for Pattern Recognition*. Oxford University Press, 2005.

[30] S. Lu and B. Hogg, "Dynamic nonlinear modelling of power plant by physical principles and neural networks," *Electrical Power and Energy Systems*, vol. 22, pp. 67–78, 2000.

[31] P. Agachi, Z. Nagy, M. Cristea, and A. Imre-Lucaci, *Model Based Control*. Wiley-VCH, 2007.

[32] R. Murray, "Control in an Information Rich World: Report of the Panel on Future Directions in Control," *Dynamics, and Systems. SIAM*, 2003. [Online]. Available: http://www.cds.caltech.edu/ murray/cdspanel

[33] B. Bouamama, A. Samantaray, K. Medjaher, M. Staroswiecki, and G. Dauphin-Tanguy, "Model builder using functional and bond graph tools for FDI design," *Control Engineering Practice*, vol. 13, pp. 875–891, 2005.

[34] A. Azuma, "Modeling and simulation of a steam power station," Master's thesis, Mechanical Engineering department at the Massachusetts Institute of Technology, 1975.

[35] G. Thomas, "Dynamic modeling and control of a 50 MW OTEC power plant," Master's thesis, Mechanical Engineering department at the Massachusetts Institute of Technology, 1980.

[36] P. Usoro, "Modeling and simulation of a Drum Boiler-Turbine power plant under emergency state control," Master's thesis, Mechanical Engineering department at the Massachusetts Institute of Technology, 1977.

[37] X. Yan, "Dynamic analysis and control system design for an advanced nuclear gas turbine power plant," Ph.D. dissertation, Mechanical Engineering department at the Massachusetts Institute of Technology, 1990.

[38] N. Rees and C. Lu, "Some thoughts on the advanced control of electric power plants," *Transactions of the Institute of Measurement and Control*, vol. 24, pp. 87–106, 2002. [Online]. Available: http://tim.sagepub.com/cgi/content/abstract/24/2/87

[39] K. Chien, E. Ergin, C. Ling, and A. Lee, "Dynamic analysis of a boiler," *ASME Transactions*, vol. 80, pp. 1809–1819, 1985.

[40] C. Weng, A. Ray, and X. Dai, "Modelling of power plant dynamics and uncertainties for robust control synthesis," *Appl. Math. Modelling*, vol. 20, pp. 501–512, 1996.

[41] K. J. Åström and R. Bell, "Drum-boiler dynamics," *Automatica*, vol. 36, pp. 363–378, 2000.

[42] S. J. Qin and T. A. Badgwell, "A survey of industrial model predictive control technology," *Control Engineering Practice*, vol. 11, pp. 733–764, 2003.

[43] C. Fazekas, S. G., and K. Hangos, "A simple dynamic model of the primary circuit in VVER plants for controller design purposes," *Nuclear Engineering and Design*, vol. 237, pp. 1071–1087, 2007.

[44] H. Li, X. Huang, and L. Zhang, "A simplified mathematical dynamic model of the HTR-10 high temperature gas-cooled reactor with control system design purposes," *Annals of Nuclear Energy*, vol. 35, pp. 1642–1651, 2008.

[45] H. Kazeminejad, "Thermal-hydraulic modeling of flow inversion in a research reactor," *Annals of Nuclear Energy*, vol. 35, pp. 1813–1819, 2008.

[46] A. Y. Ying, A. Raffray, and M. Abdou, "Benefits of natural convection in solid breeder blankets with poloidal coolant channels under LOFA conditions," *Fusion Engineering and Design*, vol. 17, pp. 313–319, 1991.

[47] C. Bonivento, P. Castaldi, and D. Mirotta, "Predictive Control vs PID Control of an Industrial Heat Exchanger," in *9th Mediterraneon Conference on Control and Automation*, Dubrovnik, Croatia, June 2001.

[48] E. Varga, K. Hangos, and F. Szigeti, "Controllability and observability of heat exchanger networks in the time-varying parameter case," *Control Engineering Practice*, vol. 3, pp. 1409–1419, 1995.

[49] L. Antelo, I. Otero-Muras, J. Banga, and A. Alonso, "A systematic approach to plant-wide control based on thermodynamics," *Computers and Chemical Engineering*, vol. 31, pp. 677–691, 2007.

[50] B. Dorneanua, C. Bildeab, and J. Grievinka, "On the application of model reduction to plantwide control," *Computers and Chemical Engineering*, vol. 33, pp. 699 – 711, 2009.

[51] G. Prasad, G. Irwin, E. Swidenbank, and B. Hogg, "A hierarchical physical model-based approach to predictive control of a thermal power plant for efficient plant-wide disturbance rejection," *Transactions of the Institute of Measurement and Control*, vol. 24, pp. 107–128, 2002. [Online]. Available: http://tim.sagepub.com/cgi/content/abstract/24/2/107

[52] H. Tummescheit and J. Eborn, "Design of a thermo-hydraulic model library in Modelica," in *European Simulation Multiconference ESM'98*, Manchester, United Kingdom, 1998.

[53] P. Colonna and H. van Putten, "Dynamic modeling of steam power cycles. Part I - Modeling paradigm and validation," *Applied Thermal Engineering*, vol. 27, pp. 467–480, 2006.

[54] H. van Putten and P. Colonna, "Dynamic modeling of steam power cycles: Part II - Simulation of a small simple Rankine cycle system," *Applied Thermal Engineering*, vol. 27, pp. 2566–2582, 2007.

[55] MathWorks, *Help File*, 2008. [Online]. Available: http://www.mathworks.com/

[56] D. Karnopp, D. Margolis, and R. Rosenberg, *System dynamics: Modelling and Simulation of Mechatronic systems*. Johan Wiley & Sons Inc, 2006.

[57] J. Thoma, *Introduction to bond graphs*. Pergammon Press, 1975.

[58] J. Granda, "The CAMP-G/MATLAB-SIMULINK Computer Generated Solution of Bond Graph derivative causality," *Department of Mechanical Engineering, California State University Sacramento*. [Online]. Available: http://gaia.csus.edu/ grandajj

[59] W. Minten, B. de Moor, and J. Vandewalle, "State equations of nonlinear dynamic systems," in *International conference on bond graph modelling and simulation (ICBGM'95)*, 1995.

[60] R. Rosenberg, "Modelling and simulation of large-scale, linear, multiport systems," *Automatica*, vol. 9, pp. 87–95, 1973.

[61] A. Filho and J. Gonçalves, "Automatic modelling of lumped parameter dynamic systems," *SBA Controle & Automaçã*, vol. 10, pp. 1–12, 1999.

[62] K. Altun, T. Balkan, and B. Platin, "Extraction of state variable representations of dynamic systems employing linear graph theory," in *The Sixth International Conference on Mechatronic Design and Modelling*, Cappadocia, Turkey, September 2002.

[63] K. Altun, B. Platin, and T. Balkan, "Systematic state equation derivation for linear systems using the normal tree method," in *2003 ASME International Mechanical Engineering Congress & Exposition*, Washington D.C, November 2003.

[64] J. van der Merwe, "Simulation of heat and momentum transfer in the high temperature test reactor," Master's thesis, School of Mechanical Engineering at the NWU Potchefstroom campus, September 2003.

[65] M. Milman and W. Pertrick, "A note on the solution to a common thermal network problem encountered in heat-transfer analysis of spacecraft," *Applied Mathematical Modelling*, vol. 24, pp. 861–879, 2000.

[66] R. Dorf and R. Bishop, *Modern control systems*, 10th ed. Pearson Prentice Hall, 2005.

[67] B. Munson, D. Young, and T. Okiishi, *Fundamentals of fluid mechanics*, 5th ed. Wiley & Sons, 2006.

[68] C. Bodenstein, "Process Modelling," 2006, Lecture Notes.

[69] H. Cohen, G. Rogers, and H. Saravanamuttoo, *Gas Turbine Theory*. Longman Group Ltd., England, 1996.

[70] *Flownex 6.8 User Manual - Part 2*, M-Tech Industrial, August 2005.

[71] S. Dixon, *Fluid mechanics and thermodynamics of turbomachinery*, 4th ed. Butterworth-Heinemann, 1998.

[72] L. Cilliers and Nieuwoudt, "Demonstration plant operations summary," PBMR, Tech. Rep., 2002.

[73] A. George, "Introduction to the Pebble Bed Modular Reactor (PBMR)," PBMR, Tech. Rep., 2002.

[74] L. Euler, "Solutio Problematis ad Geometriam Situs Pertinantis," *Academimae Petropolitanae 8*, pp. 128–140, 1736.

APPENDIX A

REVIEW OF GRAPH THEORY

A very large range of problems in engineering can be solved by means of graph theory. One of the distinctive properties of graph theory is that it can graphically represent almost any physical or conceptual problem having discrete objects. It can also describes the relationship between these objects.

Graph theory originated from a problem encountered in the early seventeen hundreds. It was called the Königsberg bridge problem and Leonhard Euler (1707-1783) was the first to solve it in 1736, by means of a graph. Euler's paper [74] proving that this problem does not have a solution was the first paper in graph theory. He is therefore considered as the father of graph theory. The Königsberg bridge problem is stated as follows:

The Pregel river isolates two islands C and D, as shown in Fig. A.1. The two islands are connected to each other with one bridge. Six bridges connect the islands with the banks A and B. The problem states that you can start at any of the four land areas, A, B, C or D, and then you have to walk over each of the bridges once, and return to your starting point. Euler represented this problem by means of a graph, as shown in Fig. A.2. The vertices or nodes represent the banks and the islands, and the edges represent the bridges.

A.1 Notation and basic definitions

Considering Fig. A.2 one can think of a graph as a set of points in a plane and a set of line segments where each joins two points, or joins a point to itself. A thorough explanation of the definitions and notations is needed to place the application of graphs on a solid footing [10].

Definition A.1.1. A **graph** $G = (\mathbf{N}, \mathbf{L})$ is a mathematical structure consisting of two finite sets **N** and **L** where $\mathbf{N} = \{n_1, n_2, \ldots, n_N\}$ and $\mathbf{L} = \{l_1, l_2, \ldots, l_L\}$. The elements of the set **N** are called **nodes** (or **vertices**) and the elements of the set **L** are called **links** (or **edges**). Each link

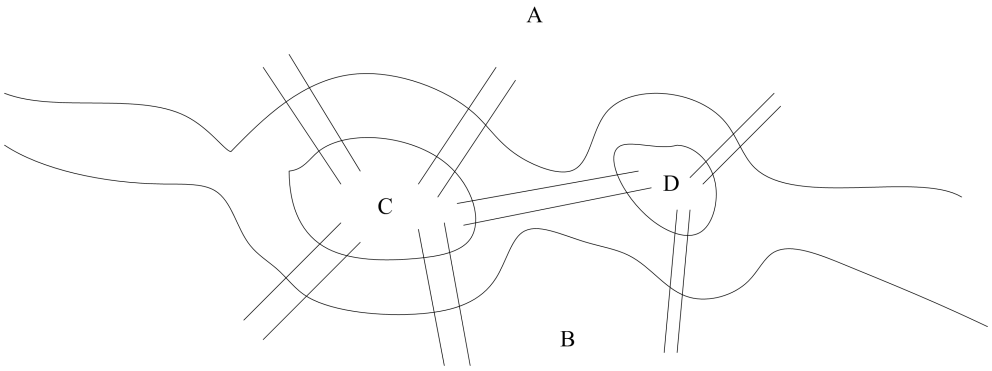

Figure A.1: Königsberg bridge problem

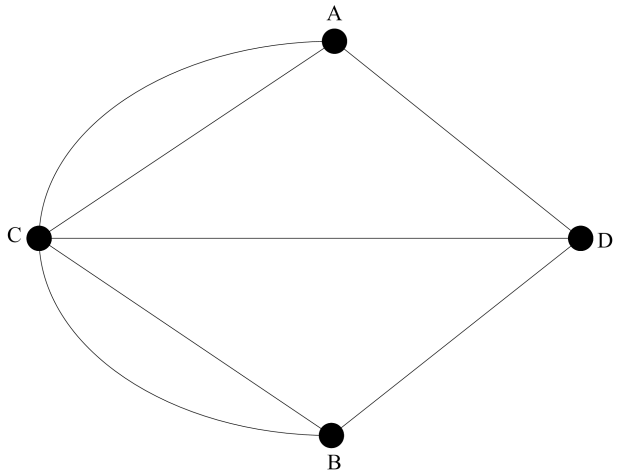

Figure A.2: Graph of the Königsberg bridge problem

has a set of one or two nodes associated with it, which are called the **end nodes**.

The links may also be directed. This is a very useful property especially when modelling physical systems such as flow networks with valves and orifices in the pipes or electrical networks. In this study directed graphs will be used mainly.

Definition A.1.2. A **directed graph** (also called a digraph) G_d consists of a set of nodes **N**, and a set of links **L**, and a mapping Φ that maps each link onto some ordered pair of nodes (n_i, n_j).

In Fig. A.3 a node is represented by a point and a link by a line with an arrow between the node pair. When the arrow is directed from n_i to n_j the node pair will be given by (n_i, n_j) and if its directed from n_j to n_i it will be given as (n_j, n_i). The mapping Φ is usually given by a *connection matrix*. There are two fundamental types of connection matrices namely an *adjacency matrix* and an *incidence matrix* which will be discussed in detail later on.

Definition A.1.3. A **multi-link** is a collection of two or more links having the same node pair. The **link multiplicity** is the number of links within the multi-link.

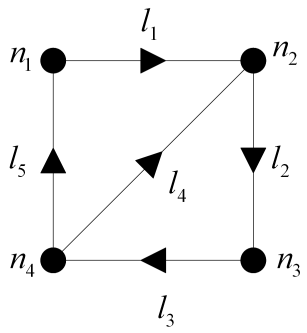

Figure A.3: Directed graph

Definition A.1.4. A **simple graph**, is a graph that has neither self-loops nor multi-links.

Definition A.1.5. A **general graph**, is a graph where multi-links and self-loops are allowed.

Definition A.1.6. A graph is called **connected** if there exists at least one path between every pair of nodes in a graph G. If this is not the case the graph is disconnected as shown in Fig. A.4.

Graphs used for dynamic systems modelling are often called **linear graphs**. The term *linear* in this case does not refer to algebraic linearity but is associated with the word line. In engineering a linear graph may also consist of more than one part as shown in Fig. A.4. Disconnected graphs can be used to model systems containing more than one physical domain. For example a thermo-fluid system can be represented by a graph representing the thermal domain and a graph representing the hydraulic domain.

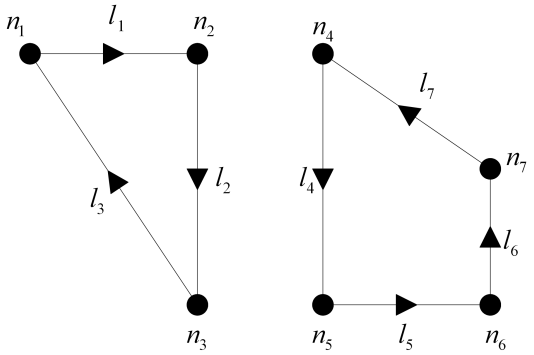

Figure A.4: Disconnected graph

Definition A.1.7. A **sub-graph** is a sub-set of the original graph-set constituting connected links and nodes that are incident with the original graph.

In this study graphs are described in terms of **sub-graphs**. A linear graph and one possible sub-graph of the original graph is shown in Fig. A.5.

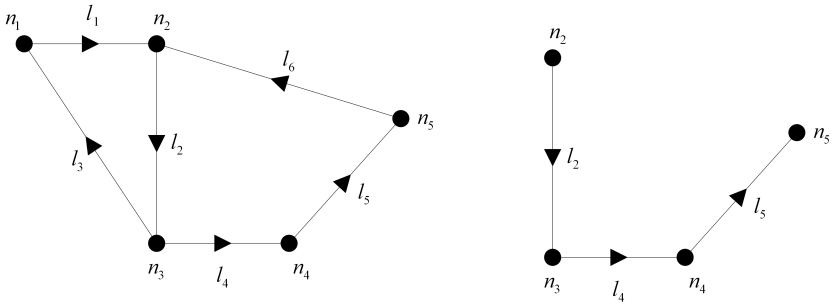

Figure A.5: Original graph and one possible sub-graph

A.2 Trees and co-trees

The concepts of trees and co-trees in graph theory are very important especially when applying graphs to dynamic system modelling. Trees play an important role in understanding the structure of graphs and form the backbones of optimally connected networks [62]. More terms concerning trees and co-trees used in modelling applications will also be discussed as well as the relationships between trees, co-trees, cut-sets and loop-sets.

Definition A.2.1. A **tree**,**T** is a connected graph with no loops.

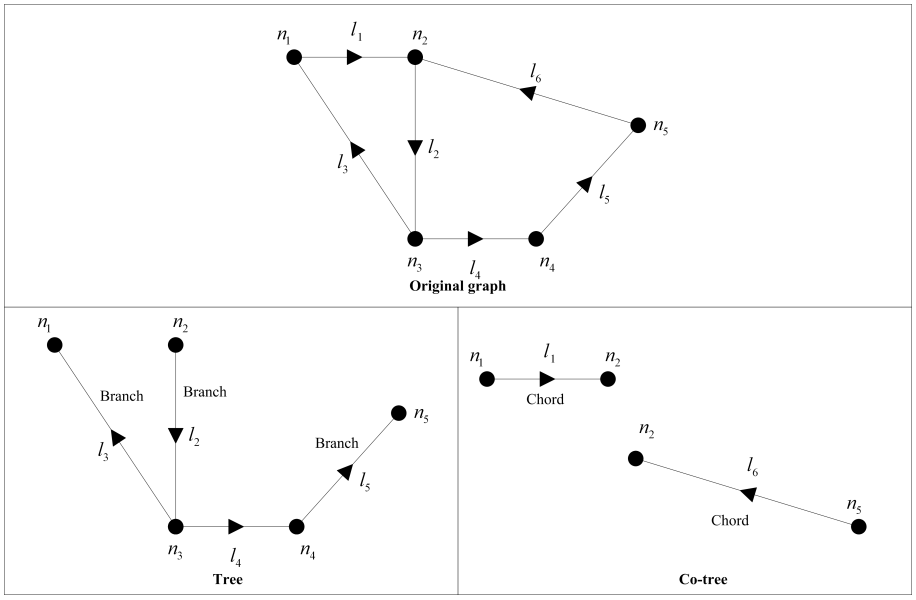

Figure A.6: A graph with one possible tree and co-tree

Definition A.2.2. A **spanning tree**, $\mathbf{T}_S$ of a graph is a connected sub-graph containing all the nodes of the graph and no loops. From here onwards the term **tree**,**T**, will **exclusively be used for a spanning tree**. The compliment of a tree is called a **co-tree**, $\mathbf{T}_C$ and is the part of the graph that remains when the tree is removed. Fig. A.6 shows a graph with one possible tree and co-tree.

Spanning trees (trees) provide a stepping stone for a systematic analysis of the loop structure of a graph.

Definition A.2.3. The links of a tree are called **branches** and the links of a co-tree are called **chords**.

It can easily be seen that by adding a link between any two nodes of a tree, a loop will be created. A tree can therefore be considered as a *saturated* sub-graph [62].

Definition A.2.4. A **fundamental loop** for a specific tree is a loop-set consisting of one chord and some or all of the branches of the tree.

It is very important to notice that a loop is fundamental only with respect to a specific tree. A given loop may therefore be fundamental to one tree of a graph, but not to another tree of the same graph. The concept of a fundamental loop plays a great role in electrical circuit analysis and was first introduced by Kirchhoff. This allows the engineer to consider only the fundamental loops, the rest of the loops are combinations of the fundamental loops [10].

Definition A.2.5. A **cut-set** is a set of links of a connected graph such that cutting these links separates the graph into two connected graphs.

Definition A.2.6. A **fundamental cut-set** is defined for a specific tree as a cut-set consisting of one tree branch and some or all of the co-tree chords.

It is interesting to see the parallelism between a fundamental loop-set and a fundamental cut-set and the fact that a tree is essential for defining them. In Fig. A.7 a specific tree of a graph is shown in bold and the basic cut-sets and loop-sets are indicated respectively.

A.3 Matrix representation of graphs

Graphs can assist the engineer to visualise a physical problem, but an algebraic representation is needed to be able to process the problem on computer. Matrices turn out to be the most natural way of representing graphs. Graph-theoretic properties previously discussed can be linked to matrix properties and finally to modelling concepts.

Two kinds of matrices are often associated with the representation of a graph. It all depends if a graph contains self-loops or multi-links. If a graph contains no self-loops, the graph can be completely described by an *incidence* matrix. If the graph contains no multi-links it can be completely described by an *adjacency* matrix. When modelling physical systems such as thermal-fluid networks there will be multi-links but no self-loops and therefore the incidence matrix representation will be used.

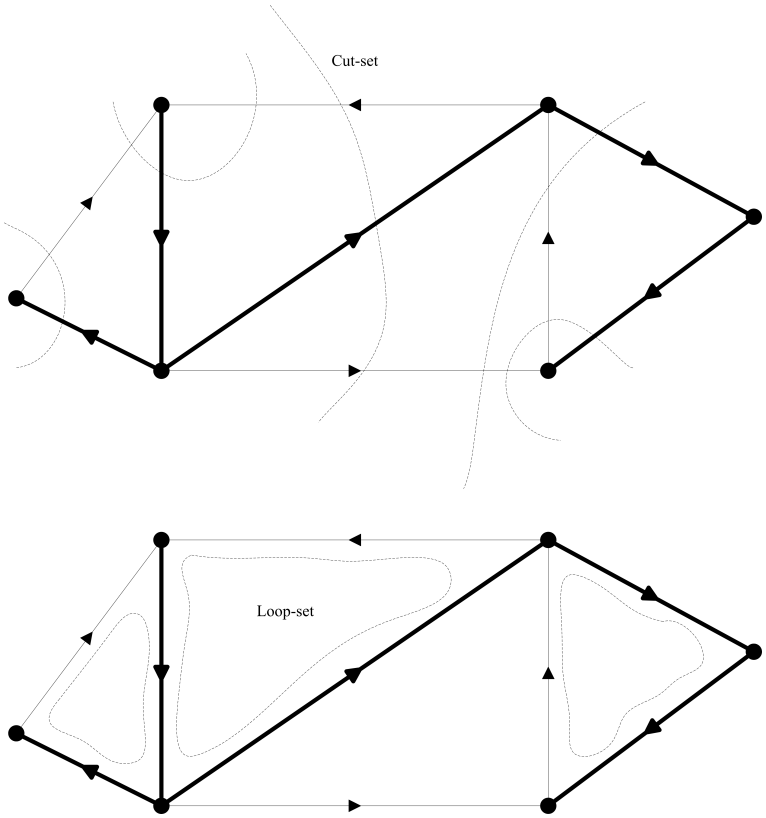

Figure A.7: Fundamental cut-sets and loop-sets

Definition A.3.1. Let G_d be a directed graph with N nodes and L links. Let G_d contain **no self-loops**. Define a N by L matrix $\mathbf{A}_I = [a_{ij}]$, whose N rows correspond to the N nodes and the L columns correspond to L links. Now let each matrix element

a_{ij} = 1, if link j is connected to node i and
the arrow is oriented away from node i,
= -1, if link j is connected to node i and
the arrow is oriented towards node i,
= 0, if no link is connected to node i.

Such a matrix $\mathbf{A}_I$ is called an **incidence matrix**.

If the graph considered is a connected graph such as the graph in Fig. A.8, then the incidence matrix may be reduced by eliminating any single row [63]. The node related to the row eliminated is called the *reference node* and the reduced incidence matrix will be indicated as $\mathbf{A}_R$.

For the connected graph with one possible tree in bold as shown in Fig. A.8, the incidence matrix is written as:

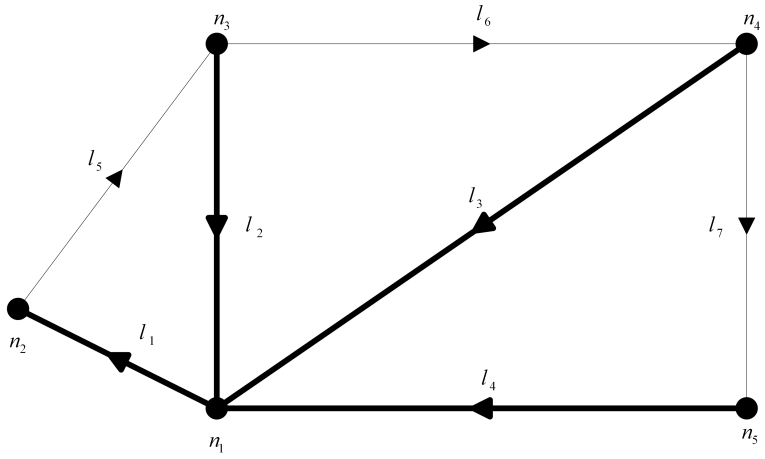

Figure A.8: Connected graph with a specific tree indicated in bold

$$\mathbf{A}_I = \begin{bmatrix} 1 & -1 & -1 & -1 & 0 & 0 & 0 \\ -1 & 0 & 0 & 0 & 1 & 0 & 0 \\ 0 & 1 & 0 & 0 & -1 & 1 & 0 \\ 0 & 0 & 1 & 0 & 0 & -1 & 1 \\ 0 & 0 & 0 & 1 & 0 & 0 & -1 \end{bmatrix}$$

Let n_1 be the reference node, then the reduced incidence matrix is given as:

$$\mathbf{A}_R = \begin{bmatrix} -1 & 0 & 0 & 0 & 1 & 0 & 0 \\ 0 & 1 & 0 & 0 & -1 & 1 & 0 \\ 0 & 0 & 1 & 0 & 0 & -1 & 1 \\ 0 & 0 & 0 & 1 & 0 & 0 & -1 \end{bmatrix}$$

When using incidence matrix representations of graphs in systems modelling it, is desirable to derive other useful matrices from the incidence matrix concerning a specific tree. Two such matrices are the *fundamental loop matrix* and the *fundamental cut-set matrix*. In order to derive these matrices it is necessary to first rearrange the reduced incidence matrix into two sub-matrices with respect to a specific tree. The first sub-matrix should contain all the chords of the co-tree and the second sub-matrix all the branches of the tree. This rearranged matrix will be called the *fundamental incidence matrix*:

$$\mathbf{A}_F = [\mathbf{A}_{co}|\mathbf{A}_{tr}] \tag{A.1}$$

where $\mathbf{A}_{co}$ consists of $L - N + 1$ columns corresponding to the chords of the co-tree and $\mathbf{A}_{tr}$ consists of $N - 1$ columns corresponding to the branches of the tree. The number of rows is the same as that of $\mathbf{A}_R$. For the graph and a specific tree in Fig. A.8 the fundamental incidence matrix is given by:

$$\mathbf{A}_F = [\mathbf{A}_{co}|\mathbf{A}_{tr}] = \left[\begin{array}{rrr|rrrr} 1 & 0 & 0 & -1 & 0 & 0 & 0 \\ -1 & 1 & 0 & 0 & 1 & 0 & 0 \\ 0 & -1 & 1 & 0 & 0 & 1 & 0 \\ 0 & 0 & -1 & 0 & 0 & 0 & 1 \end{array}\right]$$

where the columns of $\mathbf{A}_F$ are ordered in terms of increasing number of links for each sub-matrix as follows:

$$\left[\begin{array}{ccc|cccc} l_5 & l_6 & l_7 & l_1 & l_2 & l_3 & l_4 \end{array}\right]$$

The fundamental loop matrix can be derived from the sub-matrices of $\mathbf{A}_F$ by using (A.2).

$$\mathbf{F}_l = [\mathbf{I}|\mathbf{F}] = [\mathbf{I}| - \mathbf{A}_{co}^T(\mathbf{A}_{tr}^{-1})'] \tag{A.2}$$

The rows of the fundamental loop matrix $\mathbf{F}_l$ correspond to a set of fundamental loops of a graph. $\mathbf{F}_l$ can be arranged into two sub-matrices namely an identity matrix, $\mathbf{I}$ and a matrix corresponding to the branches of the specific tree, $\mathbf{F}$. The fundamental loop matrix for the graph in Fig. A.8 is given as:

$$\mathbf{F}_l = [\mathbf{I}|\mathbf{F}] = \left[\begin{array}{ccc|cccc} 1 & 0 & 0 & 1 & 1 & 0 & 0 \\ 0 & 1 & 0 & 0 & -1 & 1 & 0 \\ 0 & 0 & 1 & 0 & 0 & -1 & 1 \end{array}\right]$$

The rows of the fundamental cut-set matrix $\mathbf{F}_c$ correspond to a set of fundamental cut-sets with respect to a specific tree. Again $\mathbf{F}_c$ can be arranged into two sub-matrices namely an identity matrix, $\mathbf{I}$ and a matrix corresponding to the chords of the specific co-tree, $\mathbf{H}$. The fundamental cut-set matrix can be derived from the sub-matrices of $\mathbf{A}_F$ by using (A.3):

$$\mathbf{F}_c = [\mathbf{H}|\mathbf{I}] = [\mathbf{A}_{tr}^{-1}\mathbf{A}_{co}] \tag{A.3}$$

The fundamental cut-set matrix for the graph in Fig. A.8 is given as:

$$\mathbf{F}_c = [\mathbf{H}|\mathbf{I}] = \left[\begin{array}{rrr|rrrr} -1 & 0 & 0 & 1 & 0 & 0 & 0 \\ -1 & 1 & 0 & 0 & 1 & 0 & 0 \\ 0 & -1 & 1 & 0 & 0 & 1 & 0 \\ 0 & 0 & -1 & 0 & 0 & 0 & 1 \end{array}\right]$$

The definitions derived in this section are focussed on modelling of dynamic systems such as thermal-fluid networks, electrical networks and even mechanical systems. A whole lot more information can be extracted from a graph that may be useful for other applications such as transport systems, computer networks and computer software development.

APPENDIX B

SYMBOLIC STATE SPACE MODEL EXTRACTION

B.1 Symbolic A and B matrix elements

A11 = 1/C1*(-1/R1-1/R2-(R5*R6+R5*R4+R6*R7+R6*R4+R7*R4)/(R5*R6*R7+
R5*R3*R6+R7*R5*R4+R3*R5*R4+R6*R7*R3+R6*R3*R4+R6*R7*R4+R7*R3*R4))

A12 = 1/C1*(1/R2+R6*R7/(R5*R6*R7+R5*R3*R6+R7*R5*R4+R3*R5*R4+R6*R7*R3+
R6*R3*R4+R6*R7*R4+R7*R3*R4)+(R5*R6+R5*R4+R6*R4)/(R5*R6*R7+R5*R3*R6+
R7*R5*R4+R3*R5*R4+R6*R7*R3+R6*R3*R4+R6*R7*R4+R7*R3*R4))

A21 = 1/C2*(1/R2+R6*R7/(R5*R6*R7+R5*R3*R6+R7*R5*R4+R3*R5*R4+R6*R7*R3+
R6*R3*R4+R6*R7*R4+R7*R3*R4)+(R5*R6+R5*R4+R6*R4)/(R5*R6*R7+R5*R3*R6+
R7*R5*R4+R3*R5*R4+R6*R7*R3+R6*R3*R4+R6*R7*R4+R7*R3*R4))

A22 = 1/C2*(-1/R2-(R7*R5+R3*R5+R3*R6+R6*R7+R7*R3)/(R5*R6*R7+R5*R3*R6+
R7*R5*R4+R3*R5*R4+R6*R7*R3+R6*R3*R4+R6*R7*R4+R7*R3*R4)+
2*R3*R6/(R5*R6*R7+R5*R3*R6+R7*R5*R4+R3*R5*R4+R6*R7*R3+
R6*R3*R4+R6*R7*R4+R7*R3*R4)-(R5*R6+R5*R4+R3*R6+R6*R4+
R3*R4)/(R5*R6*R7+R5*R3*R6+R7*R5*R4+R3*R5*R4+R6*R7*R3+R6*R3*R4+
R6*R7*R4+R7*R3*R4))

B11 = 1/C1/R1

B12 = 1/C1*((R5*R6+R5*R4+R6*R7+R6*R4+R7*R4)/(R5*R6*R7+R5*R3*R6+
R7*R5*R4+R3*R5*R4+R6*R7*R3+R6*R3*R4+R6*R7*R4+R7*R3*R4)-
R6*R7/(R5*R6*R7+R5*R3*R6+R7*R5*R4+R3*R5*R4+R6*R7*R3+R6*R3*R4+
R6*R7*R4+R7*R3*R4)-(R5*R6+R5*R4+R6*R4)/(R5*R6*R7+R5*R3*R6+
R7*R5*R4+R3*R5*R4+R6*R7*R3+R6*R3*R4+R6*R7*R4+R7*R3*R4))

B21 = 0

```
B22 = 1/C2*(-R6*R7/(R5*R6*R7+R5*R3*R6+R7*R5*R4+R3*R5*R4+R6*R7*R3+
R6*R3*R4+R6*R7*R4+R7*R3*R4)-(R5*R6+R5*R4+R6*R4)/(R5*R6*R7+R5*R3*R6+
R7*R5*R4+R3*R5*R4+R6*R7*R3+R6*R3*R4+R6*R7*R4+R7*R3*R4)+(R7*R5+
R3*R5+R3*R6+R6*R7+R7*R3)/(R5*R6*R7+R5*R3*R6+R7*R5*R4+R3*R5*R4+
R6*R7*R3+R6*R3*R4+R6*R7*R4+R7*R3*R4)-2*R3*R6/(R5*R6*R7+R5*R3*R6+
R7*R5*R4+R3*R5*R4+R6*R7*R3+R6*R3*R4+R6*R7*R4+R7*R3*R4)+(R5*R6+
R5*R4+R3*R6+R6*R4+R3*R4)/(R5*R6*R7+R5*R3*R6+R7*R5*R4+R3*R5*R4+
R6*R7*R3+R6*R3*R4+R6*R7*R4+R7*R3
```

APPENDIX C

CODE IMPLEMENTATION

C.1 State space model extraction: U-tube

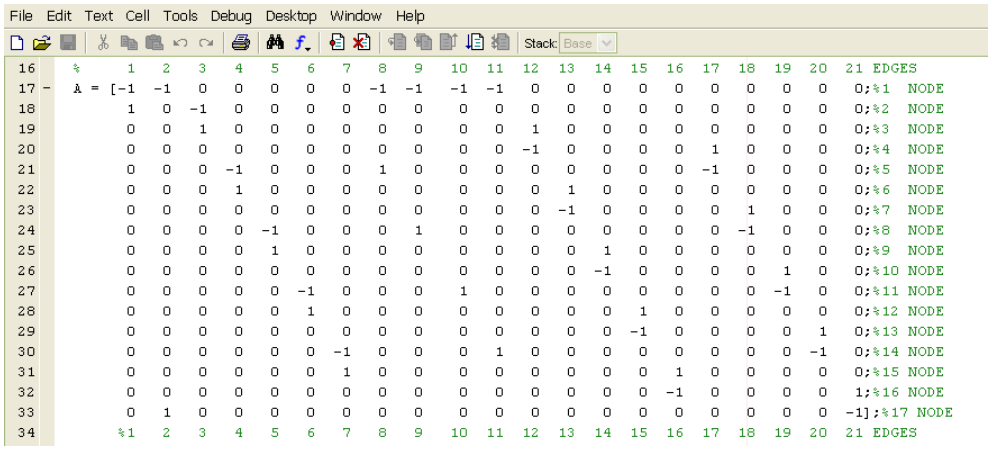

```
%     1   2   3   4   5   6   7   8   9   10  11  12  13  14  15  16  17  18  19  20  21 EDGES
A = [-1  -1   0   0   0   0   0  -1  -1  -1  -1   0   0   0   0   0   0   0   0   0   0;%1  NODE
      1   0  -1   0   0   0   0   0   0   0   0   0   0   0   0   0   0   0   0   0   0;%2  NODE
      0   0   1   0   0   0   0   0   0   0   0   1   0   0   0   0   0   0   0   0   0;%3  NODE
      0   0   0   0   0   0   0   0   0   0   0  -1   0   0   0   0   1   0   0   0   0;%4  NODE
      0   0   0  -1   0   0   0   1   0   0   0   0   0   0   0   0  -1   0   0   0   0;%5  NODE
      0   0   0   1   0   0   0   0   0   0   0   0   1   0   0   0   0   0   0   0   0;%6  NODE
      0   0   0   0   0   0   0   0   0   0   0   0  -1   0   0   0   0   1   0   0   0;%7  NODE
      0   0   0   0  -1   0   0   0   1   0   0   0   0   0   0   0   0  -1   0   0   0;%8  NODE
      0   0   0   0   1   0   0   0   0   0   0   0   0   1   0   0   0   0   0   0   0;%9  NODE
      0   0   0   0   0   0   0   0   0   0   0   0   0  -1   0   0   0   0   1   0   0;%10 NODE
      0   0   0   0   0  -1   0   0   0   1   0   0   0   0   0   0   0   0  -1   0   0;%11 NODE
      0   0   0   0   0   1   0   0   0   0   0   0   0   0   1   0   0   0   0   0   0;%12 NODE
      0   0   0   0   0   0   0   0   0   0   0   0   0   0  -1   0   0   0   0   1   0;%13 NODE
      0   0   0   0   0   0  -1   0   0   0   1   0   0   0   0   0   0   0   0  -1   0;%14 NODE
      0   0   0   0   0   0   1   0   0   0   0   0   0   0   0   1   0   0   0   0   0;%15 NODE
      0   0   0   0   0   0   0   0   0   0   0   0   0   0   0  -1   0   0   0   0   1;%16 NODE
      0   1   0   0   0   0   0   0   0   0   0   0   0   0   0   0   0   0   0   0  -1];%17 NODE
     %1   2   3   4   5   6   7   8   9   10  11  12  13  14  15  16  17  18  19  20  21 EDGES
```

Figure C.1: Incidence matrix representing the hydraulic graph of the U-tube

```
%     1    2    3    4    5    6    7    8    9   10   11   12   13   14   15   16    EDGES
A = [-1   -1   -1   -1   -1   -1   -1   -1    1    1    1    1    1    1    1    1;%1 NODE
      1    0    0    0    1    0    0    0   -1    0    0   -1    0    0    0    0;%2 NODE
      0    1    0    0    0    1    0    0    0   -1    0    0    0   -1    0    0;%3 NODE
      0    0    1    0    0    0    1    0    0    0   -1    0    0    0   -1    0;%4 NODE
      0    0    0    1    0    0    0    1    0    0    0   -1    0    0    0   -1];%5 NODE
```

Figure C.2: Incidence matrix representing the thermal graph of the U-tube

```
80    %Resistors
81 -  syms R1 R2 R3 R4 R5
82 -  Resistors_cotree = [0];
83 -  Resistors_tree   = [R1,R2,R3,R4,R5];
84 -  Rt = diag(Resistors_tree);
85 -  Rc = diag(Resistors_cotree);
86
87    %Capacitors
88 -  syms C1 C2 C3 C4
89 -  Capacitors_cotree = [0];
90 -  Capacitors_tree   = [C1,C2,C3,C4];
91 -  Ct = diag(Capacitors_tree);
92 -  Cc = diag(Capacitors_cotree);
93 -  C = Ct + HCC*Cc*HCC';
94
95    %Inductors
96 -  syms L1 L2 L3 L4 L5
97 -  Inductors_cotree = [L1,L2,L3,L4,L5];
98 -  Inductors_tree   = [0];
99 -  Lc = diag(Inductors_cotree);
100 -  Lt = diag(Inductors_tree);
101 -  L = Lc + HLL'*Lt*HLL;
```

(a)

```
66    %Resistors
67 -  syms R1 R2 R3 R4
68 -  Resistors_cotree = [R1,R2,R3,R4];
69 -  Resistors_tree   = [0];
70 -  Rt = diag(Resistors_tree);
71 -  Rc = diag(Resistors_cotree);
72
73    %Capacitors
74 -  syms C1 C2 C3 C4
75 -  Capacitors_cotree = [0];
76 -  Capacitors_tree   = [C1,C2,C3,C4];
77 -  Ct = diag(Capacitors_tree);
78 -  Cc = diag(Capacitors_cotree);
79 -  C = Ct + HCC*Cc*HCC';
80
81    %Inductors
82 -  syms L1
83 -  Inductors_cotree = [0];
84 -  Inductors_tree   = [0];
85 -  Lc = diag(Inductors_cotree);
86 -  Lt = diag(Inductors_tree);
87 -  L = Lc + HLL'*Lt*HLL;
```

(b)

Figure C.3: Element matrices: (a) Hydraulic (b) Thermal

```
200   %States
201   %=========================================
202 -  syms m1 m2 m3 m4 m5  %m =  massflows
203 -  syms P1 P2 P3 P4     %P = internal pressures of each control volume
204 -  eCt = [P1;P2;P3;P4];
205 -  fLc = [m1;m2;m3;m4;m5];
206   %=========================================
207
208   %Sources
209   %=========================================
210 -  syms P01 P02                          %Pressure references
211 -  syms Ph1 Ph2 Ph3 Ph4 Ph5              %Pressure sources due to height differences
212 -  e1 = [P01;P02;Ph1;Ph2;Ph3;Ph4;Ph5];  %Effort sources
213 -  f2 = 0;                              %Flow sources
214   %=========================================
```

Figure C.4: Hydraulic sources and state variables

```
186   %States
187   %=========================================
188 -  syms m1                        %m =  massflows
189 -  syms T1 T2 T3 T4               %T =  internal temperatures
190 -  eCt = [T1;T2;T3;T4];           %4 control volumes
191 -  fLc = [0];                     %no flow variables in this case
192   %=========================================
193   %Sources
194   %=========================================
195 -  syms Qin1 Qin2 Qin3 Qin4
196 -  syms dotQ1 dotQ2 dotQ3 dotQ4   %Flow sources, dotQ
197 -  e1 = [0];
198 -  f2 = [Qin1;Qin2;Qin3;Qin4;dotQ1;dotQ2;dotQ3;dotQ4];
199   %=========================================
```

Figure C.5: Thermal sources and state variables

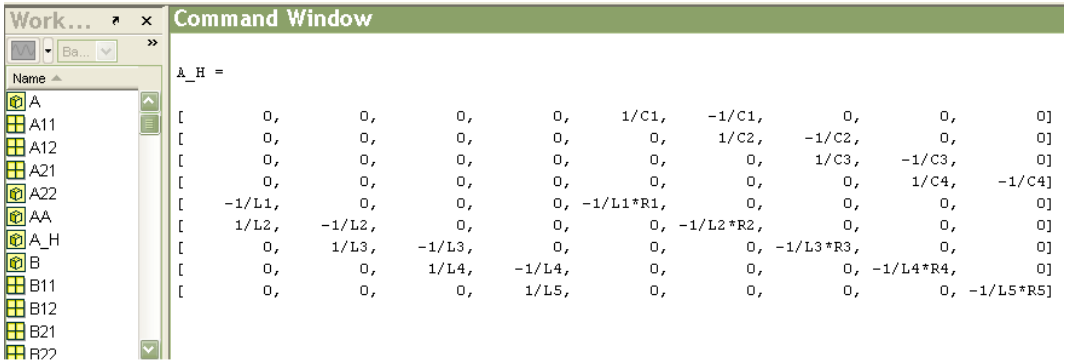

Figure C.6: Extracted hydraulic **A**-matrix

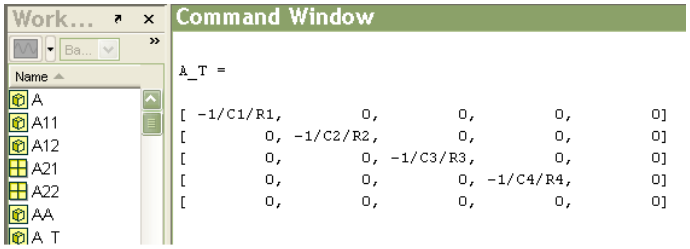

Figure C.7: Extracted thermal **A**-matrix

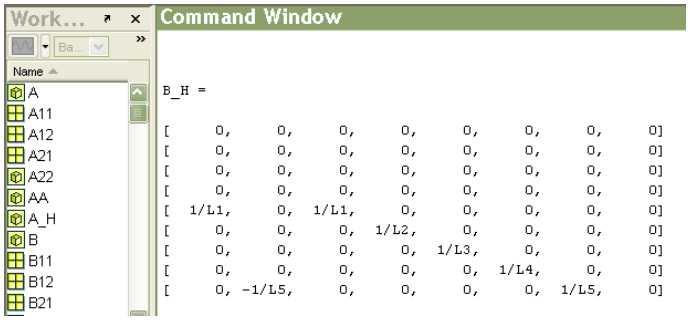

Figure C.8: Extracted hydraulic **B**-matrix

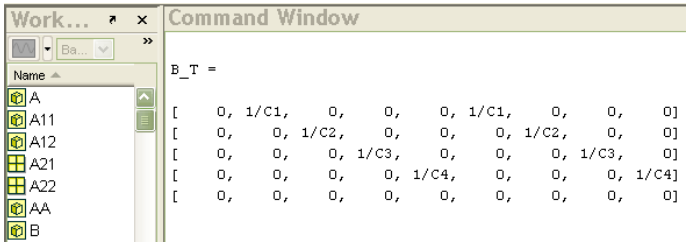

Figure C.9: Extracted thermal **B**-matrix